Some hydrodynamic aspects of a boiling water channel

SOME HYDRODYNAMIC ASPECTS OF A BOILING WATER CHANNEL

F. J. M. DIJKMAN

SOME HYDRODYNAMIC ASPECTS OF A BOILING WATER CHANNEL

SOME HYDRODYNAMIC ASPECTS OF A BOILING WATER CHANNEL

PROEFSCHRIFT

TER VERKRIJGING VAN DE GRAAD VAN DOCTOR IN DE TECHNISCHE WETENSCHAPPEN AAN DE TECHNISCHE HOGESCHOOL TE EINDHOVEN, OP GEZAG VAN DE RECTOR MAGNIFICUS PROF. DR. IR. A.A.TH.M. VAN TRIER, HOOGLERAAR IN DE AFDELING DER ELEKTROTECHNIEK, VOOR EEN COMMISSIE UIT DE SENAAT TE VERDEDIGEN OP DINSDAG 30 DECEMBER 1969 DES NAMIDDAGS TE 4 UUR.

DOOR

FREDERICUS JOHANNES MARIA DIJKMAN

GEBOREN TE AMSTERDAM

TECHNISCHE HOGESCHOOL EINDHOVEN

Dit proefschrift is goedgekeurd door de promotor

PROF. DR. M. BOGAARDT

Voor Tonny,
Michiel, Birgit, Lidwien en Joost.

CATCH WORDS

natural circulation
boiling water
axial void distribution
instabilities
phase differences
axial heat distribution
non-linear model

TABLE OF CONTENTS

NOMENCLATURE

a	amplitude	
a_1, a_2, a_3	constants in slip-correlation	
A_1, A_2 ... A_{11}	see Appendix C	
A_d	cross-section of downcomer	m^2
A_r	cross-section of boiling channel	m^2
b	amplitude	
C_K^+	dimensionless velocity of kinematic wave	
C_o	distribution parameter	eq.3.11.
	integration constant in TFA block diagram	2.11.
d_e	outer diameter heating element	m
D	hydraulic diameter of boiling channel	m
D_d	hydraulic diameter of downcomer	m
f_{ch}	friction factor boiling channel	
f_d	friction factor of downcomer	
F	friction term in momentum equation	kg/m^2sec^2
g	acceleration due to gravity	m/sec^2
G	constant in TFA block diagram	
h_{sw}	heat of vaporisation	J/kg
h_s	enthalpy of steam	J/kg
h_w	enthalpy of water	J/kg
h_z	enthalpy of water at saturation temperature	J/kg
H	constant in TFA block diagram	
I	attenuated gamma-ray intensity	
I_m	imaginary part	
I_o	original gamma-ray intensity	
k_c, k_i, k_d	specific conductivity	Ωm
		eq. 2.3.
k_{in}	inlet loss factor	

k_o	constant in TFA block diagram	
k_p	conversion factor for pitot-tube	
K	parameter in slip-correlation	eq. 3.5.
l	dimensionless distance	eq. 3.1.
L	length of shroud	m
L_b	boiling length	m
m	exponent	eq. 3.1.
n	exponent	eq. 3.2.
	upper integration limit	
p	pressure	N/m^2
Δp	pressure difference	N/m^2
q	heatflux	W/m^2
q_m	heat input per unit volume	W/m^3
q_o	axially averaged heatflux	W/m^2
Q	integrated heating power	
Q_{tot}	total channel power	
r	exponent in slip-correlation	eq. 3.6.
Re	real part	
S	slipfactor	
t	time	sec
t^+	dimensionless time	
t_1, t_2, t_3, t_4	time derivatives	
T	liquid temperature	^oC
T_o	integration time	eq. 2.11.
T_s	liquid temperature at departure of nucleate boiling	^oC
T_{sat}	saturation temperature	^oC
ΔT_{sub}	subcooling temperature at the inlet	^oC
u^+	radial velocity distribution	
v_{in}	inlet flow velocity	m/sec
v_{in}^+	dimensionless inlet flow velocity	
v_p	void propagation velocity	m/sec
v_s	local steam velocity	m/sec
v_w	local water velocity	m/sec
V_{gj}	drift velocity of vapour	m/sec
V_{vl}	drift velocity of liquid	m/sec

V_{v2}	drift velocity of gas	m/sec
w_1	volumetric flux density of liquid	m/sec eq.3.10.
w_2	volumetric flux density of gas	m/sec eq.3.9.
w_m	volumetric flux density of mixture	m/sec eq.3.9.
W	total mass flow rate	$kg/secm^2$
x	measuring signal steam quality	
X	reduced measuring signal	
y	measuring signal	
Y	reduced measuring signal	
z	axial distance	m

Greek symbols

α	void fraction	
α^+	radial void distribution	
Γ^+	vapour source term	
δ	layer thickness	m
ε_f	relative amplitude of flow perturbation	
ε_p	relative amplitude of power perturbation	
κ	heat distribution parameter	
ρ_{st}	density of steam	kg/m^3
ρ_w	density of water	kg/m^3
$\Delta\rho$	$\rho_w - \rho_{st}$	kg/m^3
σ	standard deviation	
Σ	absorption cross-section	m^{-1}
ϕ	phase angle	degrees
Φ	parameter defined in eq. 4.2.	
Φ_{xx}	power spectrum of x-signal	
Φ_{xy}	power spectrum of y-signal	
Φ_{yy}	cross-spectrum	
ω	radian frequency	sec^{-1}
ω^+	dimensionless radian frequency	
Ω^+	dimensionless reaction frequency	

ABSTRACT

The main subject of study has been the influence of subcooling, of a sine-shaped heatflux, and of a combination of both on the steady-state and dynamic characteristics of a natural-circulation, pressurised, boiling water system. In natural-circulation boiling systems hydrodynamic instabilities may occur at constant power. They appear to arise from a dependence of the vapour volume production rate upon the flow-rate as a result of energy conservation and simultaneously the flow-rate depends upon the resident vapour volume in the system as a result of momentum conservation and continuity. The steam pressures were taken 15.5 and 30 atm, corresponding to saturation temperatures of 200°C and 234°C respectively.

Although the experimental results disclose the fact that the transition from stable to unstable behaviour is not accompanied by a discontinuous change of all physical variables, preference has been given to a classification of the experiments in steady-state and dynamic measurements. It was preferred to incorporate the transfer function measurements in the dynamic part.

Chapter 2 describes the experiences with void measurements by applying the impedance technique in addition to data concerning the loop dimensions and the measuring equipment. The calibration of gauges has been referred to Maxwell's theory.

Chapter 3 deals with the measurements under steady-state conditions of the inlet velocity, the axial void distribution and pressure drops at different conditions of channel power, subcooling at the inlet, flux-shape and pressure. Data reduction was applied to calculate local values of the slipfactor and of two-phase friction. The slipfactor has been represented by adopting the correlations derived by Bankoff and Zuber. The values of two-phase friction were established according to Martinelli-Nelson.

Chapter 4 covers the results of the analysis of steady-state noise and of oscillations under unstable conditions in terms of amplitudes and

phase differences of Δp_{inlet} and the axially distributed voids. The conditions were chosen equal to those of chapter 3. The void propagation velocities have been compared with the expression derived by Neal from the energy equation.

A limited number of transfer function measurements between the channel power as the perturbed quantity, and the dependent variables Δp_{inlet} and the various axial voids, supplemented the experiments. The void propagation velocity as a function of frequency has been compared with the expression of Zuber, based on the theory of kinematic waves.

Chapter 5 describes a theoretical study based on a solution of the familiar laws of conservation, with the addition of suitable expressions for the slipfactor, two-phase friction multiplier and the heat-distribution parameter in the region of subcooled boiling. No special attention has been paid to the boiling boundary, the external system and estimated second order effects. For the solution procedure, a profitable application was made of the CSMP-program, developed by IBM, which facilitated the programming of the integration process. The results of the computations were surprising owing to the close agreement with the experimental results with respect to the threshold-powers, the frequency, the destabilising effect of moderate subcooling and the influence of a non-uniform heatflux.

Chapter 6 summarises the main conclusions to be drawn from the present study. The value of two-phase two-component measurements with the aim of transposition to boiling-water conditions is doubted. The equations of Neal and Zuber for the void propagation velocity are discussed. The influence of a non-uniform heatflux on the system stability is reviewed and its consequence is stated for dynamic boiling water experiments and for the anticipated stability of steamboilers in general and of boiling water reactors in particular.

Where it was possible and profitable chapters and parts of it have been completed with conclusive remarks.

Note: A small part of the experiments to be reported here is similar to the experiments described by Spigt (S 2). Comparison between both sets of results is impossible as void-fraction is concerned (see ch. 2.2.). Other results can deviate some per cent. owing to the use of different heating elements.

I INTRODUCTION

For many years an innumerable number of investigators have strenuously studied the phenomenon of boiling under high heatloads, as present in nuclear reactors of the boiling water type, as well as in more conventional equipment. Because of the existing number of publications each new publication is like carrying owls to Athens, but the exponentially increasing number (H 1) finds its justification in the intransparancy of boiling phenomena which leads to an insatiable need for more data. One of the causes of this need is undoubtedly the fact that it is not possible to define exactly all parameters which influence boiling (L 1). One is familiar with the principal measurable parameters such as power, pressure, mass flowrate and temperatures, but a number of quantities exist which cannot or hardly be measured. Most notorious are the void-fraction and, related to this, the void and flow-profiles; the latter are interchangeable owing to the inextricable relationship between both. Really, void itself is a quantity that is impossible to be measured directly, which is understandable from the original meaning of "void", i.e. a lack of material, a gap in the fluid. In fact, all methods applied to detect void measure the thickness of the accumulated liquid layers, and the void-fraction is found by subtracting this thickness from the one which would be present if the total cross-section was filled with liquid. This has important consequences for the measurements, as the void manifests itself in many appearances and is very sensitive to pressure variations. It is impossible to classify the different appearances in clean-cut regions. A rough classification is given by Baker (B 1) who distinguishes bubbly, slug, plug, churn-turbulent, and annular flow, completed by Hewitt (H 1) with whispy annular flow, but all regions change noiselessly from one into another.

This presence of different regions results in the existence of void-profiles, which constitute a subject of study by, for instance, Zuber

and Bankoff (Z 1, B 2). It amplifies the measuring problem to an unsolvable extent. By means of especially developed techniques as, for instance, the narrow-beam gamma-ray technique (P 1, S 1) and the electrical-resistivity probe (N 1, L 3) void-profiles have been measured in low pressure, symmetrical test sections with a constant cross-section along the vertical axis, but the reality is that operating pressures are above 100 atm and that many flow disturbing objects are present in the channel. In one test section the whole scale of void configurations from bubbly to annular flow can be present. Therefore, although it is known that the key of the boiling problem has to be looked for in the void-fraction, and in particular in the appearances and in the detailed distribution of void, it only shifts the problem because of the secrecy of the key.

Consequently, one is urged to resort to conceptions such as slipfactor and two-phase friction multiplier, derived from measurable but averaged quantities. Although the slipfactor itself was a known quantity,it lasted until 1960 before Bankoff (B 2) related the slipfactor to the void-profile and derived a simple expression for it. It is remarkable that in spite of this new approach the expression still contains the average void-fraction. Lateron Zuber made an extensive study of void (Z 1).

Another not directly measurable but necessary quantity is the steam quality. It is to be calculated from a heat balance, and then the second problem arises. In case the fluid enters the test section at a saturated condition and the heat losses are known, an accurate heat balance can be made, but the scene changes if the fluid is subcooled. Observations of several authors (B 3, L 2, R 1) have shown that though the fluid is subcooled considerably, bubbles are still formed. The methods by which these authors attack this question differ. Bowring, who was the first to develop a useful model of subcooled boiling based his upon the criteria of Jens and Lottes (J 1) and conceived a distribution rate between heat used for warming up the water and that used for generating steam. Levy (L 2) confines himself to the calculation of the starting point of bubble formation and of the amount of steam, present at the boiling boundary, and having done this, connects both points by an exponential function.

In spite of all these efforts the subcooled boiling models have not been applied quite successfully. This implies that in the region of subcooled boiling the void fraction and the steam quality are very dubious parameters, and, consequently, the derived slipfactor is equally unreliable. In the region of bulk boiling the slipfactor is reliable so far as one has confidence in the void-fraction measurements.

An analogous reasoning can be set up with respect to two-phase friction. Commonly accepted is the conception of Martinelli and Nelson (M 1), who defined a multiplication factor R, which indicated the ratio between the real pressure drop due to two-phase friction and the pressure drop that would exist if it was caused by the same mass flow under one-phase condition. The value of R is always greater than one, but smaller than it would be if the pressure loss was caused by one-phase friction and taking into account the local liquid velocity. In that case the factor R should be equal to $(\frac{1}{1-\alpha})^2$ because the local liquid velocity can be expressed by

$v_{local} = (\frac{1}{1-\alpha})v_{inlet}$, α representing the local void-fraction.

It means that it is not the friction of the liquid along the walls which determines the pressure loss, and that the presence of void diminishes the friction. It is evident that the extent to which the channel walls are covered by void, i.e. the void-profile, plays an important role. It follows that the two-phase friction multiplier appears to be as arbitrary as the slipfactor.
What further complicates the picture is the presence of flow disturbing objects in operational boiling channels as, for instance, grids. It is impossible to calibrate the pressure losses of these objects in one-phase or adiabatic two-phase flow and transfer the values obtained to boiling conditions. Besides, the roughness of the walls is of interest, more with regard to the density of the nucleation site population than to the friction. The problem is further complicated by the effect of mixing between subchannels and by the complexity of the channel geometry. The consequence of the elusivity of the void is a limited ability to extrapolate experimental results towards other rigs irrespective of the type of conditions in which they differ, to trans-

late them into design rules and to predict the hydraulic behaviour by using mathematical models.

The last ten years have shown a boom in models in abundant variety: linearised and non-linear, lumped and distributed parameter type, suitable for an analogue or a digital computer, etc. Two extensive studies of Neal (N 2) and Bjørlo (B 4) have proved that the accuracy of the predictive properties is poor, and the relative usefulness of models is emphasised by the building of large full-scale rigs (6 MW Winfrith, 8 MW Studsvik) in order to carry out experiments under conditions as close as possible to the operational ones. In view of the limitations on the experimental as well as the theoretical side it is unreasonable to expect numerical or absolute accuracy of models. It would already be very promising if a model showed qualitatively correct values, i.e. if it predicted correctly the effect of pressure, restrictions, subcooling, shape of heating power, etc. By adapting this model to a small-scale system it must be possible to predict the hydraulic behaviour of the operational system provided they have an identical geometry.

This exposition forms the basic thinking of the study under consideration. It contains the results of a number of experiments of a qualitative nature. Natural convection was chosen as the main driving head based upon the consideration that the only effect of forced circulation is a stabilising one. It damps the system by breaking the flow-void interaction and conceals some important elements of the hydraulics. To what extent the pump has a stabilising effect depends on the ratio between the driving head of the pump and the pressure drop across the boiling channel. The larger this ratio, the more stable the system will be.

The variable parameters were the system pressure, the power, the subcooling at the inlet of the channel and the shape of the heat flux in axial direction. Each of these parameters was considered to affect substantially the hydrodynamic properties of the system. We were, however, aware of the limited pressure of the system and of the unicity of the geometry, and this also was a motive to emphasise the performance of qualitative experiments. For this reason less attention has

been paid to the occurrence of burn-out. Where, however, burn-out has been unintentionally encountered, the values of the determining quantities have been registered.

2. EXPERIMENTAL EQUIPMENT AND TECHNIQUES

2.1. Boiling Loop

The system designed for a maximum operating pressure of 40 atm consists of four main components, viz. the pressure vessel, which contains the test assembly, the condenser, the subcooler and the pump, the latter being an optional additive. The material of all parts that do not conduct the electrical current, is stainless steel. The components will be described with reference to Fig. (2.1.), giving the flowsheet of the loop.

2.1.1. Pressurised part

The cylindrical pressure vessel has an inner diameter of 150 mm and a length of 3 m. A widening at the top acts as a drum where the velocity of the fluid is slowed down, the steam collected and the moving of the water surface tempered. Next to the steam drum is a separate drum, which is in connection with the downcomer and the steam space in order to stabilise the water level during operation. A 75 mm steam line leads to the condenser. The vessel is provided with a number of sleeve pieces for allowing thermocouples and electrical conducting wires to pass through the vessel wall.

The steam is condensed in a number of vertical tubes, placed in a row, on both sides of which a reservoir is mounted one wall of which is perforated. The holes have been drilled in such a way that they form a sloping straight line and the diameters decrease in upward direction. The momentary cooling capacity depends upon that length of the condenser tubes which is wetted by the sprinkling water, and this length is again dependent on the water level in the reservoirs. Condenser control is achieved by automatic adjustment of the water level. The control reacts on the temperature in the steam space and compares it to an adjusted reference value. The controlaction is proportional, integrating and differentiating.

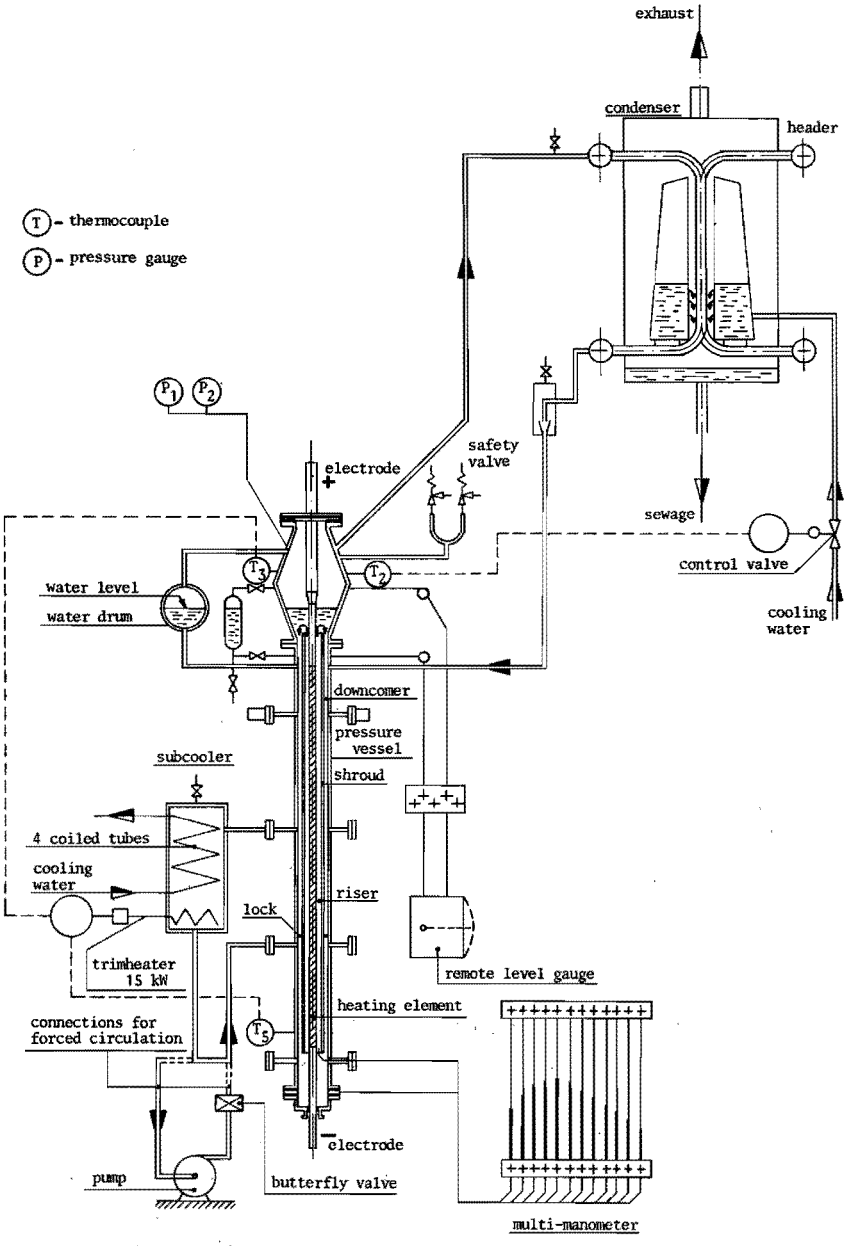

2.1. Flow sheet of the pressurised boiling water loop

The heating element consists of a stainless steel tube, on both ends provided with solid copper electrodes. The upper electrode pierces a copper flange and has been soldered on to it. The flange is connected to the positive voltage of the power supply and insulated from the pressure vessel by means of a gasket made of ferrobestos. The lower electrode is enclosed in a cylindrical stuffing box which allows for expansion of the heating element. This element is surrounded by a shroud with an inner diameter of 50 mm. The water rises through the annular passage, between heating element and shroud returns - so far as it has not been evaporated - through the downcomer between pressure vessel and shroud downwards. A locking device in the downcomer forces the water to pass through a subcooler, placed in parallel with the downcomer.

In view of the relatively small driving head inherent to natural convection, the subcooler has been constructed so as to have a very small pressure loss. Placed inside a drum through which the primary water flows, four helical tubes with cocks can be fed separately by cooling water, streaming in counter-current direction to the fluid on the primary side, which makes possible an exact adjustment of the inlet temperature of the test section. A preheater installed in the subcooler balances the heatlosses of the downcomer if zero subcooling is desired and raises the adjustability of the subcooled inlet temperature.

The construction of the pipe going from the bottom of the subcooler to the downcomer is such that a pump can be installed. Of this facility use has been made when calibrating the impedance void gauges.

2.1.2. Test assembly

The shroud with an inner diameter of 50 mm, consists of 9 identical parts, each of which has a length of 335 mm and is provided at both ends with three lugs for the purpose of fastening the housings of the impedance gauges, one of which is mounted between each two shroud parts (Fig. 2.2.). The length of the shroud extends at both ends beyond the heated length of the element. The upper non-heated part, i.e. the chimney, has a length of 246 mm. Pressure tappings have been soldered in the wall of the shroud, one in the middle of each of the 9 shroud-

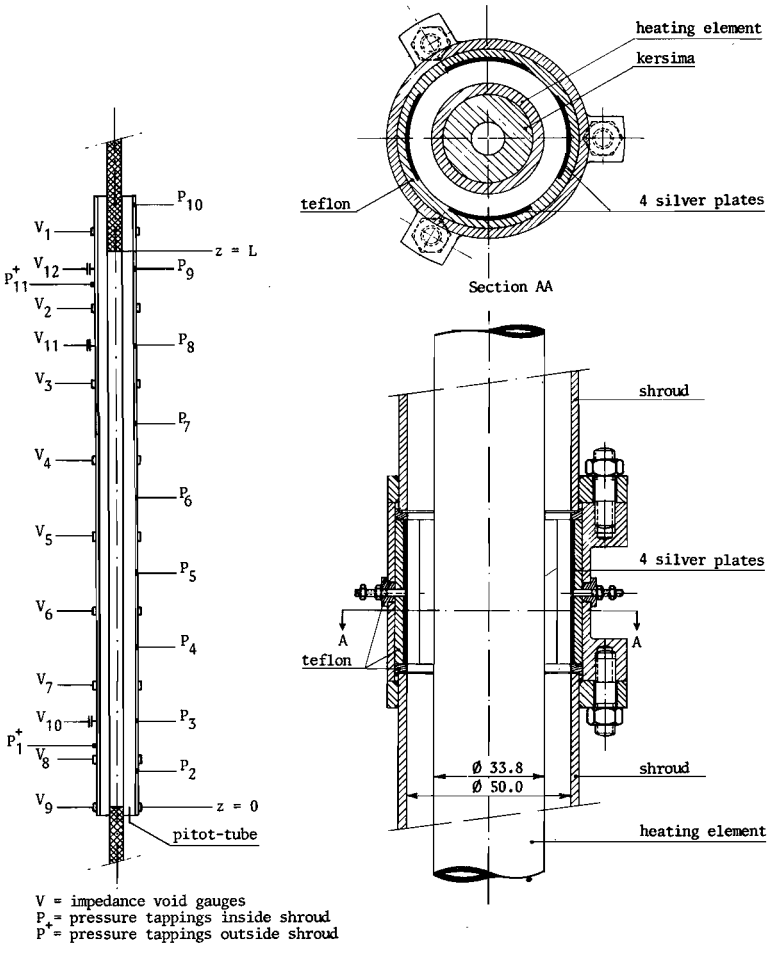

2.2. Diagram of test section and impedance void gauge

elements, offering the possibility to measure the pressure drop along the channel axis. At the lower end there are two extra tappings, one detecting the pressure outside and one detecting it inside the shroud. Their object is to measure the pressure loss across the entrance, which is a measure for the inlet velocity. A pitot tube in the entrance makes it possible to check the value of the inlet velocity. Screw joints connect the pressure tappings to a measuring ring, mounted at the bottom of the pressure vessel between two flanges. This ring is

provided with a number of drilled holes, providing a connection between the inside pressure tappings and those outside the vessel.

The insulated passage of conducting wires through the vessel wall has been achieved by means of Conax multi-hole packing glands with lava sealant, fitted in one of the sleeves of the vessel. The shroud is electrically insulated from the pressure vessel in view of the observed effect on the readings of the impedance gauges.

The heating element has an outer diameter of 33.8 mm and an electrical resistance of 8 mΩ. Two types have been applied, generating a uniform and a sine-shaped heatflux respectively. Since the latter could not be manufactured with a continuously changing wall thickness, for lack of special machine tools, it was composed of 12 pieces welded together, each having a length of 20 cm. Every piece was internally turned with a tapering diameter. The diameters have been tabulated in figure (2.3.).

The axial distribution of the resistance was calibrated by using two electrodes of a special construction. Each consisted of two sets of three sharp-edged feelers lying in one plane at 120^{o}, the distance between the two sets being exactly 4 mm. Three feelers belonging together were interconnected electrically. One electrode was then fixed at one end of the tube and the second was moved along the tube with discrete steps of 6 mm. In this manner it was possible to calibrate at the same time the integrated resistance from the fixed electrode to the moving one as well as the local resistance over a length of 4 mm. The second measurement provided information necessary to check the quality of the welded joints in view of avoiding hot-spots. Owing to the conical inner shape of the separate parts the shape of the axial distribution of the resistance of each part is a little concave. The deviation from the designed shape was, however, small enough to permit the application of the expression for the designed shape.

The largest difference appears in the middle of the rod, where the tube was turned cylindrically. The heatflux as a function of axial distance to either end of the rod can be represented by:

$$q = \frac{0.515}{0.9\ \pi\ d_e}\ \sin\left(\frac{0.215 + z}{0.9}\right).\ Q_{tot} \qquad \text{eq. 2.1.}$$

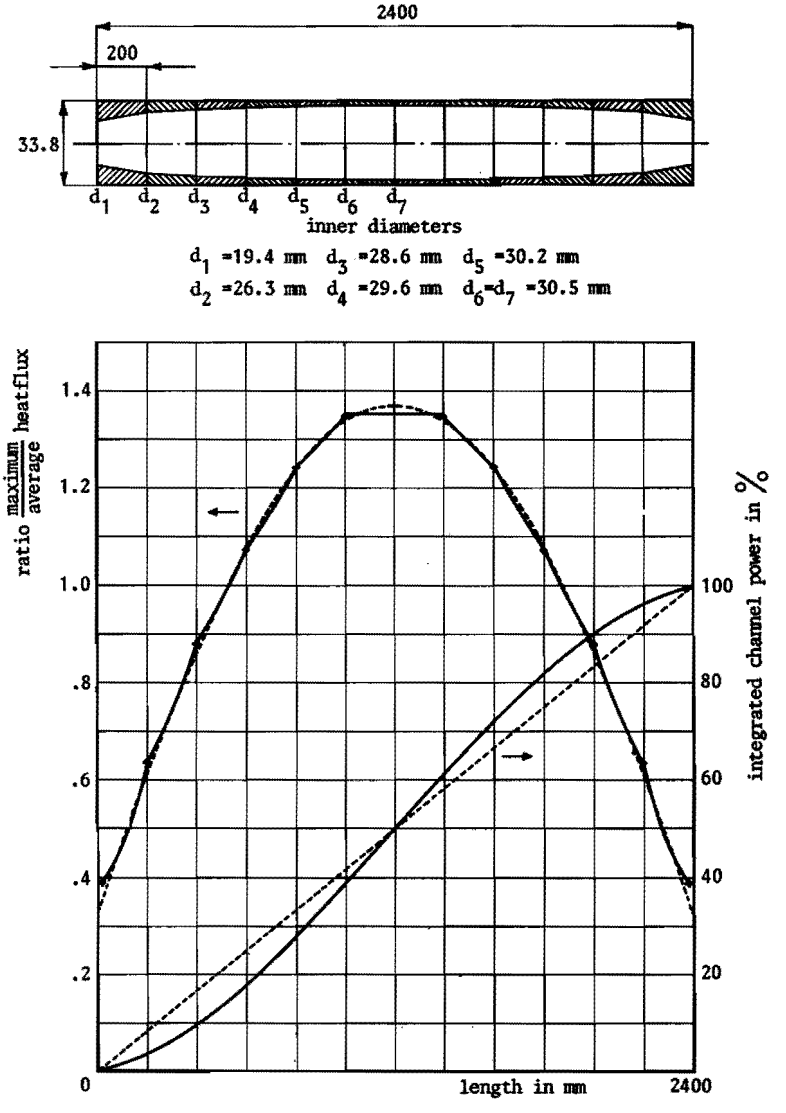

2.3. Dimensions of heater tube with varying wall thickness and axial distribution of heatflux ratio

and the local heating power, integrated over z, by:

$$Q = 0.5 - 0.515 \cos \left(\frac{0.215 + z}{0.9}\right) . Q_{tot} \qquad \text{eq. 2.2.}$$

d_e represents the outer diameter of the heating element
z the axial distance to the beginning of the heated part
, and
Q_{tot} the total power input.

The heatflux is symmetrical and the ratio between maximum and average heatflux is 1.38.

In order to allow a fair comparison between the results obtained with a sine-shaped and a uniform heatflux, a cylindrical heating element was ordered, and it was manufactured in the same way, resulting in equality of the surface roughness. It is remarked that in earlier experiments the heating elements consisted of commercially available tubes.
The relevant dimensions have been summarised in table 2.1.

Table 2.1.

Relevant dimensions and values of the test loop

inner diameter of pressure vessel	150.0	mm
inner diameter of shroud	50.0	mm
length of shroud	2.695	m
outer diameter of heating element	33.8	mm
heated length	2.4	m
distance between lower end of heated part and entrance shroud	49	mm
length of chimney	246	mm
distance between centres of two subsequent void gauges	335	mm
distance between two subsequent pressure tappings	335	mm
distance between lowest void gauge and entrance of shroud	207	mm
Weissbach friction factor of downcomer f_d	0.04	
Weissbach friction factor of boiling channel f_{ch}	0.0314	
inlet loss factor of the shroud k_{in}	1.64	

2.1.3. Power supply

The channel power was supplied by a unit, consisting of a transformer, connected to the 10 kV mains, and a rectifier. The maximum values of voltage and current were 70V and 14,000 A respectively, which means that for an optimal resistance of the heating element (5 mΩ) the maximum channel power is 1 MW. A transductor circuit at the primary side of the transformer made possible continuous control of the power and sinusoidal perturbation at a maximum frequency of 8 Hz.

The power supplied to the heating element was measured in steady-state conditions by means of a precision volt and ammeter and a light-spot wattmeter. The voltmeter was connected to the electrodes at both ends of the heating element. Current indication was obtained from a direct-current transductor, reducing the current by the ratio 3000:1.
The power was measured under dynamic conditions by making use of a Hall generator. This device produces a signal which is proportional to the product of voltage and current. It was calibrated under steady-state conditions against the light-spot wattmeter. The linearity was better than 0.1% in a range of channel powers from 10 to 400 kW.

The dynamic response did not necessitate corrections of gain and phase.

2.2. Measuring facilities

Sensors

The temperatures have been measured by using ordinary insulated thermocouples with an outer sheath diameter of 1 mm. They were calibrated for an accuracy of 0.25°C. The reliability of the thermocouples was so good that all experiments could be performed with the same set of thermocouples.

The absolute pressure was measured by a Bourdon spring manometer connected to the steamspace. The pressure differences were measured

under steady-state conditions by means of a multimanometer and under dynamic conditions with pressure transmitters (type SEL). These transmitters, applied only for the detection of the pressure loss across the inlet and of the pressure difference indicated by the pitot tube, were of the inductive type. The displacement of a membrane is converted into a change in the inductance of a coil.

For use during steady-state conditions the pressure-gauges were calibrated against the multimanometer. The linearity was within 1%.

Examination of the dynamic characteristics mentioned in (S 2) indicated that for frequencies up to 2 Hz no corrections were necessary where amplitude and phaseshift are concerned.

The pressure loss across the entrance of the channel as a function of inlet velocity was calibrated conscientiously for a range of Reynolds' numbers. The procedure was that by means of a separate, suitable centrifugal pump a dosed flowrate was pumped through the system at room temperature. The flowrate was measured by weighing on a balance the amount of water that was poured forth during a certain period. The pressure drop across the inlet, after conversion of the multimanometer reading, can be written as a function of the inlet velocity according to

$$\Delta p = \tfrac{1}{2}\, k_{in} \cdot \rho_w \cdot v^2_{in},$$

where k_{in} represents the inlet loss factor. The dependence of k_{in} on the Reynolds' number decreases with increasing value of Re (Fig. 2.4.).

In order to approximate closely the experimental values of Re it was necessary to perform the calibration at flowrates up to 3.1 m/sec. For the calculation of the inlet velocity from the experimental Δp-values $k_{in} = 1.64$ was used. The corresponding value for the pitot tube was $k_p = 1.39$.

A disadvantage of this method of measuring the inlet velocity is the impossibility to translate under dynamic conditions the Δp-values into values of the inlet velocity owing to the non-linear relation between pressure drop and velocity.

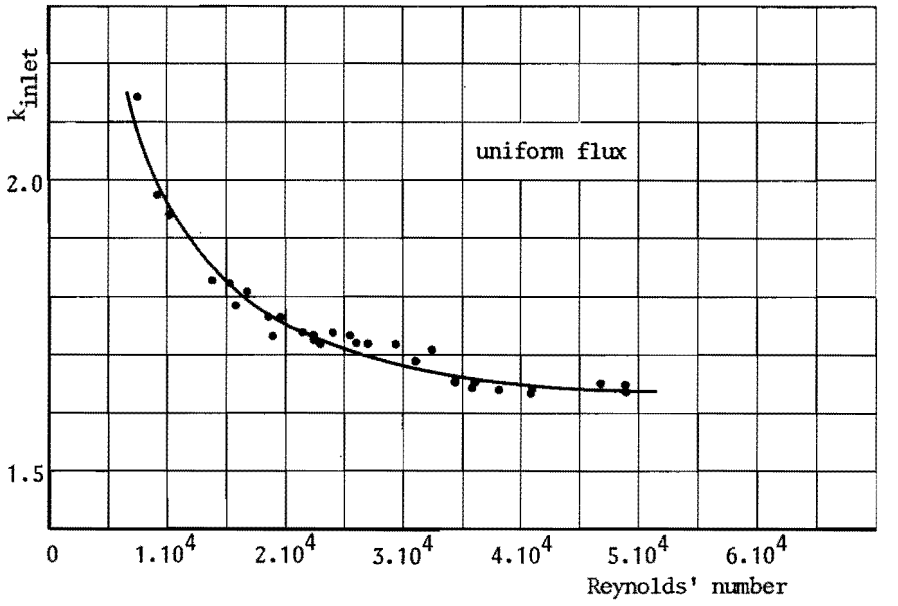

2.4. Calibration curve of the inlet loss factor

Because the position of the pressure tapping detecting the inlet pressure loss, is a little distant from the entrance of the channel, the measured value of that loss includes also a contribution of the frictional pressure losses in downcomer and heated channel. The use of k_{in} in the mathematical model needs therefore a correction for these additional losses, resulting in $k_{in} = 1.45$.

V o i d f r a c t i o n

Two techniques of measuring void fraction were available, viz. the gamma-ray method and the impedance method.

(1) The gamma-ray method is based upon the attenuation of a beam of gamma-rays when passing through layers of different materials. The attenuation is an exponential function of the sum of the thickness of different layers multiplied by the individual specific macroscopic cross-section for absorption, according to the absorption law

$$I = I_o e^{-\sum_{i=1}^{n} (\Sigma_i \delta_i)} ,$$

where I represents the actual radiation intensity,

I_o the original intensity,

Σ_i the specific macroscopic cross-section and

δ_i the layer thickness.

When the method is applied to void fraction measurements, one of the layers, consisting of boiling water, has a variable density and consequently a variable absorption. The absolute void value is determined by means of interpolation between the intensity at zero void and that at 100% void.

In the present case a 350 mCurie Thulium-170 source was placed inside the heating element in a fixed position. The annular cross-section of the channel involved this complicated assembly. Around the source four scintillation counters were mounted into the wall of the pressure vessel in the form of a straight cross. The apparatus possessed some particular features. The amplification of each photomultiplier was kept constant by continuous calibration against the gamma-spectrum of a 10 mCurie Caesium source, fixed to the water-cooled photocrystal, and subsequent control of the high voltage. The pulses of the four scintillation counters were mixed and counted by a 10 MHz scaler. The counting-rates of the four counters were established to be of comparable magnitude. The ratio of the intensity, measured in the empty loop, to that measured in the loop, when filled with water, commonly named the empty to full ratio was about 1.10, attained by carefully discriminating over the Thulium peak in the energy spectrum (84 KeV).

(2) The impedance method is based upon the change of impedance of a waterlayer owing to the presence of gas-bubbles. The relation between the impedance and the content of bubbles, however, is neither linear nor exponential. The basic theory that is generally accepted by investigators was derived by Maxwell in 1881 (M 2). He regarded a carrier fluid and a suspension of small spherical particles in it. As an essential characteristic he assumed the distance between the particles to be large compared to their diameter. Representing the specific conductivity of the mixture by k_α, the
30 specific conductivity of the continuum phase by k_c, that of the

suspended spheres by k_i and the volumetric fraction of particles by α, the relation between the impedance of the mixture and the relevant parameters is

$$\frac{k_\alpha - k_c}{k_\alpha + 2k_c} = \alpha \frac{k_i - k_c}{k_i + 2k_c} \qquad \text{eq. 2.3.}$$

This expression can be represented in a diagram and has been generally used in that form (O 1, C 1, S 2).
Realisation of the impedance technique was first tackled by Olsen (O 1). He made an extensive study, directed to the applicability of the method in boiling water channels. An investigation was made as to the influence of the geometry of the electrodes, the influence of the void profile and the flow-dependence of the measurements. The different gauges were carefully calibrated in an air-water system, equipped with quick-closing valves. The maximum void fraction that was attained was 55%. He measured appreciable flow dependence at low velocities, which seemed not to be attributable to the velocity or void profile. The strong dependency of the bubble size on the superficial water-velocity was assumed to be the main cause of the flowrate dependency on the void signals. Later on, however, it was stated that at low velocities there might be a considerable difference between the measured average void fraction in the test section and the local void fraction in the gauge, owing to a decrease of slip-ratio in the void gauge, having a smaller cross-section than the channel.
By applying a correction factor that takes this effect into account the flowrate dependency could be reduced substantially.
Ultimately it was established that there were three conditions that had to be fulfilled in order to obtain reliable results, viz.

(1) the electric field must be homogeneous
(2) the distance between the electrodes must be large in comparison with the diameter of the bubbles
(3) the flow must be undisturbed. The slip, and consequently, the void fraction are substantially altered by a change of the cross-section.

In the conclusions (O 1) it was stated that "the measurements of the void fraction in a two-phase fluid by means of the impedance method are generally subject to large uncertainties. However, by a careful electrode design, and by use of the instrument in flow regimes for which it is designed, adequate results are possible."

It was found that the preferential design was a gauge with two plate electrodes spaced 17.5 mm apart. The void-signals from this type of gauge were measured to be in good agreement with the corresponding values found with Maxwell's formula when the void meter was used in bubble flow. In slug flow the electrode geometry was expected to have no influence. This is the more astonishing because it is conflicting with the third condition.

Bjørlo et al. (B 5) reported void measurements with a gauge consisting of a number of concentric, ring-shaped electrodes, which could only satisfy the first condition. The gauge was calibrated against the turbine-flowmeter, but it is not mentioned whether the results followed the Maxwell curve or not.

The second experience that has been reported was obtained by Cimorelli (C 1). The test section used was of an annular geometry. The electrodes were formed by the central cylindrical tube and the shroud itself, thus not introducing a disturbance of the flow. In this manner the integral void fraction over the channel length was measured, which was compared with the results obtained by the dilatation technique. The calibration was not carried out in an air-water system but in a boiling water loop. The operation-pressure was 1.15 kg/cm^2 and the steam was produced by flashing at the entrance of the test section. The water was preheated and passed through an orifice under forced circulation, causing a pressure drop and consequent flashing. The inlet steam quality was evaluated by measuring the temperatures before and after the orifice. The reliability of the results was greater for the higher void fractions owing to the scatter of the experimental points in the region of low voids ($< 40\%$). An encouraging correspondence with the Maxwell curve was established for void fractions smaller than 0.5 and an increasing deviation at higher void fractions (< 0.85), although the diffe-

rence did not exceed 10% void. The deviation increased with decreasing flowrate, contradictory to the observations of Olsen.

However, the results having been published, reflections on the experimental uncertainties aroused doubts concerning the correctness of the observations (E 1), in particular with respect to the higher void fractions. It was felt that extrapolation from lower voids to higher values is quite a precarious venture.

The third investigator who adopted the impedance method was Spigt (S 2). The annular cross-section enabled him to apply a very clean design of the void gauge (Fig. 2.2.). The heating element itself acted as the first electrode and the second electrode consisted of 4 silver plates, mutually interconnected and placed in an insulating material, in this case Teflon, and fitted in a stainless steel housing. The housing was clamped between flanges of the shroud parts. The cumulative circumference of the silver plates equalled that of the heating element with a view to creating a homogeneous electric field. The electrode plates were flush with the inner surface of the shroud, so that the flow was not at all disturbed. The second condition of Olsen was fulfilled so far as the distance between the electrodes was as large as possible, equal to the distance of the channel walls. The height of the plates was 5 cm in order to obtain a quiet void signal by the integrating action of the axial dimension of the gauge. The four plates were interconnected and only one wire per gauge left the pressure vessel, insulated by a Conax-packing gland.

As for the agreement of the void as measured by the impedance method and that measured in the same position by the gamma-ray method, Spigt claimed a deviation of only 3% void. A preliminary examination had been carried out before in an air-water loop, where the gas content was determined from the rise of the water level. The results sustained the observations under boiling conditions.

Since Spigt completed his series of experiments, the present author has prepared a new series of experiments to be carried out in the same rig, using the same instrumentation.
The whole equipment was inspected quite thoroughly and the shroud,

being the most important part of the rig, was dismantled and re-assembled very carefully. In particular, much attention was paid to the insulation of the wires that interconnected the silver plates and that conducted the signal to the outside of the pressure vessel. When starting the experiments, values of the void fraction were obtained that exceeded 95%. This observation implicated figures of the slipfactor being smaller than one. This is physically impossible, certainly for those high void fractions. The apparatus was carefully re-checked, however, no differences with the previous equipment being established that could explain the void fraction to be 20% greater than before. It was only known afterwards that formerly less care had been given to the proper insulation of the wires than

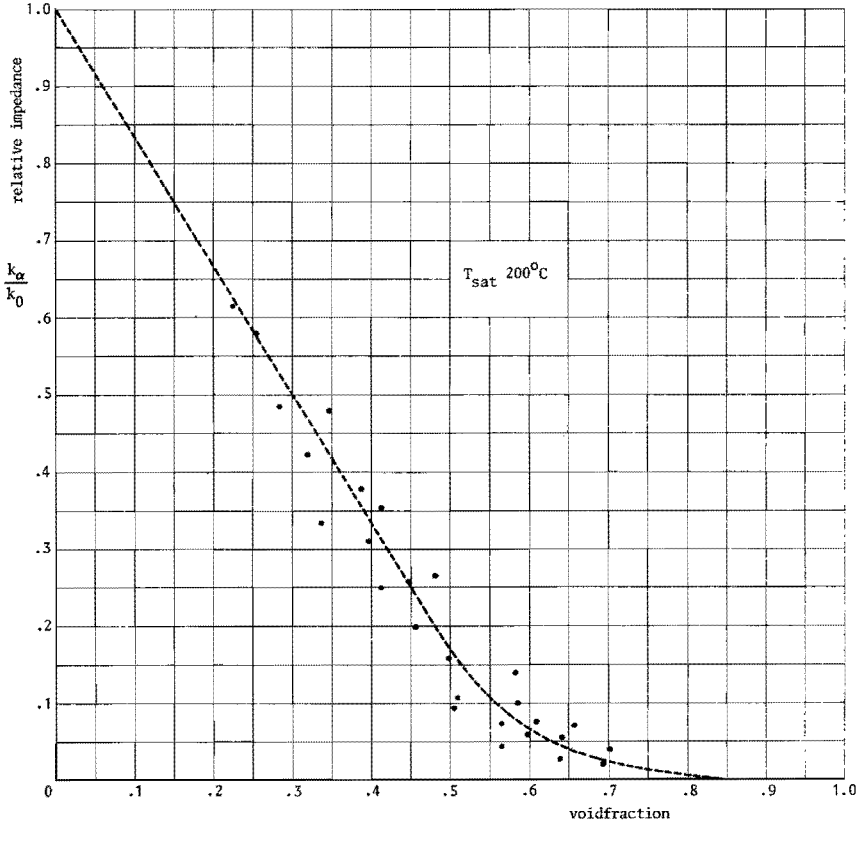

34 2.5. Calibration curve of the relative impedance T_{sat} 200°C

was done later on. It can be argued that leakage of the current from the void gauges to the surrounding wall decreases the values of the measured void fraction. This led to ascribe the present deviating results to better insulation of the conducting wires.

The impossibly large void fractions required a re-calibration against the gamma-ray method. Owing to the fixed position of the gamma-source the calibration could only be performed for that upper void. In order to gauge low void fractions too, forced circulation was applied. By accepting the gamma-ray method as the standard and measuring the impedance of the mixture, the results no longer corresponded to the Maxwell curve. Already at small void fractions the results started to deviate (Fig. 2.5.). It appeared inevitable to

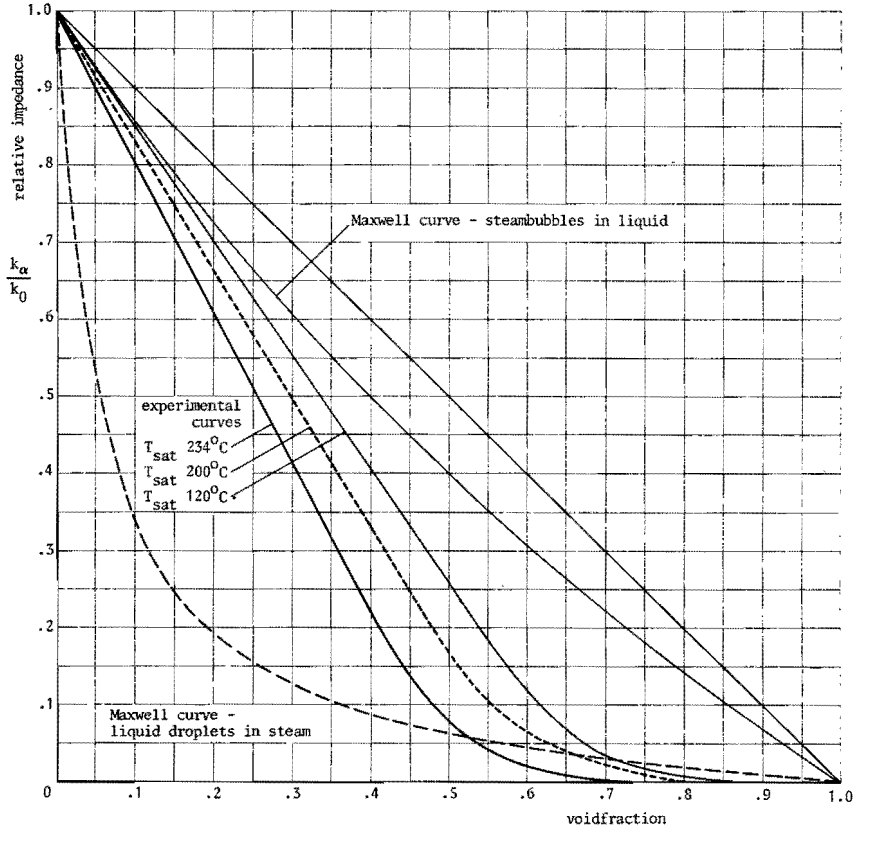

2.6. Experimental and theoretical curves of the relative impedance

accept new calibration curves that deviated considerably from the Maxwell curve. Two curves are given, corresponding to the two operation pressures (Fig. 2.6.). Varying the flowrate did not essentially affect the results. At most it increased the scatter of the points. Up to values of 40% void the relationship between impedance and void fraction is linear. At high values of void fraction the method is less sensitive but still usable.

Conclusive remarks

Calibration in air-water systems indicates a rather fair correspondence to the Maxwell curve, provided that some special precautions are taken with respect to the geometry of the gauge. Calibration in steam-water mixtures or boiling systems indicates deviations, although their magnitude differs for each investigator. This is an inducement to distrust calibration in an air-water system. An essential difference between an air-water and a boiling mixture is the presence of two completely independent components. They exert forces upon each other, but no one-component phase relationship exists. In the case of boiling there exists a strong interchangeability between the two phases. The bubbles grow and contract as they exchange heat with the surrounding liquid. This has an effect on the shape of the bubbles and on their agglomeration. When boiling takes place all along the channel, then there is also a difference in velocity and void profile. With natural circulation the void profile in boiling-tubes is strongly related to the velocity profile and it is very questionable whether this also holds for an air-water mixture.

A deviation from the Maxwell curve is very acceptable since the latter has been derived for small spherical particles and with a relatively large distance between them. This situation is only present at very low void fractions and, on the other hand, also at very low liquid content. A similar curve can be drawn for a dispersion of liquid droplets in steam (C 1). At high void fractions it is expected that the second situation is approached. In fact, it is not correct to extrapolate the Maxwell curve to high void fractions, just as it is not correct to extrapolate the second curve to the region of very low void fractions. Both curves represent theoretical, extreme

situations and practical conditions will lie in between. This indeed is reflected by the new curves.

The afore-mentioned remarks tend to emphasise the necessity to calibrate the impedance gauges as far as possible in the test section itself. This can be realised by means of the gamma-ray technique. It is interesting to evaluate both methods in comparison with each other.

Characteristics of the gamma-ray method

(1) easy interpolation between the limits of zero and 100% void, which makes a calibration over a long range redundant.
(2) It involves a long measuring period in view of the necessary counting time of the pulses. This objection can partly be overcome by using a strong source (S 1)(safety problems).
(3) item (2) leads to the impossibility to use it for dynamic measurements, unless a strong source is applied (S 1).
(4) Although principally possible it is very laborious to take measurements at different locations along the channel axis.
(5) The apparatus needs permanent care and control owing to its great complexity.

Characteristics of the impedance method

(1) The calibration is quite difficult and must be performed in the test section itself.
(2) The measuring time is zero owing to the electrical nature of the method.
(3) It lends itself admirably to dynamic measurements.
(4) The gauges are of a simple construction and may easily be built into the boiling channel.
(5) The apparatus is easily manageable and quite reliable.
(6) The shape of the cross-section of the channel is often too complicated for a suitable gauge construction. Even an ordinary cylindrical cross-section is difficult to handle (A 1, Å 1).

Other devices as, for instance, the dilatation technique (P 2), the electrical probe (L 3, O 1) and the isokinetic probe (A 3) have been omitted because the first does not detect local void fractions and the latter two do not measure average values.

The experiences of the author himself as well as of the investigators referred to make it very hazardous to guarantee the accuracy of the absolute void values. This was one of the motives to lay the emphasis of the experiments on qualitative and relative measurements. However, reasonable confidence can still be put in the absolute magnitude of the void fractions, which is sustained in (B 4), where it is noticed that the void fractions measured by Spigt exceed by about 15% (absolute) the predictions of the models studied in (B 4), whereas the predictions for experiments of other investigators fit quite satisfactorily. The difference need not, therefore, be imputed to a deficiency of the model.

The apparatus used is practically identical to that applied by Spigt (S 2). The gauges consist of four interconnected silver plates in a Teflon housing. Along the length of the shroud nine gauges have been mounted at equal distances from each other. The lowest gauge, placed in the non-heated part, detects the instantaneous conductivity of the water and acts as the reference gauge.

The shroud was given the same potential as the silver plates, thus eliminating edge effects in axial direction. The voltage between the electrodes had a frequency of 3000 Hz.

Burn-out detector

In order to avoid burn-out of the heating element, a burn-out detector was applied as a safety device. The resistances of the upper and lower halves of the heating element formed the variable branch of a Wheatstone bridge. When the difference of the resistance values between the two halves exceeded a preset value, the power was switched off with a time lapse of about 100 msec. In view of the relatively large heat capacity of the heating element this period was sufficiently short to guarantee a perfectly safe operation of the loop.

Slow variations in the out-of-balance voltage, caused, for instance, by an increase in heating power, were controlled manually.
In practice the heating power was always switched back just before the burn-out detector would come into action since it took about two hours to reach the operating condition after switching off power.

Recorders

For temperature readings under steady-state conditions ordinary mV-recorders were available.
For recording purposes under dynamic conditions the following apparatus have been used.
A U.V. recorder enabled important signals to be visualised continuously on photographic paper.

A 12-channel FM-magnetic tape recorder, Ampax manufacture, was applied to store the signals in view of the off-line analysis afterwards. Owing to the limited number of available preamplifiers, only six channels could be used at the same time. The play-back as well as the recording speed were chosen $7\frac{1}{2}$ ins. per sec.

2.3. Analysing Equipment

Transfer function analyser

The name does not really cover the properties of the apparatus. This special purpose analogue computer was purchased in two parts. The first part computed transfer functions between an internally generated sinusoidal perturbing input signal and a responding output-signal. It implicated that the computer could only be used on-line with the experimental rig. The second part, when coupled with the first part, was capable of computing point-to-point transfer functions between two arbitrary output signals in response to a transient or sinusoidal perturbation of an adequate input signal, and to compute power spectra of two arbitrary off-line signals.
The ability to compute related quantities between two off-line signals led to the application of only the second feature of the computer. All signals which were estimated to be of interest in order

to determine the characteristics of the boiling system were recorded on the magnetic tape and analysed afterwards. For this reason a short description is given of only the computation process concerned with the power spectra. The block diagram is given in Fig. 2.7.

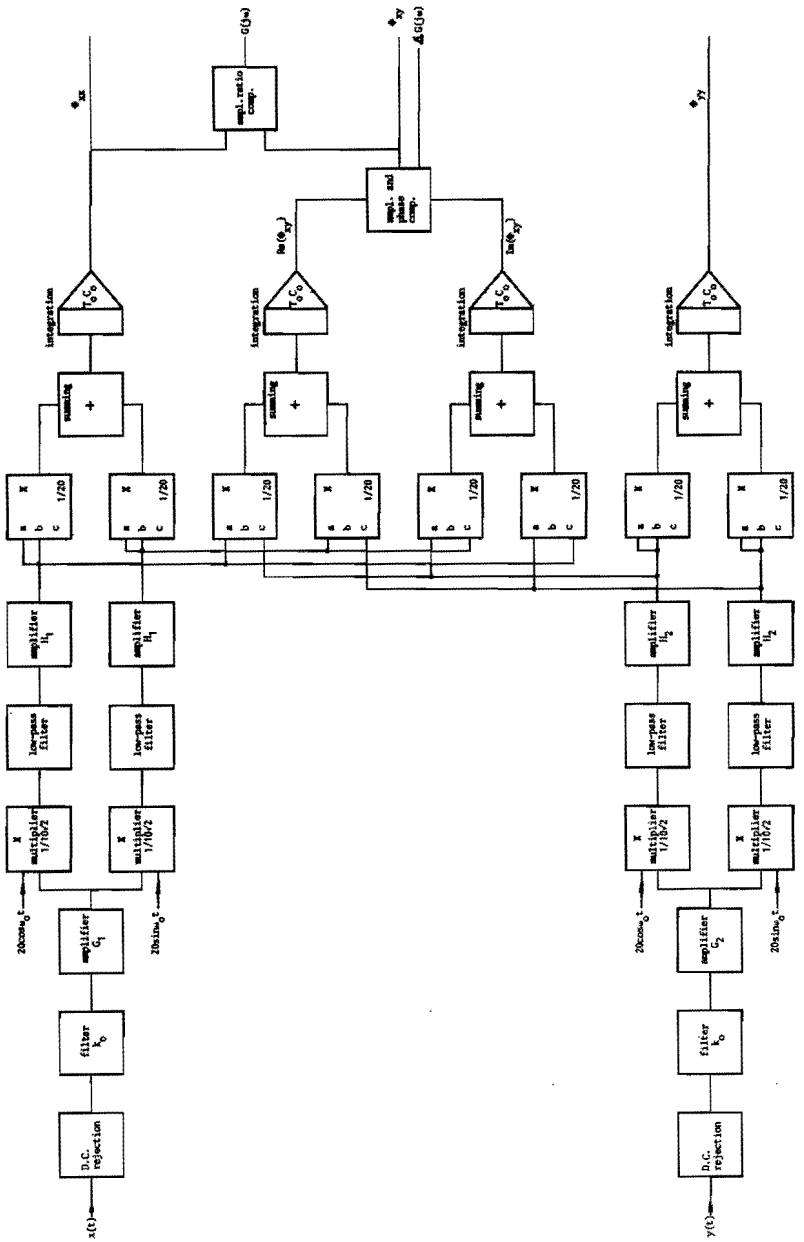

2.7. Block diagram of the Transfer Function Analyser

The power spectrum of a signal is a measure for its energy content at a certain frequency ω within a bandwidth $\pm \Delta\omega$. The relationship between two signals is determined by the cross-spectrum. It is superfluous to mention in detail the sense and derivation of power and cross-spectra. The mathematical background is sufficiently known (T 1) and the technique has been applied by many investigators (M 3, B 5, S 2).

After rejection of the DC-component from the signal under consideration, each signal passes through a bandpass filter in order to improve the signal-to-noise ratio. The signal is amplified with the aim to start from a reasonable input voltage by which accuracy is increased. The signal is fed into the multipliers to be multiplied by the internally generated sinusoidal signals of an adjusted frequency $\sin \omega_o t$ and $\cos \omega_o t$ respectively. The doubled number of signals pass subsequently through the low-pass filter, that cuts off at the adjusted frequencies $\omega_o + \Delta\omega$ and $\omega_o - \Delta\omega$, and again through an amplifier, in order to obtain proper output values of the integrators. Starting from the original signals:

$$x(t) = \sum_{i=1}^{n} a_i \sin(\omega_i t + \phi_{\omega ix}) \qquad \text{eq. 2.4.}$$

$$y(t) = \sum_{i=1}^{n} b_i \sin(\omega_i t + \phi_{\omega iy}), \qquad \text{eq. 2.5.}$$

where $\phi_{\omega ix}$ and $\phi_{\omega iy}$ represent the phase differences with respect to the multiplicative signals $\sin \omega_o t$ and $\cos \omega_o t$, the signals after the above operations can be represented by:

$$X_1(t) = k_o G_1 H_1 \sqrt{2}.x(t)\cos \omega_o t = k_o G_1 H_1 \sqrt{2}. \sum_{i=1}^{n} a_i \sin(\omega_i t + \phi_{\omega ix})\cos \omega_o t =$$

$$= k_o G_1 H_1 \sqrt{2}. \sum_{i=1}^{n} \left[a_i \sin\{(\omega_i - \omega_o)t + \phi_{\omega ix}\} + a_i \sin\{(\omega_i + \omega_o)t + \phi_{\omega ix}\} \right]$$

eq. 2.6.

and after the low-pass filter

$$X_1(t)=k_oG_1H_1.\tfrac{1}{2}\sqrt{2}\sum_{\omega_i=\omega_o-\Delta\omega}^{\omega_i=\omega_o+\Delta\omega} a_i \sin\{(\omega_i-\omega_o)t+\phi_{\omega ix}\} \qquad \text{eq. 2.7.}$$

$$X_2(t)=k_oG_1H_1.\tfrac{1}{2}\sqrt{2}\sum_{\omega_i=\omega_o-\Delta\omega}^{\omega_i=\omega_o+\Delta\omega} a_i \cos\{(\omega_i-\omega_o)t+\phi_{\omega ix}\} \qquad \text{eq. 2.8.}$$

$$Y_1(t)=k_oG_2H_2.\tfrac{1}{2}\sqrt{2}\sum_{\omega_i=\omega_o-\Delta\omega}^{\omega_i=\omega_o+\Delta\omega} b_i \sin\{(\omega_i-\omega_o)t+\phi_{\omega iy}\} \qquad \text{eq. 2.9.}$$

$$Y_2(t)=k_oG_2H_2.\tfrac{1}{2}\sqrt{2}.\sum_{\omega_i=\omega_o-\Delta\omega}^{\omega_i=\omega_o+\Delta\omega} b_i \cos\{(\omega_i-\omega_o)t+\phi_{\omega iy}\} \qquad \text{eq. 2.10.}$$

The amplification constants correspond to the blocks in the illustration. The signals then become squared or multiplied crosswise, added up two and two, and fed into integrators that ultimately provide the desired quantities Φ_{xx}, Φ_{yy}, $Re(\Phi_{xy})$, $I_m(\Phi_{xy})$ representing the power spectrum of the x-signal, that of the y-signal, the real vector of the cross-spectrum, and its imaginary vector, respectively. The results read:

$$\Phi_{xx} = 2(k_oG_1H_1)^2\, T_oC_o(a_{rms})^2 \qquad \text{eq. 2.11.}$$

$$\Phi_{yy} = 2(k_oG_2H_2)^2\, T_oC_o(b_{rms})^2 \qquad \text{eq. 2.12.}$$

$$Re(\Phi_{xy}) = k_o^2G_1G_2H_1H_2\, a_{rms}.\, b_{rms}.T_oC_o \cos(\phi_x-\phi_y) \qquad \text{eq. 2.13.}$$

$$I_m(\Phi_{xy}) = k_o^2G_1G_2H_1H_2\, a_{rms}.\, b_{rms}.T_oC_o \sin(\phi_x-\phi_y) \qquad \text{eq. 2.14.}$$

T_o and C_o represent the integration time and the integration constant respectively. The phase angle and the cross-spectrum Φ_{xy} are computed from the vectors $Re(\Phi_{xy})$ and $I_m(\Phi_{xy})$. The amplitude ratio Φ_{xy}/Φ_{xx} defines the gain of the transfer function and is expressed in decibels.

P r o c e d u r e

The output of two particular signals of the magnetic tape recorder were connected to the x and y inputs of the TFA. The proper values of amplifications, analysis frequency and other constants of importance were adjusted and the analysis started. In order to obtain reproducible values, taking into account the stochastic character of the signals, the period of each measuring point was taken to be 100 seconds. In view of improving accuracy, each analysis was repeated twice on the same part of the signal and the results were averaged. The reproducibility of the analysed transfer function measurements was good enough to confine ourselves to only two analyses at a time.

Before starting the analysis of a series of measurements it was first investigated at what frequency, viz. the resonance frequency, the power spectrum was maximum. Owing to the bandwidth of $2\Delta\omega$ it may be expected that this maximum does not occur at one distinct frequency on both sides of which the power spectrum would drop suddenly to zero. Another reason for the existence of a finite width of the band of power spectra as a function of the frequency may lie in the low inconstancy of the resonance frequency. It varies somewhat with time. The slope of the bandcurve was less steep for noisy signals than for steady oscillating signals. The adjusted peak frequency was kept constant during the analysis of signals belonging together at one condition. It proved a weak function of heating power for some conditions.

Every series of measurements was preceded by the recording of a sinusoidal calibration signal with known amplitude and frequency. It enabled the ultimate results of power spectra to be reduced to effective values of voltage and consequently of the physical quantities.

It is quite difficult to estimate the accuracy of the computations on account of the stochastic character of the signals. In order to give an impression of the reproducibility, a random page of results has been added in Appendix A. Especially the calibrating signal gives results having an accuracy of the amplitude of $\pm$ 2% and of

the phase angle of $\pm$ 0.1°. The accuracy of the results obtained from the measuring signals can be deduced from the illustrations, which show well-fitting curves through the points.

Computers

The Pace Analogue Computer has a capacity of 110 amplifiers and 25 multipliers.
The digital computer, available at the Technological University, was an Electrologica X-8.

For the purpose of reducing the data obtained from the steady-state measurements use was made of a simple computer program. The input data were the measured quantities of local void fraction and pressure drop, the pressure loss across the entrance of the channel, channel power and inlet temperature. Taking into account subcooled boiling, the program calculated the local values of the steam quality, slipfactor, slip-correlated parameters, parameters correlated to the pressure drop, steam and water velocities,and the residence times of water and steam phase.

The digital computer applied for the theoretical study was an IBM 360-50, placed at our disposal by the Roman Catholic University of Nijmegen.

For a limited number of time-consuming computations use was made of the IBM 360-65, available at the Technological University of Delft, which reduced the computation time to one fifth of the time required by the IBM 360-50.

3. STEADY STATE MEASUREMENTS

General procedure

A sequential summary is given of the necessary actions preceding the measurements. In order to be sure of constant water properties and to avoid corrosion, each daily series of experiments was started with a check on the electrical resistance of the demineralised water. The rig was filled and an optimal level adjusted in such a way that it was high enough to cause a sufficient slowing down of the waterflow, streaming upwards, in order to achieve good separation of water and steam and to avoid the presence of outlet restriction, and low enough to maintain a reasonable steam space, acting as a buffer for variations in the steam production. The level was kept constant in all the experiments. The power unit was switched on and a low power level was adjusted to prevent extreme stresses in the material when raising the temperature. After some hours of heating the water started to boil and the system was deaerated carefully by blowing off at a proper cold location in the condenser. This was repeated several times until no more air escaped from the rig. Still at low power the system was allowed to reach the desired pressure. Actually, it was the steam temperature, measured in the steam space, which was kept constant by testing it to a preset point. Then the lowest power was adjusted, where the heat losses were just in balance and a stable condition was attained.

The desired subcooling, defined by the difference between the temperature in the steam space and the inlet temperature of the channel was then adjusted. Before taking the first measurement, the experimental apparatus was checked on correct working. After reading the instruments that recorded the most interesting variables, the power was increased stepwise and a new condition was stabilised. The successive steps in power were chosen so as to be able to define the curves of the variables by a sufficient number of points. The

measurements were continued until oscillations started to occur or burn-out was encountered.
A new condition of subcooling or pressure was adjusted and the procedure was repeated.

3.1. Basic data

A survey of the measurements is given in Appendix B. The experiments have been carried out under system pressures of 15.5 and 30 atm, corresponding to saturation temperatures of 200°C and 234°C respectively. In both cases the influence of subcooling and of the shape of the heatflux were investigated.

U n i f o r m h e a t f l u x

Inlet Velocity

Fig. 3.1. shows the change of the inlet velocity as a function of heating power for a saturation temperature of 200°C and different subcoolings. Each curve has a maximum which moves to higher powers for increased values of subcooling. Similar results have been obtained by Becker and Spigt (B 6, S 2). The common explanation is

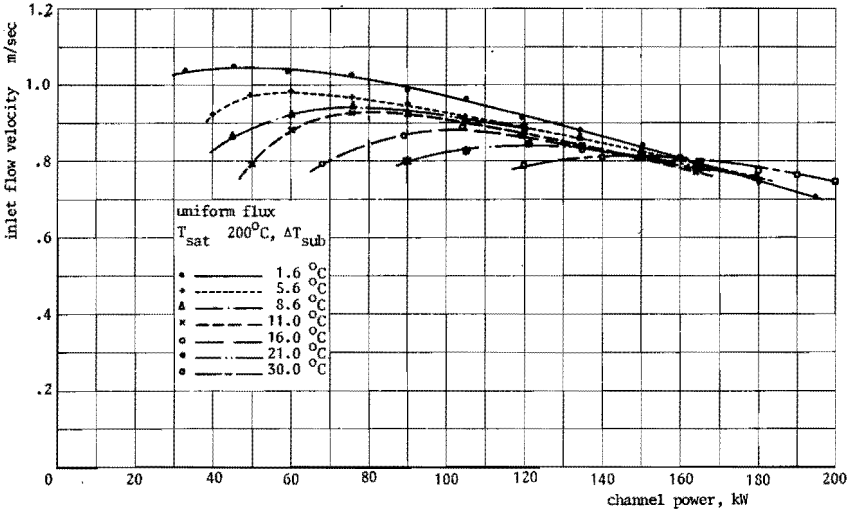

46 3.1. Inlet flow velocity versus channel power T_{sat} 200°C

given by considering the balance between driving head and total pressure drop across the channel. At low powers the driving head increases disproportionately to the pressure drop and beyond the maximum the reverse is true, causing the inlet velocity to drop continuously with power. Increasing the subcooling decreases the driving head and consequently reduces the inlet velocity. The maxima lower and move towards higher channel power. The curves intersect at 160 kW, where the inlet velocity appears to be independent of subcooling.

Generally, it can be concluded from the constant slope of the curves beyond the maximum that, when assuming the driving head to change linearly with void fraction, the sum of the pressure drops due to acceleration and friction also changes linearly with void fraction. The general trend remains the same at higher pressure (Fig. 3.2.). The only difference lies in the position of the lowest-subcooling curve with respect to the other curves, which does not give higher velocities than the others as it did at lower pressure.

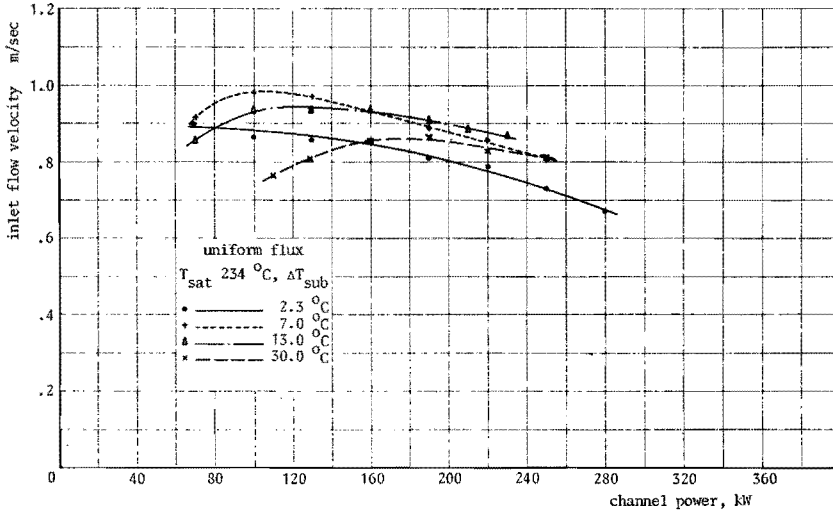

3.2. Inlet flow velocity versus channel power T_{sat} 234°C

Void fraction

The void fractions have been measured in the manner described in chapter 2.2. In the illustrations showing the void fraction as a function of the channel power, that void fraction is plotted which has been measured at position 2 (see Fig. 2.2.) being the upper position where the channel is heated and where calibration against the gamma-ray method was achieved.

For the condition of a saturation temperature of 200°C the exit void fraction (pos. 2) versus power has been plotted in Fig. 3.3.

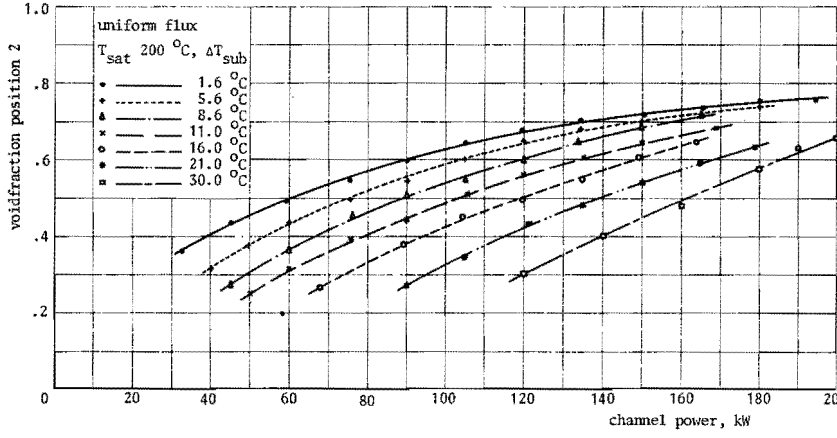

3.3. Exit void fraction versus channel power T_{sat} 200°C

for different values of inlet subcooling. The void fraction rises continuously with power, but the slope of the curves diminishes at higher powers. Subcooling reduces the void fraction considerably. When comparing figures 3.1. and 3.3. it appears that the maxima of the velocity curves correspond to constant values of the exit void, viz. 45%. For two values of subcooling, viz. 1.6°C and 11°C, considered to be representative of other values, the axial void distribution has been plotted for different values of channel power (Figs 3.4. and 3.5.). The curves run parallel to each other, the upper ones belonging to the higher powers. Near the bottom of the channel there is a rapid growth of void, visible from the steepness of the curves. The maximum void does not exceed 80%. Subcooling de-

creases the void as may be expected from the consideration that a substantial fraction of the power is used to raise the temperature of the water up to its saturation value.

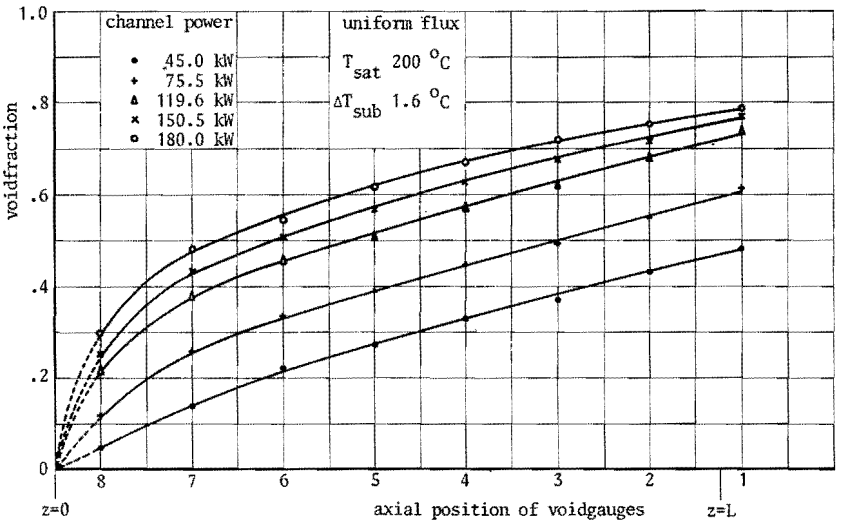

3.4. Axial void distributions T_{sat} 200°C, ΔT_{sub} 1.6°C

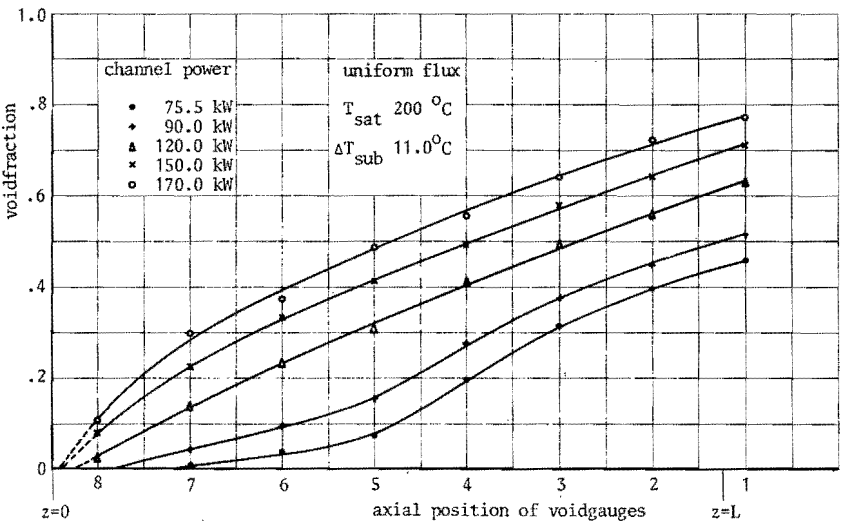

3.5. Axial void distributions T_{sat} 200°C, ΔT_{sub} 11.0°C

At an inlet subcooling of 11°C the curves for the higher powers are similar to those at 1.6°C subcooling. The other curves start with a concave part, which must be attributed to the subcooling, which consumes here a relatively large proportion of the available power. At position 8 it is sometimes even not possible to detect void.

Increase of the pressure results in substantially lower values of

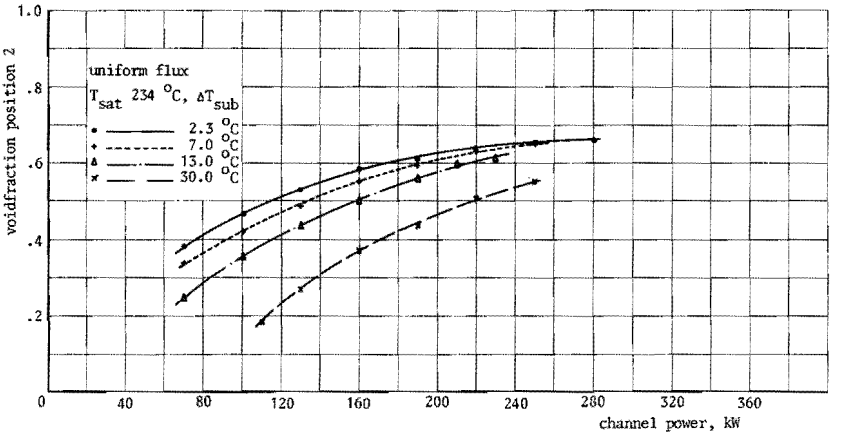

3.6. Exit void fraction versus channel power T_{sat} 234°C

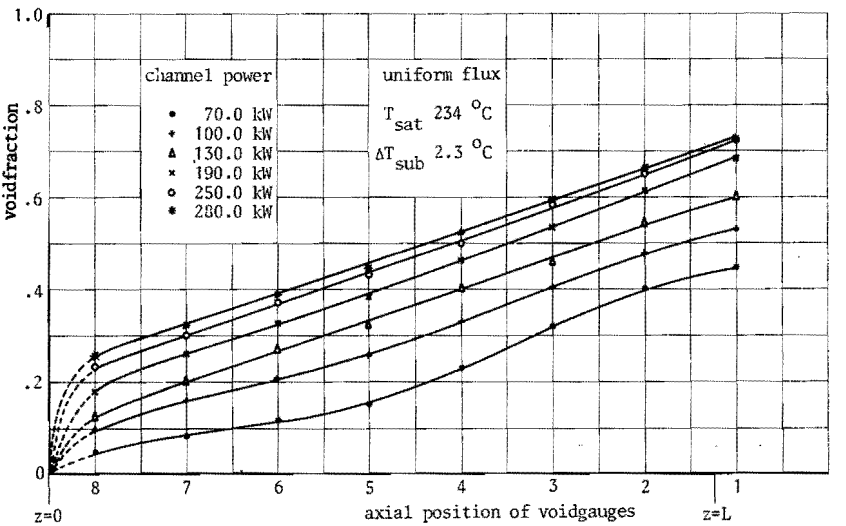

 3.7. Axial void distributions T_{sat} 234°C, ΔT_{sub} 2.3°C

void fraction (Fig. 3.6.); the difference is 15% at most. For the rest the curves are very similar. The curves of the axial void distribution are nearer to linear than at the lower pressure (Fig. 3.7.). A similar trend was measured by St. Pierre (S 1).

Pressure Drop

The pressure differences as detected by the pressure tappings have been plotted first as functions of the axial distance. These pressure tappings were fixed to the shroud between the void gauges (see Fig. 2.2.). In order to know the pressure drops at the posi-

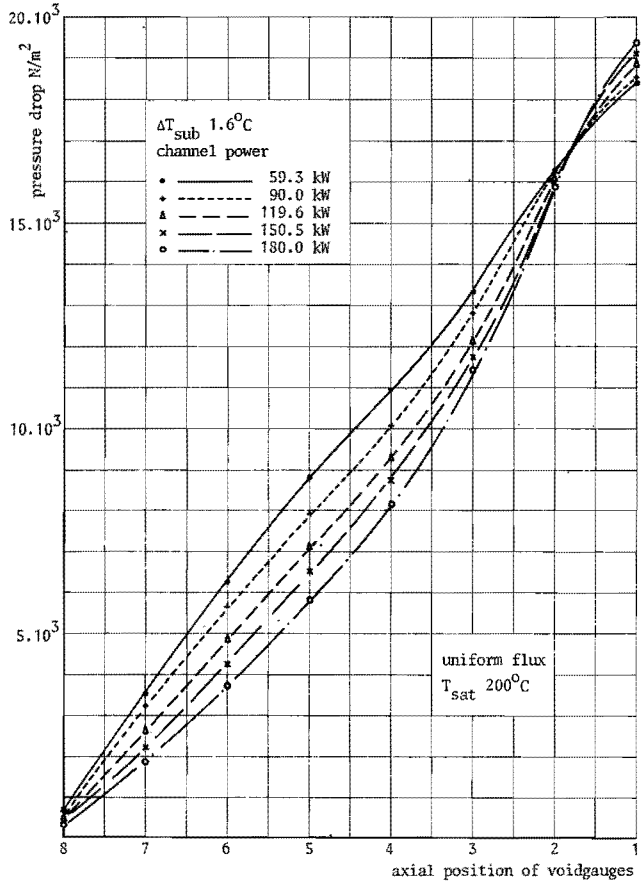

3.8. Axial pressure drop distribution T_{sat} 200°C, ΔT_{sub} 1.6°C

tions of the void gauges themselves the pressure differences were interpolated from the basis curve. For the condition of 200°C saturation temperature and lowest subcooling the pressure differences have been given in Fig. 3.8. The intersection with the ordinate shows the pressure loss across the inlet, being a function of the inlet velocity. Although the pressure loss from bottom to top ought to be constant, there still remains a small unexplained deviation at the upper position.

At the lowest channel power the curve is almost linear but the higher channel powers indicate a lower pressure drop along the lower half of the channel and a higher one along the upper half. The curves do not have a very pronounced shape, the pressure decreases rather continuously with increasing axial distance from the bottom.

S i n e - s h a p e d h e a t f l u x

Inlet velocity

The general characteristics of the curves are essentially similar to those of the uniform heatflux (Fig. 3.9.).+

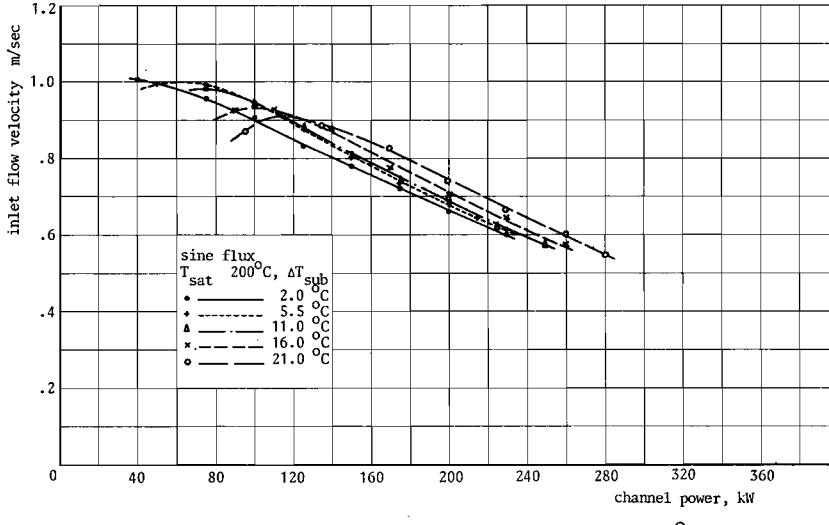

3.9. Inlet flow velocity versus channel power T_{sat} 200°C

+The reader's attention is drawn to the different scale of the abscissa.

However, gradual differences can be observed. The position of the maxima with respect to the abscissa and the slope of the curves are almost identical, but the curves have moved with respect to the ordinate in such a way that the curves are nearer together. The result is that the single crossing points has disappeared and is replaced by a number of intersections. The mutual difference between the subcooling curves has become smaller in the region of the low channel powers and larger in that of higher powers (cf. Fig. 3.10.). Another distinction is the ability to extend the curves to considerably higher powers. Anticipating chapter 4, this already indicates that the region of stable operation has expanded.

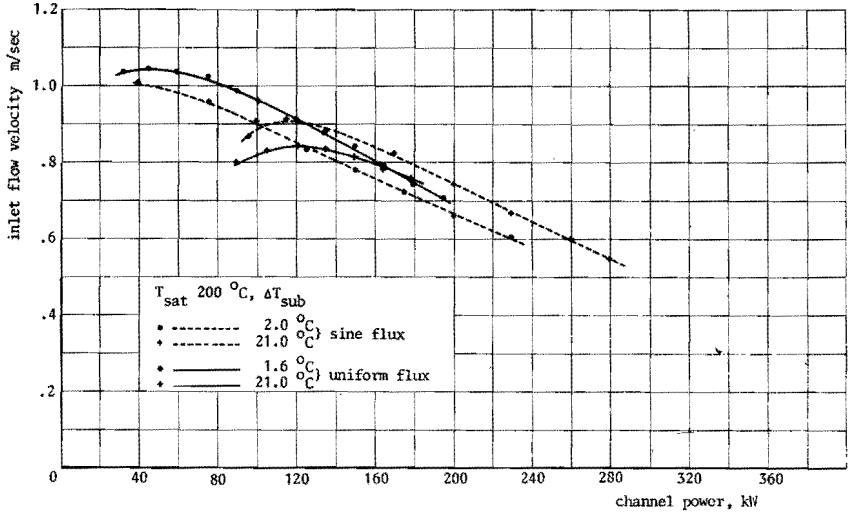

3.10. Inlet flow velocity versus channel power T_{sat} 200°C, ΔT_{sub} 2.0-1.6°C and 21°C

Void fraction

If the differences in the inlet velocity are not significant at all, the similitude of the upper void fractions is really striking, also at relatively high values of subcooling (Figs 3.11. and 3.12.). The differences could even be estimated to lie within the measuring accuracy if the curves of the void fraction versus axial distance did not affirm them (Fig. 3.13.). Especially in the lower part of

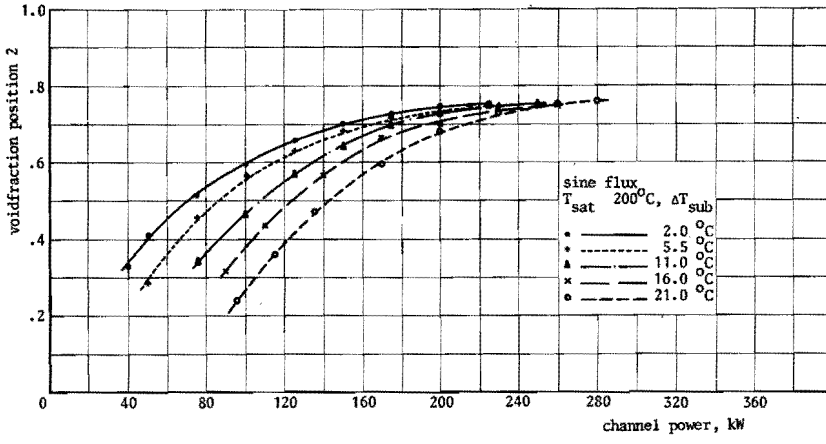

3.11. Exit void fraction versus channel power T_{sat} 200°C

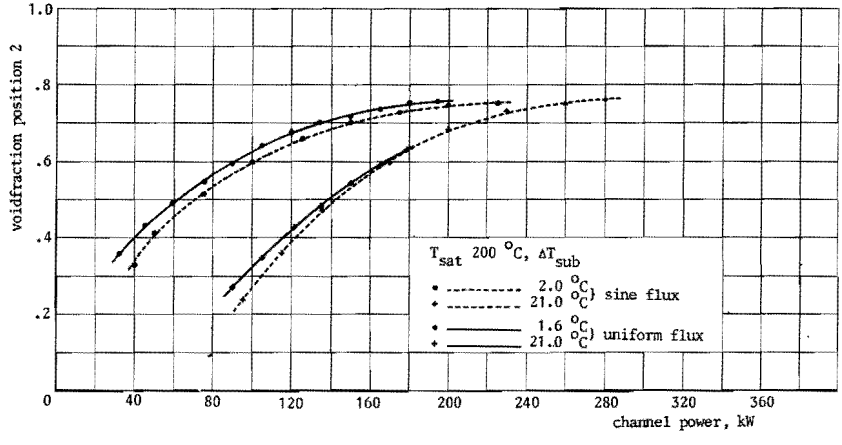

3.12. Exit void fraction versus channel power T_{sat} 200°C, ΔT_{sub} 2.0-1.6°C and 21°C

the channel the void fraction is much smaller, but when passing the centre of the channel, the curves of uniform and sine-shaped heatflux start to approach each other. This holds for both low and moderate subcoolings (Fig. 3.14.). It is evident that here the low heatflux near the bottom of the channel plays a dominant role. It suppresses the growth of the void fraction and shifts the position

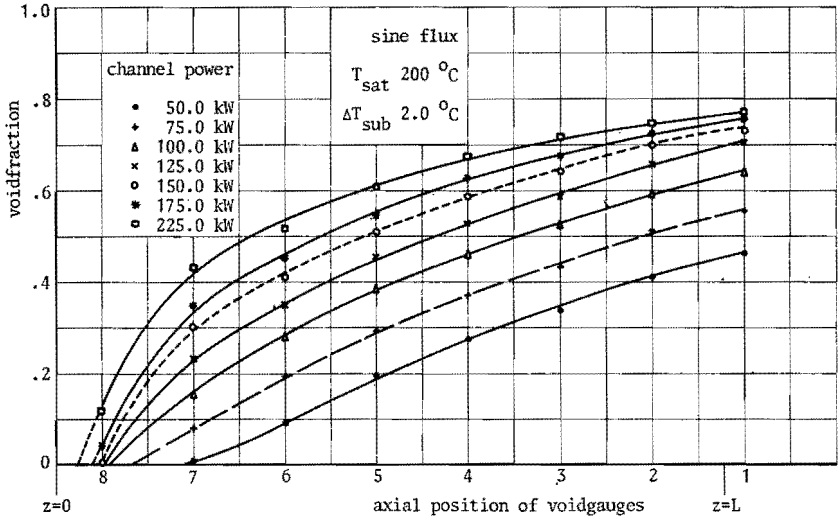

3.13. Axial void distributions T_{sat} 200°C, ΔT_{sub} 2.0°C

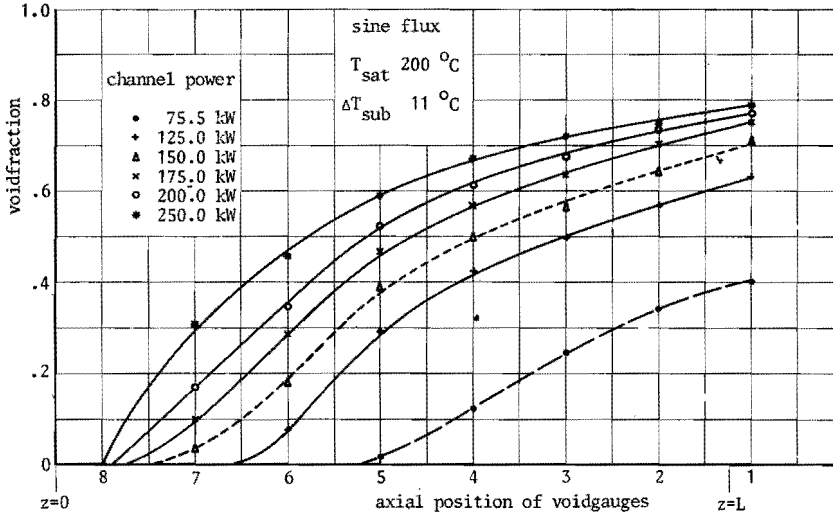

3.14. Axial void distributions T_{sat} 200°C, ΔT_{sub} 11.0°C

of the departure of nucleate boiling in an upward direction. Even at an inlet subcooling of 2°C the gauge number 8 did not detect void at the lowest channel powers.

Pressure drop

The figure of the axial distribution of the pressure drop (Fig. 3.15.) does not reveal special characteristics. The pressure drop along the lower half of the channel seems to be a little lower than for the uniform flux and that along the upper half of the channel consequently higher.

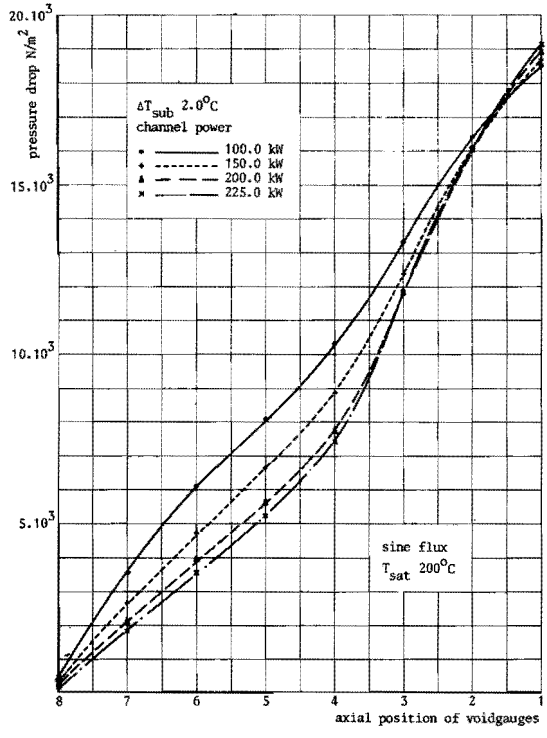

3.15. Axial pressure drop distribution T_{sat} 200°C, ΔT_{sub} 2.0°C

Effect of pressure

What has been remarked concerning the effect of the sine-shaped heatflux on inlet velocity and void fraction at 200°C saturation temperature, can be repeated for a saturation temperature of 234°C (Figs 3.16., 3.17., 3.18., 3.19.). An exception, however, has to be made with respect to the form of the curve of the axial void distribution (Fig. 3.20.). At low powers the attitude is similar

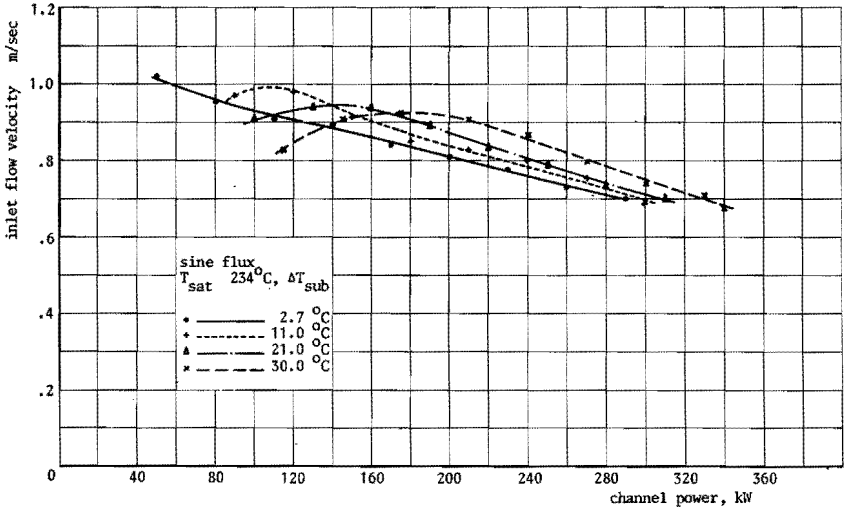

3.16. Inlet flow velocity versus channel power T_{sat} 234°C

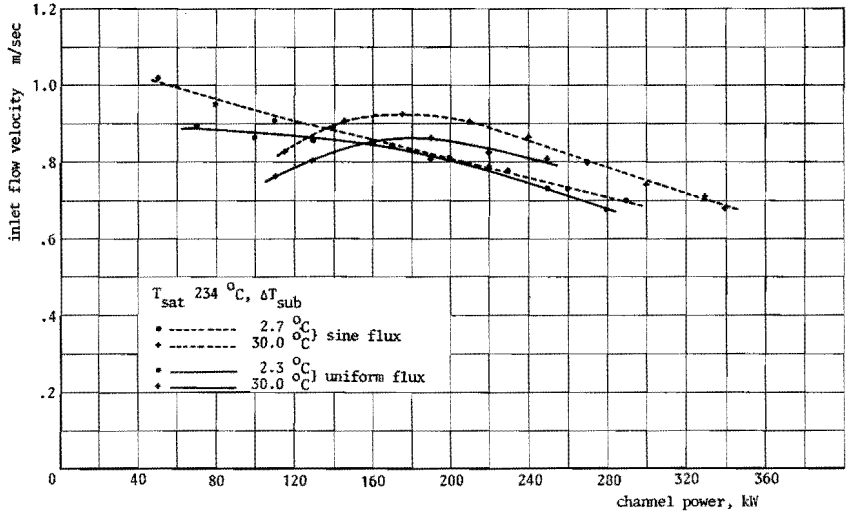

3.17. Inlet flow velocity versus channel power T_{sat} 234°C, ΔT_{sub} 2.7-2.3°C and 30°C

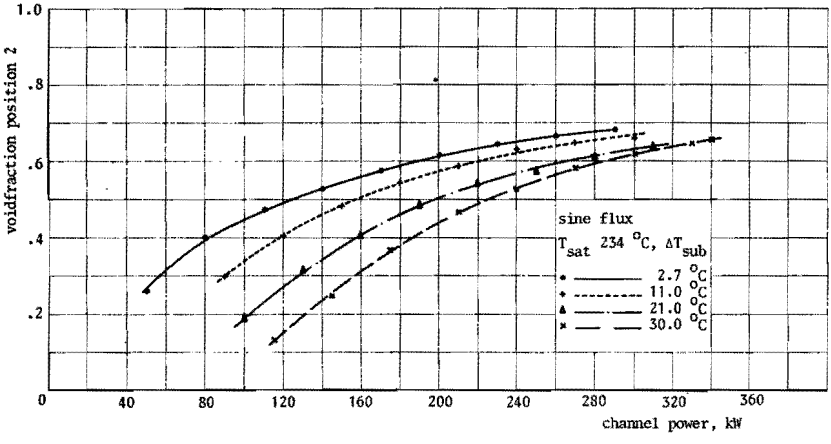

3.18. Exit void fraction versus channel power T_{sat} 234°C

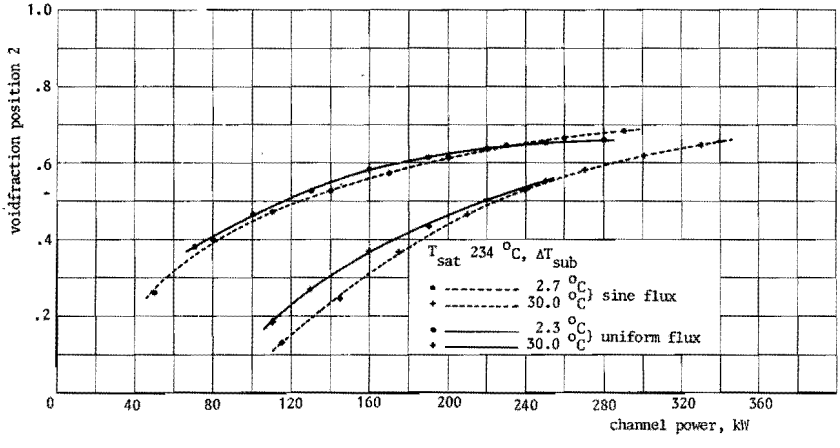

3.19. Exit void fraction versus channel power T_{sat} 234°C, ΔT_{sub} 2.7-2.3°C and 30°C

but at higher power values the curves are very equal to the corresponding curves of the uniform flux. The suppressing effect of the low heatflux on void generation near the bottom of the channel seems to be absent here.

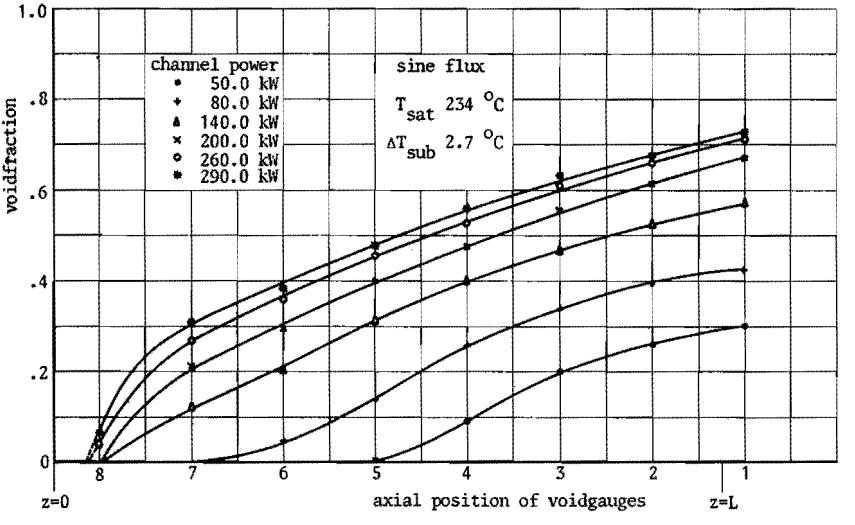

3.20. Axial void distributions T_{sat} 234°C, ΔT_{sub} 2.7°C

Conclusive remarks

The shape of the heatflux has no significant influence on the inlet velocity nor on the outlet void fraction. Both appear to be only functions of the total channel power. The void in the lower part is, however, reduced substantially. That this does not induce a change of the inlet velocity can be explained by assuming that the change in driving head is just balanced by the change in the pressure loss due to friction.

3.2. Reduction of the steady-state data

S l i p f a c t o r

When analysing experimental results it is often a serious question how to present the data. Plotting the rough data frequently shows inadmissible scattering of points. The cause may lie in the parameter itself, in a less proper choice of the parameter on which it is thought to depend or in a combination of both. It may be advisable to conceive a characteristic number of which the measured quantity forms an integrant part, but which contains other variables

too. This question arises in particular with regard to the slip correlation. When the void fraction has been measured and the steam quality has been calculated from a heat balance, the slipfactor can easily be determined. In the present case this has been done by applying the special computer program described in chapter 2. However, when plotting the slipfactor versus void fraction the scatter of points is too large for decent, usable curves to be drawn. Fortunately, two studies by Bankoff and Zuber (B 2, Z 1) are available that offer a possibility to plot the slipfactor, or rather a slip-dependent quantity, more successfully. These two authors are particularly mentioned because they base their study of the functional relationship between the steam and water phase on a physical background.

The slipfactor is defined as the ratio of the average steam flow velocity to the average liquid flow velocity. The denomination itself indicates the original idea of the difference in velocities to be attributed to a real slip between gas and liquid.

It was Bankoff (B 2) who developed the conception of void and velocity profiles. Slip is not the relative motion of separate bubbles with respect to the surrounding liquid. On the contrary, the local velocities of liquid and steam are presumed to be equal. The void is thought to be concentrated in the centre of the boiling channel where a higher flow velocity exists than near the channel wall. Because the slippage at any point is considered to be negligible, the mixture may be regarded as single fluid whose density is a function of radial position. An examination of the radial distribution function for voids must take into account buoyancy, and inertial and surface tension forces. From the derivation the ultimate expression for the slipfactor is

$$S = \frac{1-\alpha}{K-\alpha} \quad . \qquad \text{eq. 3.1.}$$

The flow parameter K was derived from assuming power law distributions for both the velocity and the void fraction:

$$u^+ = 1^{1/m} \qquad \text{eq. 3.2.}$$

and

$$\alpha^+ = 1^{1/n} \qquad \text{eq. 3.3.}$$

where

u^+ = the velocity of two-phase mixture at distance y from the wall / the velocity of two-phase mixture at tube centre line

α^+ = void fraction at distance y from the wall / void fraction at tube centre line

1 = dimensionless distance from the wall.

The derivation results in $K = \frac{2(m+n+mn)(m+n+2mn)}{(n+1)(2n+1)(m+1)(2m+1)}$ eq. 3.4.

Because of insufficient experimental information concerning values of m and n, an expression for K was based on a number of experimental data, viz.

$$K = 0.71 + 0.0001.\ p \qquad \text{eq. 3.5.}$$

where p is the pressure in psi. For an assumed value of K = 0.89 good agreement was reported with the correlation of Martinelli-Nelson over a pressure range of 100-2500 psia.

Because of the singularity of equation 3.1. at $\alpha = K$, Jones (J 2) modified it by adding a term to the denominator, giving

$$S = \frac{1-\alpha}{K-\alpha+(1-K)\alpha^r} \qquad \text{eq. 3.6.}$$

where r is the quadratic function of pressure:

$$r = 3.33 + 0.18.\ \frac{p}{1000} + 0.46\ .\ \left(\frac{p}{1000}\right)^2 \qquad \text{eq. 3.7.}$$

The empirical correlation (3.5.) for the flow parameter K was also slightly modified.

$$K = 0.71 + \frac{0.29}{0.32062}\ .\ \frac{p}{10{,}000} \qquad \text{eq. 3.8.}$$

It was Zuber's intention to provide a general method which could be used either for predicting the volumetric concentration or for analysing and interpreting experimental data. The analysis takes into account the effect of the non-uniform flow and concentration distributions of both phases across the duct as well as the effect of the local relative velocity between the two phases. In analogy with the kinetic theory of gases, volumetric densities and a drift velocity of the gas-phase with respect to the liquid phase have been defined. By making use of the continuity equations for the two phases, the following equations were developed, and the results expressed in terms of average volumetric flux densities:

$$\langle w_2 \rangle = \langle w_m \alpha \rangle + \langle V_{v_2} \alpha \rangle \qquad \text{eq. 3.9.}$$

$$\langle w_1 \rangle = \langle w_m (1-\alpha) \rangle + \langle V_{v_1} (1-\alpha) \rangle \qquad \text{eq. 3.10.}$$

Where w_2 represents the volumetric flux density of the gas phase,
w_1 that of the liquid phase,
w_m the volumetric flux density of the mixture,
α the volumetric concentration,
V_{v_2} the drift velocity of the gas phase and
V_{v_1} that of the liquid phase with respect to the volumetric flux density of the mixture.

Then a parameter C_o is introduced defined by

$$C_o = \frac{\langle w_m \alpha \rangle}{\langle w_m \rangle \langle \alpha \rangle} . \qquad \text{eq. 3.11.}$$

This quantity substituted in equation 3.9. results in

$$\frac{\langle w_2 \rangle}{\langle \alpha \rangle} = C_o \langle w_m \rangle + \frac{\langle \alpha V_{v_2} \rangle}{\langle \alpha \rangle} \qquad \text{eq. 3.12.}$$

The effect of the non-uniform flow and concentration profiles is taken into account by the first term on the right-hand side, whereas the second term on the right-hand side is the weighted average

drift velocity of the gas phase. This term accounts for the effect of the local relative velocity and of the concentration profile. Upon rearranging equation 3.12. the average volumetric concentration in a two-phase mixture is to be calculated from:

$$\langle\alpha\rangle = \frac{\langle w_2 \rangle}{C_o \langle w_m \rangle + \frac{\langle \alpha V_{v_2} \rangle}{\langle\alpha\rangle}} \qquad \text{eq. 3.13.}$$

For the term $\frac{\langle \alpha V_{v_2} \rangle}{\langle\alpha\rangle}$ in the denominator, which represents the average drift-velocity, expressions are given in case of slugflow and churn-turbulent bubbly regime. Equation 3.13., when written in usual experimental values reads:

$$\alpha = \frac{x \cdot \frac{\rho_w}{\rho_s} \cdot v_{in}}{C_o \{ x \frac{\rho_w}{\rho_s} + (1-x) \} v_{in} + \text{drift velocity}} \qquad \text{eq. 3.14.}$$

This equation defines the functional relationship between void fraction and steam quality. Although Zuber avoids the use of the term slipfactor, this function really represents the slip correlation. When the drift velocity is implied to be zero, the expression reduces to

$$S = \frac{1 - \alpha}{\frac{1}{C_o} - \alpha},$$

quite similar to the correlation by Bankoff, where $\frac{1}{C_o} = K$. The value of C_o depends on the flow and concentration profiles, and for established profiles it ranges from about $C_o = 1.5$ to $C_o = 1.0$. The first figure corresponds to pronounced parabolic profiles and the second to flat profiles. In most cases the value of C_o is close to 1.2. From the experiment; C_o can be determined by plotting the term

$$(x \frac{\rho_w}{\rho_s} + 1 - x) v_{in} \text{ versus } \frac{x}{\alpha} \cdot \frac{\rho_w}{\rho_s} \cdot v_{in}$$

According to Zuber there must exist a linear relation between these two quantities - provided the profiles are established - the slope of the straight line giving the value of C_o. The intersection of this line with the ordinate represents the value of the drift velocity. Based upon these two theories, the slipfactor is represented in K and α co-ordinates according to Bankoff, and in the co-ordinates defined heretofore according to Zuber. Figures 3.21. and 3.22. with Zuber co-ordinates show a considerable scatter of points which renders difficult the drawing of a straight line through them. A line can be drawn under different slopes while still passing through the points in an acceptable way. At low values of the abscissa parameter the line bends downwards, indicating the presence of an unestablished profile. It is clear that this occurs in the region of subcooled boiling. The slope is practically independent of the

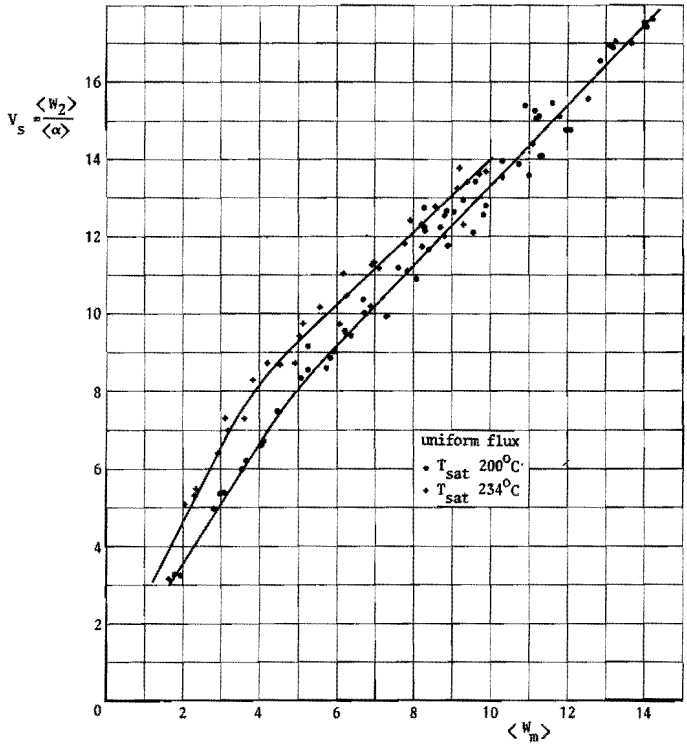

64 3.21. Void parameters defined by Zuber (Z 1) T_{sat} 200°C and 234°C

flux shape and its tangent is about one, which points to a flat void profile. In the case of the sine-shaped heatflux, the drift velocity is a little higher than for the uniform heatflux. The same holds for higher pressures.

Figures 3.23. and 3.24. plotted in the K-α plane, show much less scattering, especially at void fractions above 45%. At low void fractions the values of K have been omitted, because of the large scattering due to the presence of subcooled boiling. The void fraction in that region has been measured correctly but in order to calculate the steam quality, the assumption of the heat distribution parameter κ (see chapter 5) is necessary, and this results in poor values of the slipfactor. The lines have been extrapolated to the ordinate in view of the usability in the mathematical model.

It is remarkable that in the region of subcooled boiling, plotting of K shows unadmissible scattering, whereas the co-ordinates of Zuber allow the drawing of an acceptable curve. It is stated that

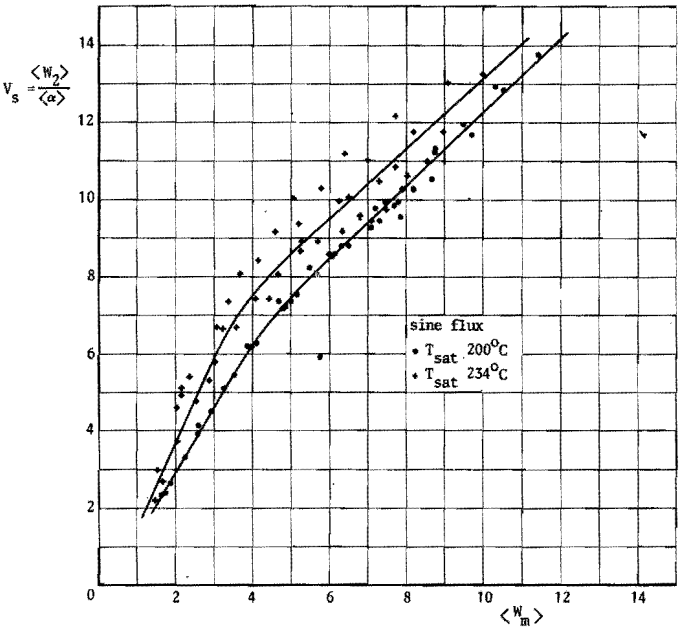

3.22. Void parameters defined by Zuber (Z 1) T_{sat} 200°C and 234°C

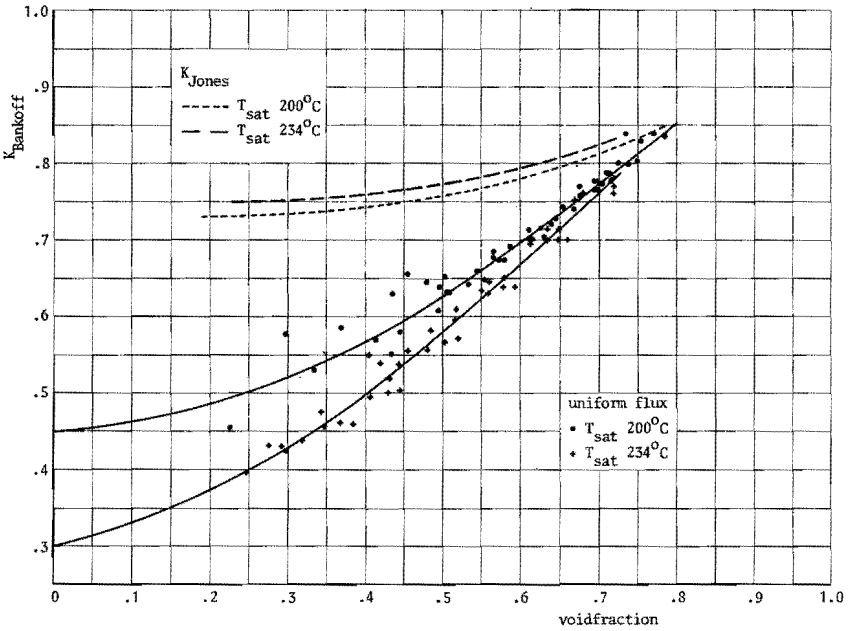

3.23. Void parameters based on study by Bankoff (B 2)
T_{sat} 200°C and 234°C

whatever model of subcooled boiling is used, the calculated values of steam quality are rather arbitrary. That a certain scattering is present in representations of related quantities is, therefore, comprehensible. When looking at the quantities suggested by Zuber for plotting void fraction and steam quality, it appears that both are linear with steam quality x, provided x is small compared to one,

reading $\frac{1}{\alpha}$. $(x \frac{\rho_w}{\rho_s})$ and $x \frac{\rho_w}{\rho_s} + 1$.

When plotted in combination, the sensitivity of the curve to steam quality is poor.
The value of K is far from constant. In figures 3.23. and 3.24. the parameter K derived from the expression by Jones has been plotted too. K_{Jones} = K eq. 3.8. +(1- K eq. 3.8.)α^r. There is only good agreement at the highest values of the void fraction, corresponding

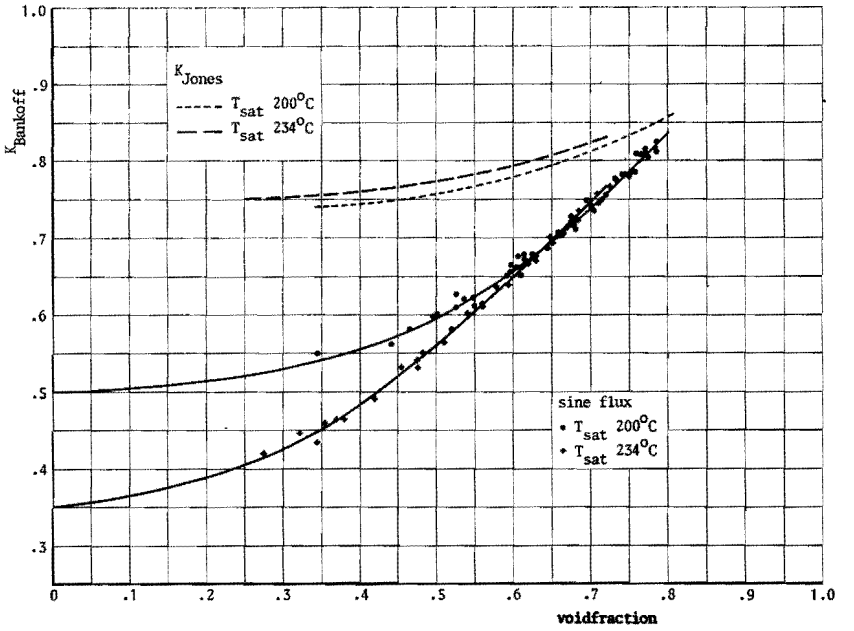

3.24. Void parameters based on study by Bankoff (B 2)
T_{sat} 200°C and 234°C

to conditions at the outlet of the channel. For lower void fractions the value of K is consistently too high, indicating low slipfactors.

Although Bankoff as well as Jones suggests the value of K to be practically constant, the experimental verification indicates a close relation to the void fraction, which increases the variation of the magnitude of K. It may be that the K as plotted is not identical to the K as derived by Bankoff, and that other parameters also play a role in determining the slipfactor. This parameter, however, cannot be the drift velocity of Zuber. If that is taken into account, the slipfactor reads:

$$S = \frac{(1-\alpha)\ \{1+ \frac{\text{drift velocity}}{C_o(1-x)}\ \}}{\frac{1}{C_o} - \alpha} \quad .$$

The drift velocity term does not essentially contribute to the variation of the slipfactor but only to its magnitude. The close dependence of K on void fraction tends to the conclusion that either C_o is not constant in the measure as claimed by Zuber, or that the conception of C_o and the drift velocity are not sufficient to define the relationship between steam quality and void fraction. Also Nassos (N 1) supposed, on the ground of his measurements of propagation velocities, a void dependence of C_o.

Petrick (P 1) performed measurements of void and velocity profiles in a forced air-water flow, supplied with some experiments in a boiling water flow. He established values of m and n (eq. 3.2. and 3.3.) and ascertained a fair discrepancy between measured values of the slipfactor and values predicted by Bankoff. Petrick even concludes his statement by saying that the phase distributions did not appear to play a major part in establishing the relative velocity between phases. This is completely contradictory to the basic assumptions of Bankoff. Besides, Petrick found that several trends of the phase distribution data were contrary to what was predicted by the models of Bankoff and Zuber. He found, for instance, that in fully developed flow the void distribution became more skewed as the velocity was increased and quality decreased, whereas one would expect flat profiles.

Compared with the theory of Zuber, in some cases values of C_o were found to indicate a skewed profile, whereas really the profile was flatter.
Lottes (L 1) reports a study of Fohrman that supports the conception of Bankoff.

However the parameter K may be defined, it appears to be a valuable tool for plotting the slipfactor. Because of the small scatter of the points and the monotony of the function, the curves of K have been used in the theoretical model for predicting the slipfactor as a function of the void fraction.

Two-phase friction

 The improbable situation arises here that a correlation derived in

1948 by Martinelli and Nelson (M 1) is still in use by many investigators and even meets little competition from other correlations. Everybody is familiar with the objections against it, the most important being the fact that it was derived for an air-water instead of a two-phase boiling system, but it does not hamper the use of the correlation. Several attempts have been undertaken since then in order to provide a reliable correlation based upon modern experiments (B 9, T 2) but each one has its limitations. The intrinsic difficulty of two-phase friction is that its verification in an experimental rig is impossible. When local pressure losses are measured it is quite easy to subtract the pressure drop due to the decrease of density, provided the void fraction is known, but the remaining pressure difference consists of two terms, namely the pressure losses due to friction and those due to acceleration. The calculation of the acceleration loss can be based upon the definition of the flow being homogeneous or heterogeneous. These two flow types give very different results.
The expressions read:

(a) steam and water completely mixed (maximum loss):

$$\Delta p_{acc} = \{(1-x) + x \frac{\rho_w}{\rho_s} - 1 \} \rho_w v^2_{in} \qquad \text{eq. 3.15.}$$

(b) steam and water completely separated (minimum loss):

$$\Delta p_{acc} = \{\frac{(1-x)^2}{1-\alpha} + \frac{x^2}{\alpha} \frac{\rho_w}{\rho_s} - 1\} \rho_w v^2_{in} \qquad \text{eq. 3.16.}$$

The ratio between the values of the two expressions for a saturation temperature of 200°C and arbitrary but realistic values of 0.1 and 0.7 for x and α respectively, is 3.3., which is not a negligible value in view of the contribution of Δp_{acc} to the total pressure drop.
In practice the flow is not identical to either of both types and the actual condition will lie between these two limits. The inability to determine experimentally the true acceleration pressure drop component causes large scatter in the frictional pressure drop

data (see also A 4). Thom (T 2) is one of the few investigators who analysed data of boiling water in a horizontal as well as a vertical pipe. He calculated per force the acceleration loss assuming a separated flow type and plotted the results for horizontal flow in a similar way as did Martinelli-Nelson i.e. the two-phase friction multiplier versus exit steam quality. At low pressures the data compare very well, but they diverge considerably at higher pressures. The deviation is largest at low steam qualities, where the curves of Thom are concave, whereas the curves of Martinelli-Nelson are convex.
The objection against the plotting procedure is the use of the quality parameter, because steam quality does not represent a physically perceptible quantity. A much better parameter should be

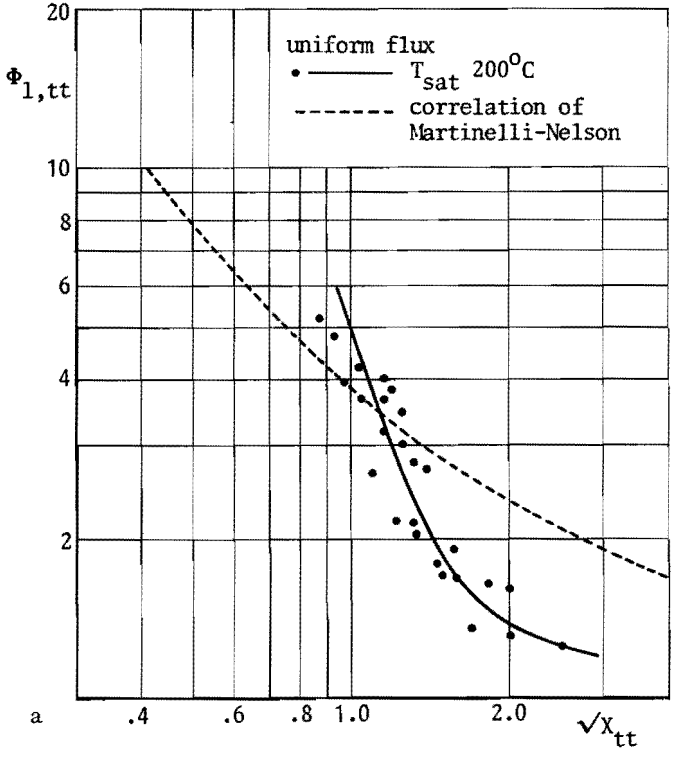

3.25. Two-phase friction parameters defined by Martinelli-Nelson (M 1) T_{sat} 200°C

the void fraction, but again we meet the difficult measurableness of it, whereas the steam quality can easily be determined from a heat balance, provided the fluid is not subcooled. Thom as well as Martinelli-Nelson assumed the steam quality to be linear with axial distance and this is by far not true with respect to the void fraction. At the same time it excludes the validity for non-uniform heatfluxes. It indicates also again the comparative merit of studies under adiabatic conditions. The void and velocity profiles are essentially different from those in boiling channels owing to the heated wall, and in air-water systems the friction due to contact with the wetted walls, is not influenced by the presence of bubbles attached to them. Experiments by Tarasova et al. (T 3) showed a definite effect of the heated wall in an annular channel.

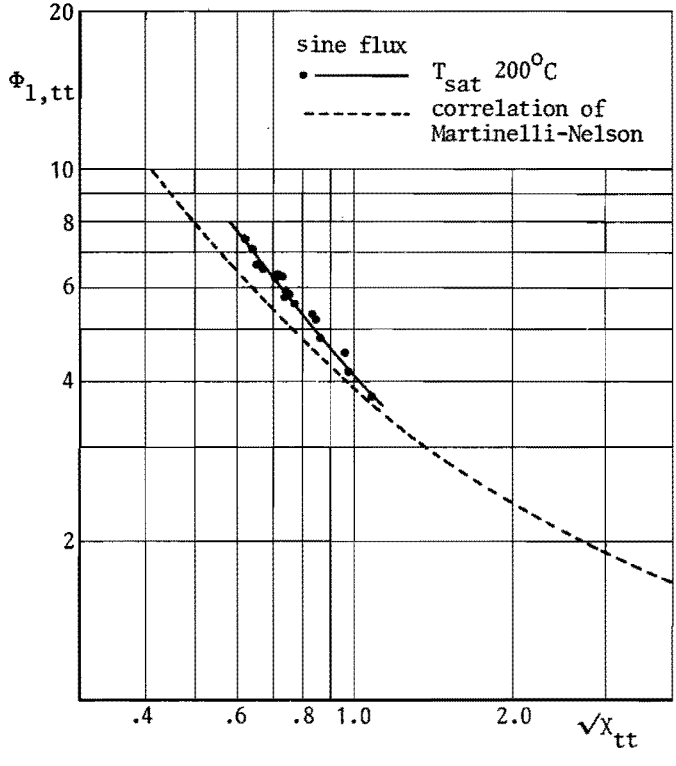

Besides, it is unsatisfactory that the two-phase friction multiplier of the figures still contains a fraction of the acceleration pressure drop, namely the difference between the actual situation and the extreme case of minimum pressure loss. The difficulty is that the frictional pressure drop component is a function of length while the acceleration pressure drop is independent of it, which precludes the possibility to incorporate the extra acceleration pressure drop in the frictional pressure drop, even though the momentum equation of all existing models is based on the acceleration loss of completely separated phases.

For want of something better the pressure loss data of the present study were plotted by making use of the correlation parameters of Martinelli-Nelson (Fig. 3.25 a and b), for a definition of which reference is made to (M 1). There exists an evident deviation from the Martinelli-curve, but the parameters satisfy reasonably as plotting quantities. It must be stressed that the figure does not exhibit overall but, instead, local values of the frictional data. The data points obtained with the sine-shaped heatflux fit very well the curve of Martinelli-Nelson.

4. DYNAMIC MEASUREMENTS

4.1. Behaviour under unsteady conditions

The oscillations to be reported here are those which are inherent to a boiling channel itself, without paying attention to other parts of the system which do not essentially exert an influence on the occurrence of instabilities. In principle the test section can be regarded as a tube being flowed through by a boiling two-phase fluid under a constant heating and a constant pressure head, which continuously balances the total pressure drop across the channel.

We would make a remark here with respect to the effect a pump would have. Neal (N 3) stated that the differences between forced and natural circulation systems are not fundamental in the sense that different instability mechanisms are involved. It can be added that the effect of a pump is twofold. On the one hand it superimposes an extra pressure head to the channel; it now depends on the ratio between the pressure drop across the channel and this extra pressure head whether instabilities can develop or not. On the other hand the stiffness of the pump is of importance because it uncouples what is known as flow-void feedback or rather the interaction between flow and the integrated void volume, and this is even worse if a part of the driving head is dissipated in a valve. In the extreme case of a plunjer pump this relationship between void and flow is completely absent. Both characteristics concur in the stabilising action of a pump.

However, a distinction must be made between a single channel and a multichannel system. If a number of parallel channels are connected together to one pump, then only the extra pressure head plays a part. Each channel encounters a fraction of the superimposed pressure head corresponding to its pressure drop. The stiffness of the pump does not come into the picture because the different channels

can freely interact while the total pressure drop remains the same. (C 2, M 3).

The threshold of instabilities is defined by making use of r.m.s. values accepted by many investigators (B 6, M 3, B 5, S 2) as valuable tools. In fact, an r.m.s. value represents the amplitude of the oscillating signal when averaged in time and magnitude, provided the shape of the signal is sinusoidal. It is therefore not necessary to use a time consuming computation when the amplitude of the signal concerned can be read directly from a recorder, but this only holds in the unstable region. The method of power spectra is especially profitable in the region of lower powers, the preambulary region, where the oscillations are developing and where it is practically impossible to distinguish visually the momentary resonance frequency of the system. As a clarification of "momentary" it must be remarked that the resonance frequency is a weak function of power in the sense that the frequency slightly increases with power.

The problem involved in the manipulation of different criteria for the determination of the threshold of instabilities has been recognised by many investigators (K 1, J 3, B 4, B 7). A comparative study has been reported by Dijkman (D 1) on the different results obtained from using various criteria. A selection was made of the available threshold definitions and these were related to the experimental results from (S 2). Along with the standard deviation σ or r.m.s. value, $1/\sigma$ and $1/\sigma^2$ also have been tested besides the ordinary amplitude, measured from recorders. The scatter in threshold power was about 10%.

On the ground of this study the choice fell on simply plotting σ because of two reasons:

(1) it enables the threshold of instabilities to be determined objectivily and in correspondence with the experimental observations
(2) it is a physically imaginable figure.

The r.m.s. value of a signal is compared to that of a recorded sinusoidal calibration signal with known amplitude which makes it possible to reduce the computed r.m.s. values of signals to amplitudes.

The region of unstable behaviour was entered, starting from a really stable condition, at least 40 kW distant from the instability threshold. Then the first measurements were taken and the signals of the significant variables recorded on the magnetic tape. The power was raised cautiously by superimposing a step of about 10 kW and the system was allowed to stabilise under a new condition. If oscillations started to appear, the condition was estimated to be stable when the oscillations showed a fairly constant amplitude.

Uniform heat flux

Amplitudes of the Δp-inlet signal have been plotted in Fig. 4.1. for two different system pressures corresponding to saturation tempe-

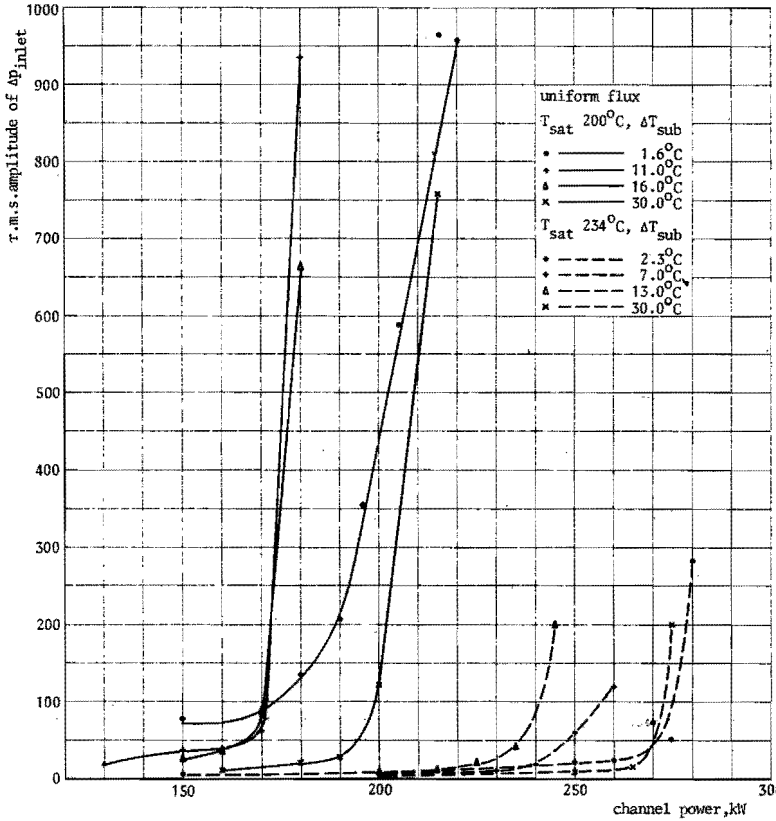

4.1. Stability curves defined by Δp-inlet T_{sat} 200°C and 234°C

ratures of 200°C and 234°C and for different subcoolings. As described by many authors (J 3, B 6, A 2, S 2, B 5) the effect of lower values of subcooling is destabilising. Arneodo established this effect on existing oscillations (A 2). The diagram indicates likewise that for the condition of 200°C saturation temperature in subcooled inlet conditions (and this holds too for high values of subcooling) the oscillations develop more rapidly than they do at almost zero subcooling; they do not announce themselves long in advance of the onset. At lowest subcooling there is a continuous lack of stability with increasing channel power without a clear onset of instabilities. The accepted threshold powers and resonance frequencies have been summarised in table 4.1. A similar behaviour is shown by the void signals. We will now first restrict ourselves to the condition of 200°C saturation temperature. The r.m.s. amplitudes of the void signals detected at the eight different positions of the channel in axial direction have been plotted in Fig. 4.2. The diagrams of the amplitudes have been corrected for the respective $d\alpha/dV$ values, as reduced from the Maxwell curve. At minimal subcooling the amplitude is obviously largest at the lowest position in the channel and decreases rapidly when going upwards, i.e. the higher the average void fraction the smaller the amplitude of the oscillations. This may

Table 4.1. Threshold powers and related frequencies measured by applying the uniform heatflux.

T_{sat} in °C	ΔT_{sub} in °C	threshold power in kW	frequency in Hz
200	1	190	1.05
	11	170	0.70
	16	170	0.50
	30	200	0.40
234	2	260	0.95
	7	240	0.85
	13	235	0.70
	30	265	0.45

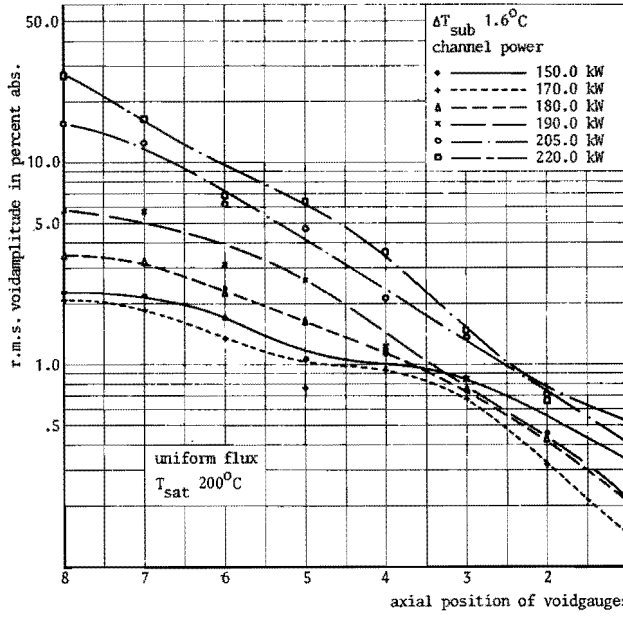

4.2. Axial distribution of void amplitudes T_{sat} 200°C, ΔT_{sub} 1.6°C

be comprehensible from a consideration of acceleration forces which are significantly larger for a certain increase in per cent. void (absolute value) at a high void fraction than for an equal increase at a low void fraction. It implies that the void oscillations when travelling from bottom to top are being damped strongly. Raising the channel power results in an increase of the void amplitude along the whole channel axis, comparable to the behaviour of the Δp-inlet signal.

It is interesting to divide the amplitude of Δp_{inlet} by that of the various void fractions. The results have been plotted in Fig. 4.3. The ratio increases exponentially with increased distance from the channel entrance. Since the amplitude of Δp_{inlet} for one channel power is fixed, the curves imply naturally the void amplitudes decreasing with increasing distance from the bottom i.e. the response of upper voids to a change of Δp_{inlet} is less pronounced than that of lower positioned voids. Comparison of the curves of different

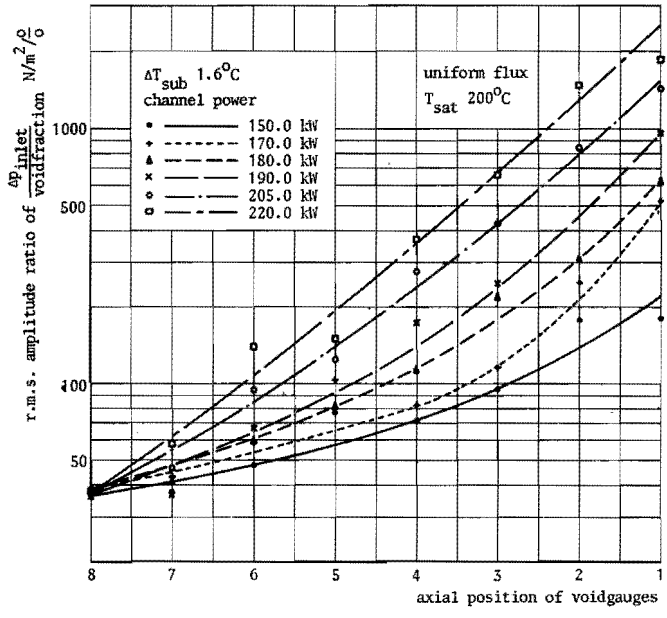

4.3. Axial distribution of amplitude ratio Δp-inlet-void T_{sat} 200°C

channel powers indicates that the reaction of the voids to Δp_{inlet} is less pronounced for higher powers than it is for lower powers, or, reversely, that the response of Δp_{inlet} to changes of void is amplified at higher channel powers. It is, however, notable that the void-to-Δp_{inlet} amplitude ratio at position 8 is constant for all powers, which means that the void fraction at that position changes linearly with Δp_{inlet}, and the reverse is, of course also true.

Fig. 4.4. shows the phase angles between void signals and the Δp_{inlet} signal. They have been computed by means of the transfer function analyser (see chapter 2.3.). The phases of the void signals have been referred to the Δp_{inlet} signal and have thus been plotted in the diagram. The phase differences between the subsequent void signals can be obtained by subtracting the phase differences with respect to the Δp_{inlet} signal. When following the change of the phase angle(in upward direction of the channel) the phase lead of the void fraction with respect to the Δp_{inlet} changes into a phase

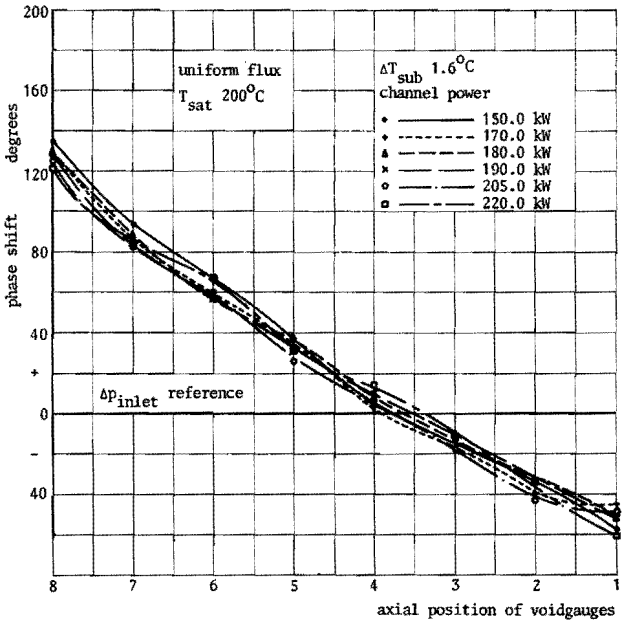

4.4. Axial phase distribution of void T_{sat} 200°C, ΔT_{sub} 1.6°C

lag. It is very remarkable that the phase differences between the mutual local voids and also between the voids and the inlet velocity are completely insensible to the channel power as well as to the measure of stability of the system. It accentuates the more the indivisible consistency of void fraction and flow-rate. It has often been suggested by authors, e.g. Neal and Lottes (N 3, L 1) that the occurrence of hydraulic instabilities should find their origin in a phase lag between void and flow-rate of 180°. If this is stated unshadedly, one has to realise that there is no question of only one void fraction but on the contrary, of an infinite number of void fractions, differing in magnitude and phase with different local, axial positions. In this connection Neal speaks of void volume, but this would require the concept of a kind of centre of gravity in which the void can be thought to be concentrated. This is, however, impossible and as figure 4.4. shows, unprofitable.

The phase angle changes from 130° phase lead for the lowest void

position to 50^{o} phase lag for the highest void position. Primarily the flow responds to the action of the integrated void volume causing a change of driving head and secondarily the void responds to the flow via the change in heat transfer. It is not the phase-shift that changes with power but the amplitude. Noise analysis could be started already at a relatively low channel power, in this case 150 kW, which is 40 kW below the accepted threshold power. It means that at this power the resonance frequency of the channel was really present and could be distinguished from the inherent noise. At a channel power of 50 kW this frequency was not present, i.e. the TFA was not able to compute a peak in the power spectrum and did not give reproducible values. Thus the resonance frequency is present very early and it appears to increase slowly with power; see table 4.2. This is supported by Del Tin (T 4). Another interesting conclusion is justified by observing Fig. 4.4. Neal (N 3) has written the conservation of energy equation in terms of the quality disturbance and the conservation of mass, and derived analytically

Table 4.2. Channel power dependence of frequency

Uniform heatflux, T_{sat} $200^{o}C$

ΔT_{sub}	channel power kW	frequency Hz
1.6	150	1.10
	190	1.10
	220	1.10
11.0	130	0.60
	150	0.65
	160	0.70
	180	0.70
16.0	150	0.50
	180	0.50
30.0	160	0.35
	180	0.40
	215	0.40

an equation for the transportation time of a vapour quality disturbance:

$$v_p = \frac{\Phi W}{(1-x)\rho_s + x\rho_w} \qquad \text{eq. 4.1.}$$

where $\Phi = \frac{x(1-x)}{\alpha(1-\alpha)} \cdot \{1 + \alpha(1-\alpha)\frac{1}{S} \cdot \frac{dS}{d\alpha}\}$ eq. 4.2.

all values indicating steady state conditions. W represents the total mass flowrate. If this propagation velocity is known from position to position one can convert it into phase angles for a measured frequency. This has been done for some powers at lowest subcooling, making use of the digital model for stationary-data reduction and the results are given in Fig. 4.5. Because the phase difference between void and Δp_{inlet} is unknown the position of the analytical phase curve with respect to the reference line of Δp-inlet is arbitrary.

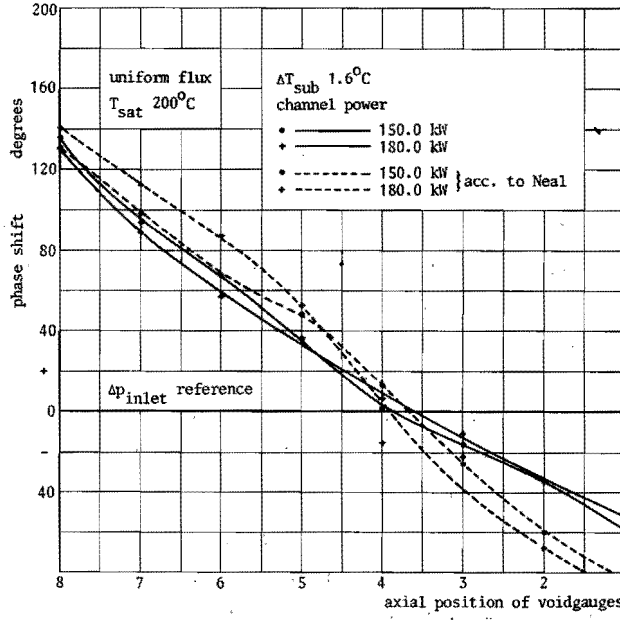

4.5. Axial phase distribution of void compared to Neal's expression T_{sat} 200°C

Owing to the unreliability of steam quality calculations in regions of subcooled boiling, the computation of propagation velocities under subcooled conditions has been omitted.
The agreement with the measured values is rather good.

The propagation velocity is indeed constant along the channel axis resulting in the phase shift changing linearly with axial distance although the slope is steeper than has been measured. The reason for this deviation is not clear. One may think of an incorrect value of void fraction but a check calculation teaches us that the equation is rather insensitive to small changes in void. The equation (4.1.) is, therefore, in principle correct, which means a support for the validity of the conservation equations and it affirms the conclusion of Neal (N 2) that a linear feedback exists between void and flow, and that non-linearities are not essential for the instability to occur, but merely affect the limit cycle.

Besides, Fig. 4.4. tends to the conclusion that the propagation velocity is constant for different channel powers, the threshold power included. If it is now assumed that the steam quality and void fraction increase from power to power in equal measure, this holds too with respect to the slipfactor; see 4.1., 4.2. The important inference to be drawn is the validity of a slip correlation, derived from steady state conditions, for dynamic calculations. This question concerning the validity is recognised by anyone who develops a mathematical model, and can be answered affirmatively. This, consequently, is also true for the correlation of the two-phase friction multiplier.
Christensen (C 2) and Davies (D 2) state that inclusion of the steady state correlations in dynamic calculations are felt to be invalid, Neal (N 4) is convinced of the permissibility, Kirchenmayer (K 2) doubts it and other people, among whom Åkerhielm (Å 2), feel uncertain about it.

Phase differences between flow and axially distributed voids in a boiling water system have been measured by Åkesson (Å 1) by making use of impedance void gauges. The reported results, however, are fairly obscure. The data inserted in the tables do not all correspond to the figures. The linearity of the curve of the axial dis-

tribution of the void phase is contradictory to the scatter revealed by the tables. The void signals of the upper positions have a scalene-saw-tooth shape. The measurement of the phase angles apparently carried out on the basis of photographic recordings leads to deviating results. Since the signal of the inlet velocity is sinusoidal the phase difference between upper voids and inlet velocity depends on whether the maximum or the minimum of a void amplitude is being considered. For the condition of a pressure of 30 atm and a subcooling of 5^{o}C the plotted curve shows that the phase difference reduced from the maxima run from 160^{o} phase-lead to 25^{o} phase-lag, going from the lower to the upper void position, which agrees reasonably well with the results of the present study. This phase shift is, however, dependent on the power. The phase shifts reduced from the minima differ considerably but are not power dependent. The phase angle between the lower positioned void and inlet velocity happens to be 180^{o}, but it is not indicated whether the system was stable or not.

In order to investigate the relationship between void propagation, frequency and transit or residence times of steam and water, these residence times have been computed from the present experiments for different subcoolings (Fig. 4.6.). The transit time of a void disturbance, calculated from eq. 4.1., as well as the period of the frequencies are indicated by marked points. The period of the frequency appears mainly related to the transit time of the water, in agreement with the prediction of Kirchenmayer (K 2) deduced from theoretical considerations. The transit time of a void disturbance (t_v) lies somewhere between the residence times of water (t_w) and steam (t_s). The ratio t_w/t_v is a little larger than the ratio t_v/t_s. Nassos (N 1) measured void and velocity profiles in a forced-circulation air-water system and derived a simple expression for the void propagation velocity based on the theory of kinematic waves. The expression needs accurate knowledge of the profiles. The qualitative agreement between theory and experiment was satisfactory, but the quantitative correspondence was poor. At liquid velocities above 0.6 m/sec the void propagation velocity was measured to be lower than the gas velocity.

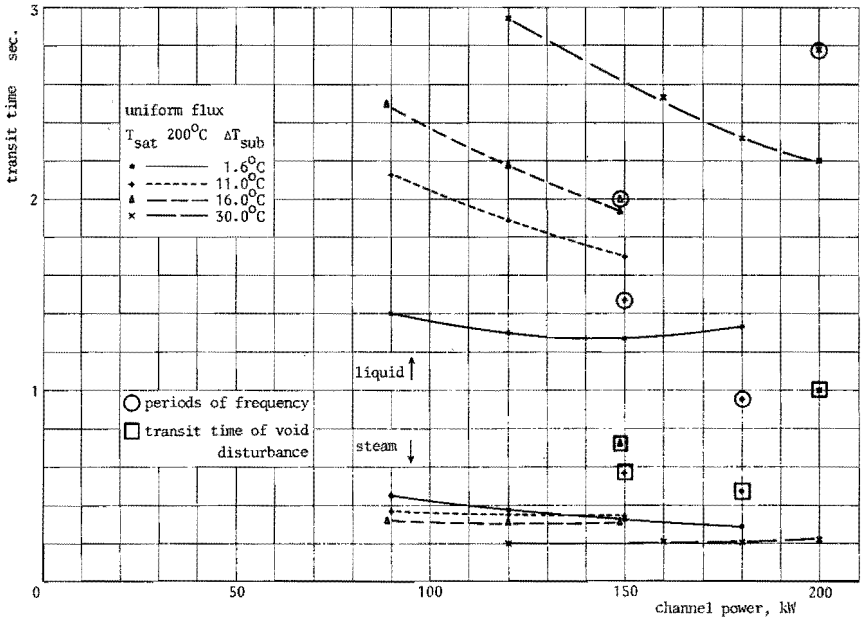

4.6. Residence times of water and steam T_{sat} 200°C

Also St.Pierre (S 1) reports the propagation velocity to lie between the steam and water velocities. We will revert to this publication later on.. Neal (N 4) mentioned a few experiments that indicated a similar trend.
Noteworthy is the notation of eq. 4.1. in terms of velocities of flow components. Substitution of the velocity definitions:

$$v_{st} = \frac{x}{\alpha} \cdot \frac{\rho_w}{\rho_s} v_{in} \text{ and } v_w = \frac{1-x}{1-\alpha} v_{in} \qquad \text{yields}$$

$$\Phi = \frac{v_{st} \cdot v_w}{v_{in}^2} \cdot \frac{\rho_s}{\rho_w} \left\{ 1 + \alpha(1-\alpha) \frac{1}{S} \cdot \frac{dS}{d\alpha} \right\} \qquad \text{eq. 4.3.}$$

Neglecting for a moment the term $(1-x)\rho_s$ in 4.1. which contributes about 10% to the denominator, it follows that

$$v_p = \frac{v_{st} \cdot v_w \cdot \rho_s}{x \rho_w v_{in}} \left\{ 1 + \alpha(1-\alpha) \frac{1}{S} \frac{dS}{d\alpha} \right\} \qquad \text{eq. 4.4.}$$

which reveals that a prediction of v_p from known steam and water velocities is not self-evident.

Influence of subcooling

Similar figures showing the amplitude of void signals and the phase shift in relation to the flow-rate have been drawn for different values of subcooling.
The influence of subcooling on the amplitude of the void signals is shown in figure 4.7.a, b, c. At lowest subcooling the following facts can be established:

(1) The amplitude decreases monotonously with increasing distance from the bottom.
(2) The amplitude increases monotonously with channel power corresponding to a similar behaviour of the Δp_{inlet} signal.
(3) The ratio of the amplitudes of lower and upper voids is relatively high.

The different values of higher subcooling concur in the following effects:

(1) The amplitude shows a maximum near the bottom. It moves upwards with increasing subcooling.
(2) The amplitude increases monotonously with channel power except for the threshold power where the amplitude increases quite rapidly, again corresponding to the behaviour of the Δp_{inlet} signal.
(3) The amplitudes of the voids along the channel are of the same order of magnitude.

It is interesting to consider item (1) in detail. The position of the maximum moves up with increasing subcooling. It is stated frequently (S 2, D 2) that this maximum should be situated at the position of the boiling boundary. However, this boiling boundary is a fictitious conception. Physically it does not exist. The figures of the axial void distribution show a steady growth of void without any discontinuity. In the subcooled region a considerable quantity of void is present and it does not change abruptly where the local

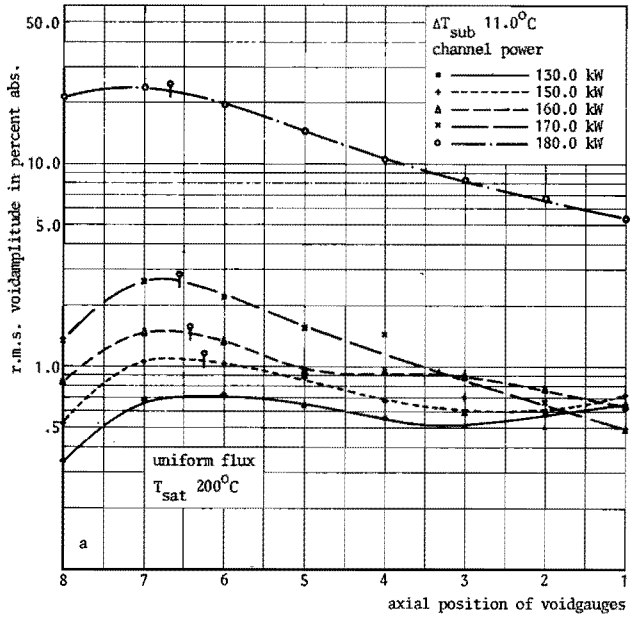

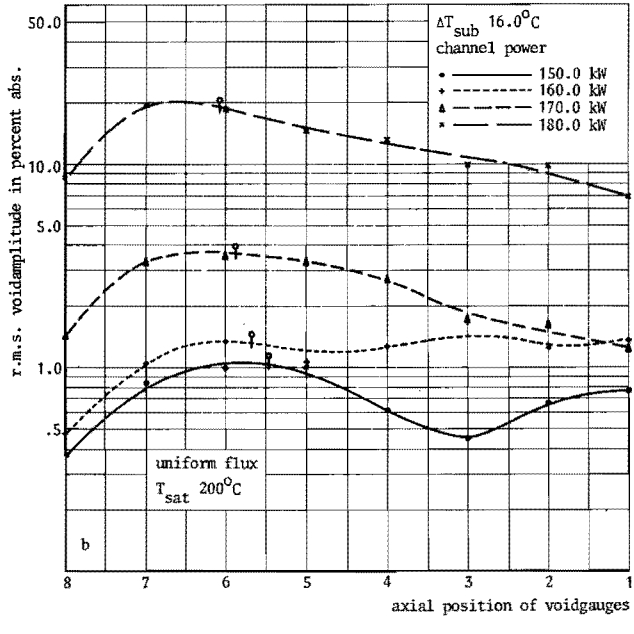

ϕ indicates position of boiling boundary in case of thermodynamic equilibrium.

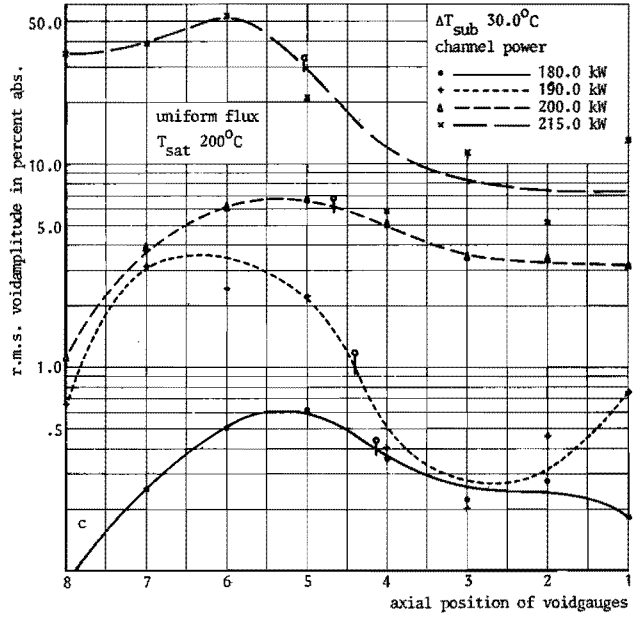

4.7.a,b,c. Axial distribution of void amplitudes T_{sat} 200°C, various subcoolings

fluid temperature starts to exceed the local saturation temperature. For some powers the position has been denoted in figure 4.7.a, b, c., where would be the thermodynamic boiling boundary resulting from a simple energy balance and the assumption of thermal equilibrium. This is approximately at the level of the maximum amplitudes. The position of the real theoretical boiling boundary is considerably further downstream. The peak is just there where the derivative of void with respect to z is high i.e. where the slope of the axial void distribution curve is steep. Here the void has the freedom to grow rapidly in steady as well as non-steady condition.

As concerns the phase curves it can be established that the straightness of the lines has disappeared; Fig. 4.8.a, b, c.
The curvature implies the existence of a larger propagation velocity in the boiling region than in the subcooled boiling one. The inherent scatter of the curves has become larger than at zero subcooling where the lines form a narrow band. The phase difference

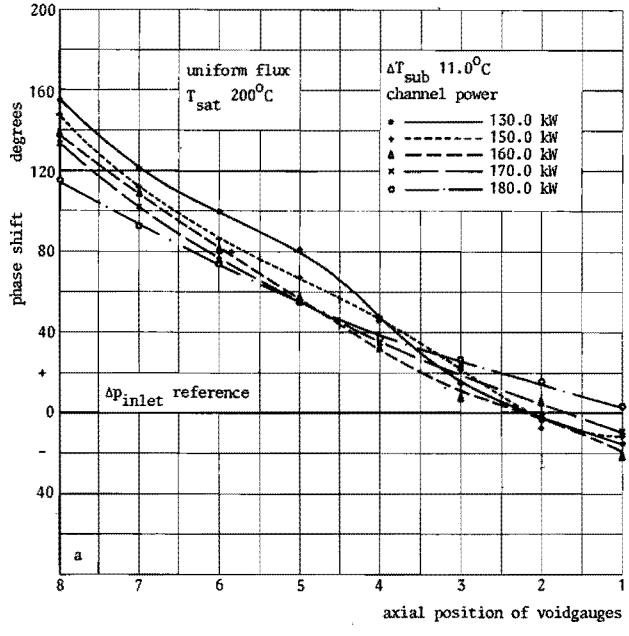
uniform flux
T_{sat} 200°C
ΔT_{sub} 11.0°C
channel power
130.0 kW
150.0 kW
160.0 kW
170.0 kW
180.0 kW
Δp_{inlet} reference
phase shift
degrees
200
160
120
80
40
+
0
-
40
a
8
7
6
5
4
3
2
1
axial position of voidgauges

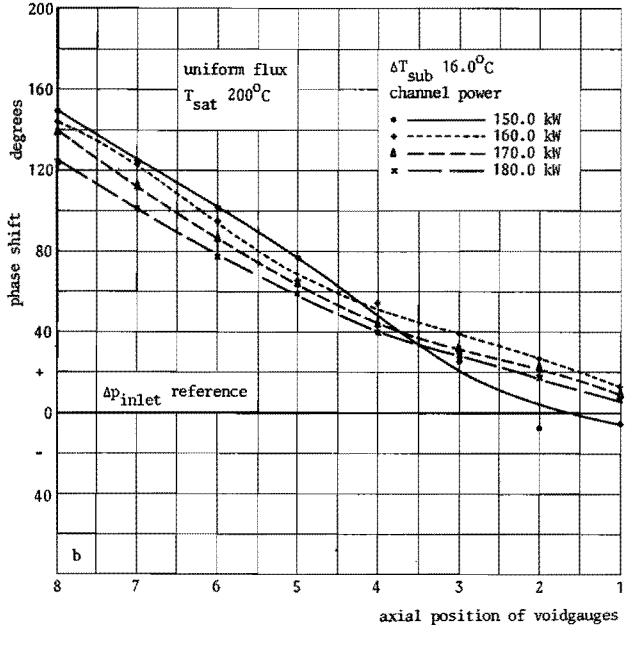
uniform flux
T_{sat} 200°C
ΔT_{sub} 16.0°C
channel power
150.0 kW
160.0 kW
170.0 kW
180.0 kW
Δp_{inlet} reference
phase shift
degrees
200
160
120
80
40
+
0
-
40
b
8
7
6
5
4
3
2
1
axial position of voidgauges

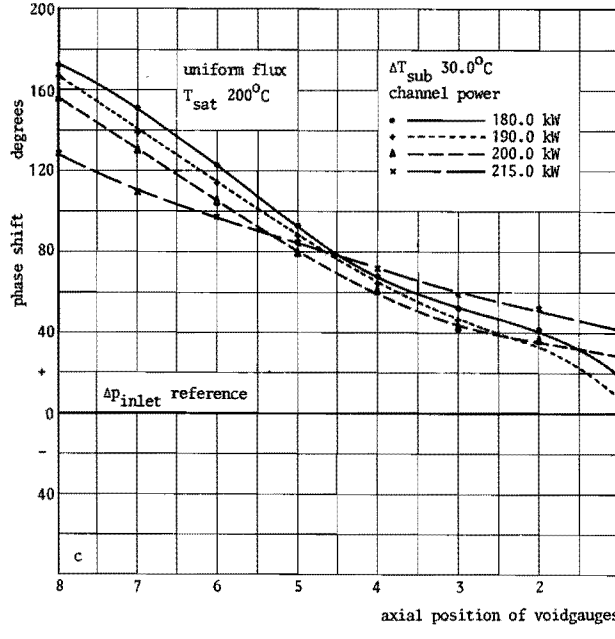

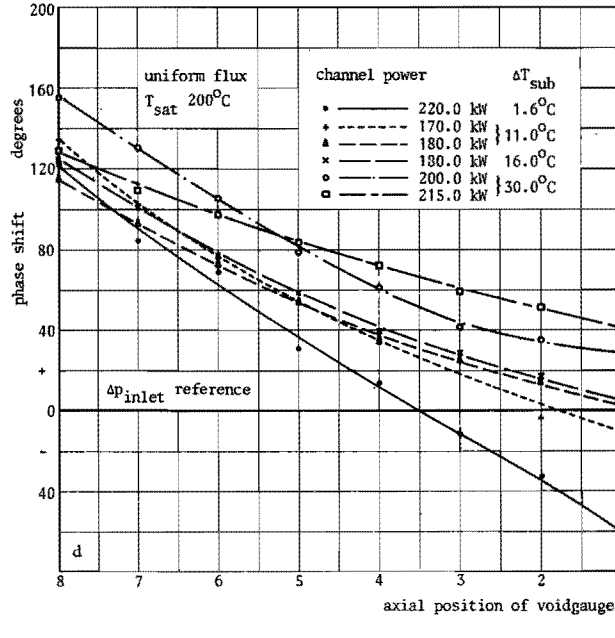

4.8. a,b,c,d. Axial phase distribution of void T_{sat} 200°C, various subcoolings

between the lower positioned void and Δp_{inlet} does not really change, but that between the lower and the upper voids decreases with increased subcooling. There is a tendency of this phase difference to decrease for higher power values.

Fig. 4.8.d is a combination of curves of the two highest channel powers of each subcooling. There is a significant difference between the curves of low, moderate and high subcooling. The conspicuous distinction is the phase shift between the extreme voids.
It decreases with increasing subcooling but not to the extent as does the frequency. On the ground of experimental data the void propagation velocity can be expressed as

$$v_p = \Delta z \cdot \frac{\text{frequency} \cdot 360}{\Delta \text{ phase}}, \qquad \text{eq. 4.5.}$$

Δz representing the length of the axial distance under consideration, Δ phase the phase difference in degrees along this Δz, and "frequency" the momentary resonance frequency. It follows that the propagation velocity of a density disturbance becomes smaller as the subcooling increases.

This should confirm the hypothesis of Neal (N 3) who supposes that the principal effect of the non-boiling length is that it introduces a transportation time delay between the occurrence of a disturbance and the appearance of the corresponding quality change in the boiling region.

Influence of pressure

It is well known (N 2) that pressure stabilises the system as is visible in Fig. 4.1. from a moving of the threshold powers to higher values as well as from a decrease of the amplitude of the flow-rate signal. The influence of subcooling is similar to that at 200°C, with the minimum threshold power likewise at about 13°C subcooling. The oscillations develop at lowest subcooling more rapidly than they do at 200°C.

As regards the amplitudes of the void signals, the difference in magnitude of lower and upper void amplitudes is less than at 200°C,

for low subcooling as well as for higher subcooling values, Fig. 4.9.a, b, c, d. Again there is a maximum in the curves that moves upwards with increasing subcooling.

It is noticeable that pressure does not act upon the void propagation velocity (Fig. 4.10.a, b, c, d). This is in accordance with the constancy of the oscillation frequency which appears to be more a function of subcooling than of pressure. The differences in phase-curves between 200°C and 234°C are merely gradual. At low subcooling the agreement is perfect although the powers are considerably different. At higher subcooling values the phase differences between upper and lower voids change less than at 200°C. This observation, too, agrees with the smaller variation of frequency with subcooling at higher pressure.

Influence of a sine-shaped heatflux

In a number of publications, of which the most recent are T 5, B 8 and S 4, the influence has been reported of a sine-shaped heatflux on the occurrence of burn-out. It is outside the scope of the study under consideration to review these publications. However, to the author's amazement no experiments are known that aim at studying the influence of a non-uniform heatflux on the stability of a boiling system. This is the more astonishing because of the essentially different behaviour of the system in comparison with that under a uniform heatflux. The publications mentioned report a small influence of sine-shaped heatflux on burn-out, it only moves the burn-out location to a lower axial position. However, the effect on stability is so radical that it is necessary to apply considerable correction factors to the results of experiments carried out with uniform heating.

The r.m.s. averaged amplitude of the signal of Δp_{inlet} has been plotted versus channel power in Fig. 4.11. for different values of subcooling and one higher pressure. What strikes the eye first is the smallness of the values of the amplitude, being on an average 15 times as small as corresponding values measured with a uniform heatflux. Comparison with Fig. 4.1. shows that the amplitudes are

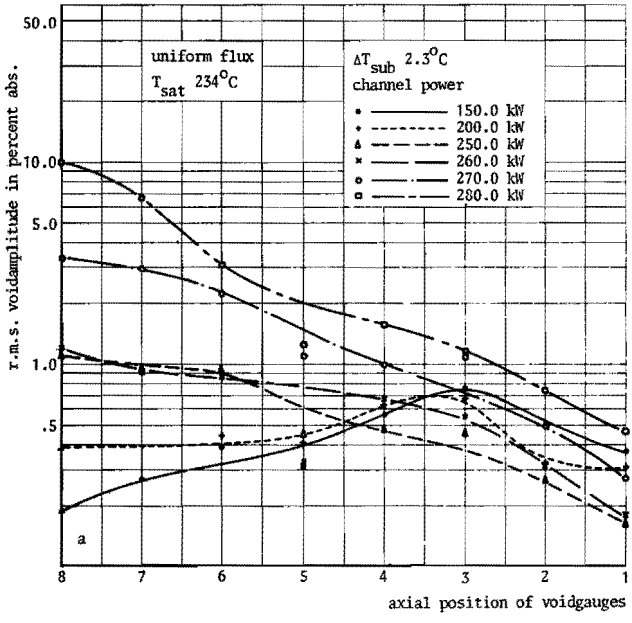
uniform flux
T_{sat} 234°C
ΔT_{sub} 2.3°C
channel power
150.0 kW
200.0 kW
250.0 kW
260.0 kW
270.0 kW
280.0 kW
r.m.s. voidamplitude in percent abs.
50.0
10.0
5.0
1.0
.5
a
8
7
6
5
4
3
2
1
axial position of voidgauges

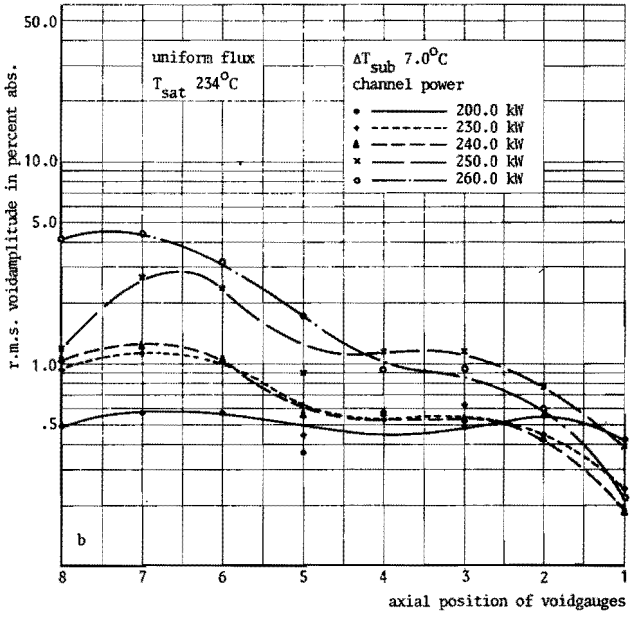
uniform flux
T_{sat} 234°C
ΔT_{sub} 7.0°C
channel power
200.0 kW
230.0 kW
240.0 kW
250.0 kW
260.0 kW
r.m.s. voidamplitude in percent abs.
50.0
10.0
5.0
1.0
.5
b
8
7
6
5
4
3
2
1
axial position of voidgauges

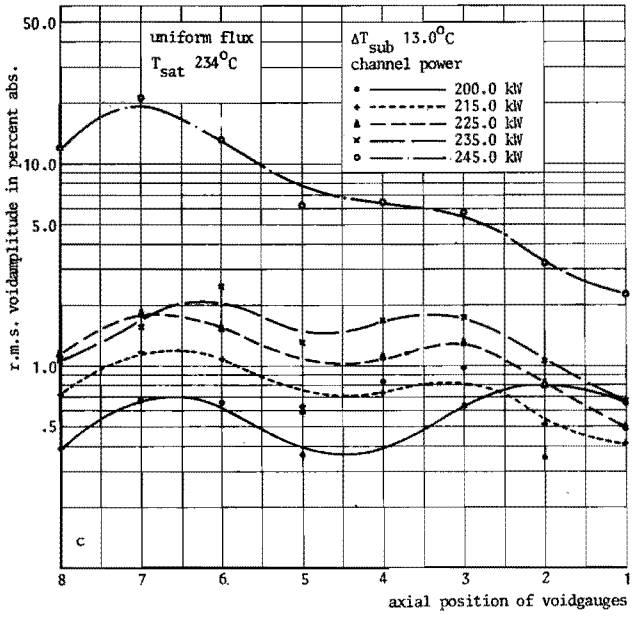

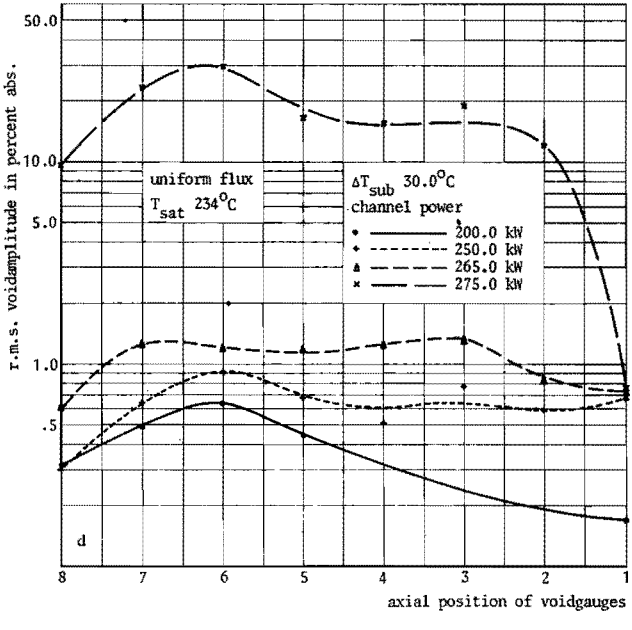

4.9. a,b,c,d. Axial distribution of void amplitudes T_{sat} 234°C, various subcoolings

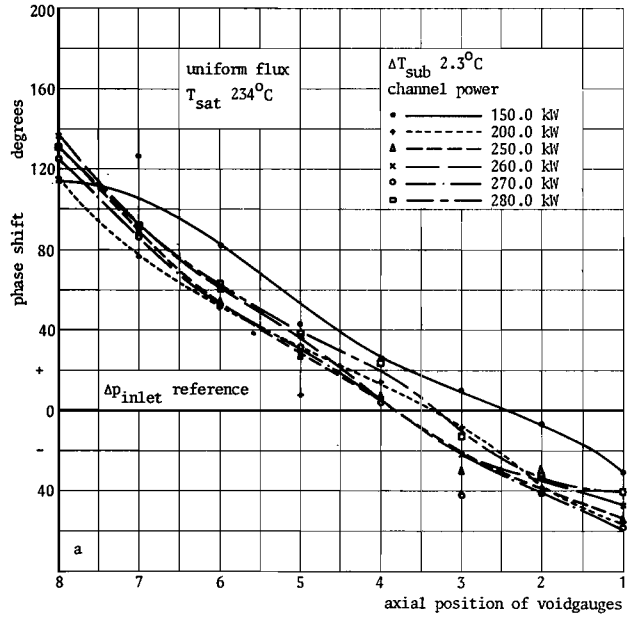
uniform flux
T_{sat} 234°C
ΔT_{sub} 2.3°C
channel power
150.0 kW
200.0 kW
250.0 kW
260.0 kW
270.0 kW
280.0 kW
Δp_{inlet} reference
phase shift
degrees
200
160
120
80
40
+
0
-
40
a
8
7
6
5
4
3
2
1
axial position of voidgauges

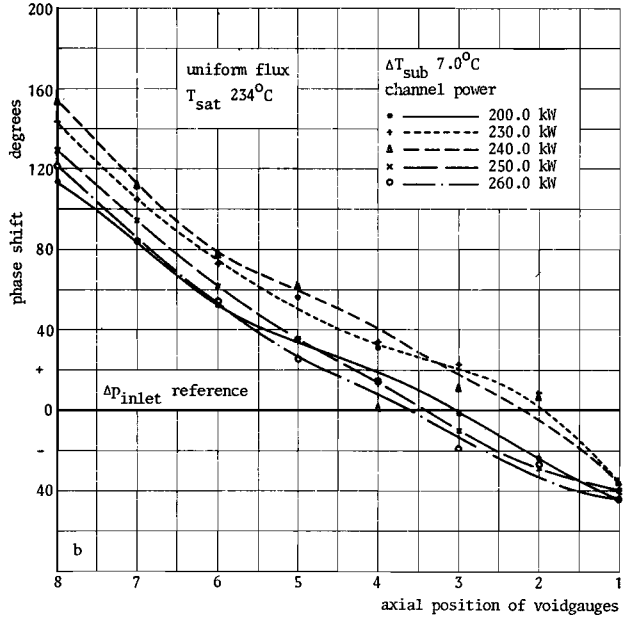
uniform flux
T_{sat} 234°C
ΔT_{sub} 7.0°C
channel power
200.0 kW
230.0 kW
240.0 kW
250.0 kW
260.0 kW
Δp_{inlet} reference
phase shift
degrees
200
160
120
80
40
+
0
-
40
b
8
7
6
5
4
3
2
1
axial position of voidgauges

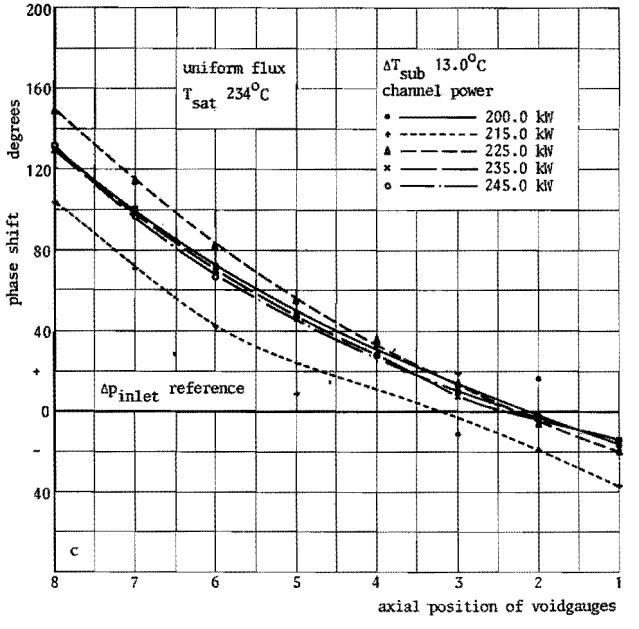

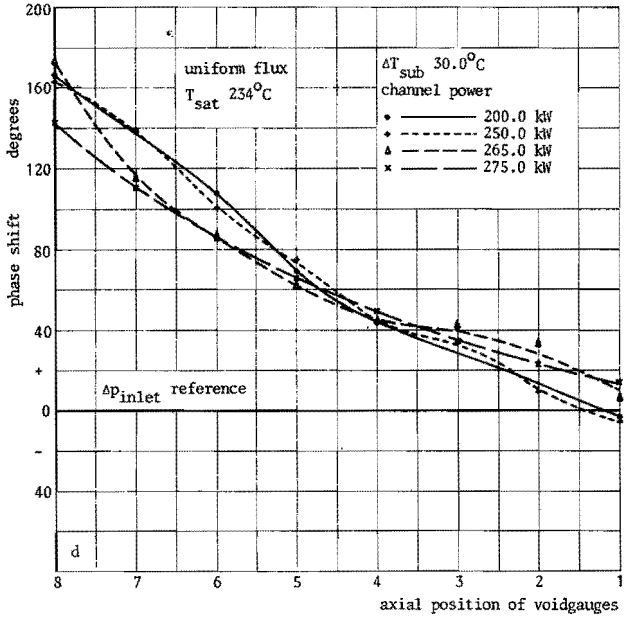

4.10. a,b,c,d. Axial phase distribution of void T_{sat} 234°C

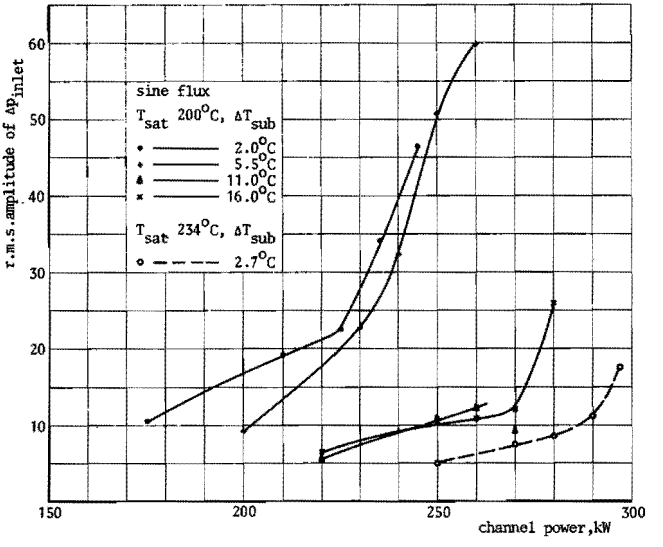

4.11. Stability curves defined by Δp-inlet T_{sat} 200°C and 234°C

even smaller than those of the corresponding signals of the uniform heatflux in the region of noise.

The second conspicuity is the fact that low values of subcooling have lost their destabilising effect. At 1.5. and 5.5.° subcooling it is hardly possible to determine a threshold power of instabilities, and at 11° and 16° it is entirely impossible. It is more correct to speak of a decline of stability than of an increase of instability. Because in all cases the burn-out was encountered before the system was really unstable, it is highly questionable whether the occurrence of burn-out is precipitated by the decrease of stability, or if the burn-out can be considered to occur under stable conditions. It means that a comparison of results obtained from measurements with a uniform and with a sine-shaped heatflux is not possible on the basis of threshold powers, nor on the basis of burn-out values. For this reason the threshold powers of the uniform flux and the burn-out powers (i.e. the ultimate powers at which the system could be established to be stable) of the sine-shaped flux have been summarised in table 4.3. For the purpose of facilitating comparison with the uniform flux table 4.1. has been included.

Table 4.3.

uniform heatflux				sine-shaped heatflux			
temp. °C	subc. °C	threshold power kW	freq. in Hz	temp. °C	subc. °C	b.o. power in kW	freq. in Hz
200	1.6	190	1.05	200	2.0	245	1.05
	11	170	0.70		5.5	265	0.9
	16	170	0.50		11	275	0.9
	30	200	0.40		16	285	0.85
234	2.3	260	0.95		21	295	
	7	240	0.85	234	2.7	305	0.90
	13	235	0.70		11	312	
	30	265	0.45		21	330	

If it is assumed that in the first case the threshold power of instabilities determines the danger situation for a reactor core and in the second case the burn-out power, then a comparison of both quantities proves convincingly the considerable influence of a sine-shaped heatflux, especially when subcooling is involved.

The results of all one-channel and multi-channel experiments aiming at studying the hydraulic behaviour of a boiling water system under high heatloads, are in principle directed to the applicability to a core design of a reactor. The results of the experiments mentioned tend to emphasise that predictions with respect to the occurrence of oscillations in reactor cores based upon loop experiments with uniform heatfluxes are fundamentally very conservative and this all the more if the fluid at the entrance is subcooled.

Neal (N 2) and Lottes (L 1) reported reactor power oscillations in the EBWR and the SPERT IA reactor respectively. In both cases, however, the oscillations were imputed to reactivity feedback and not to hydrodynamic instability.

Hansson (H 2) reports stability experiments with an axial heatflux distribution. The heatflux, however, did not change continuously with axial distance but was essentially uniform all along the channel. The heating rod was divided into three parts, each part gene-

rating a different uniform heatflux. The heatflux changed abruptly at the junction of two subsequent parts. These discontinuities disturb the flow considerably and the experimental results cannot therefore be considered to be representative for the influence of axial heatflux distribution.

Bjørlo (B 5) carried out a study on the comparison between in-pile and out-of-pile measurements. The differences between the applied test sections were very small. Two important discrepancies were still determined, namely the reactor was more stable than the loop, and the inlet velocity in the reactor was more than 20% higher. As possible causes were mentioned, among less important other ones, the different axial power distributions and the different time constant of the heater tubes. As far as our experience is concerned, neither of them, however, can be responsible for the higher flow velocity (cf. A 5). It is tempting to attribute the increased stability to the sine-shaped heatflux, but the considerably higher inlet velocity has a stabilising effect, too, although it is difficult to estimate to what extent. It is, therefore, not evident that the study by Bjørlo constitutes a support of the present results. The conclusions with respect to the stability are confirmed by the following figures. The amplitudes of voids are given in figure 4.12.a, b, c, d. At low subcooling there is a steady falling off of the amplitude in upwards direction in the channel but less steep than was the case with the uniform flux, as is clearest visible from the lower two void fractions. The absolute values are considerably smaller than for the uniform flux; in the lower part of the channel the ratio is about 20. The effect of power is small, the curves move slightly parallel to each other.

Subcooling changes the form of the curves as it did in the case of the uniform flux. A small peak appears close to the bottom of the channel, but a strange phenomen is the minimum at the position of void number 4, i.e. near to the location of the maximum heatflux. There is a certain symmetry in the curve, probably corresponding to the symmetry of the heatflux. The sequence of the curves with respect to the ordinate in the second peak is in one case (Fig. 4.13.b) similar to that in the first peak, in one case the opposite

(d) and one case (c) indifferent, thus not significant. The absolute value of the amplitude is a factor 10 or more smaller than for a uniform flux, emphasising the noisy character of the signals. Fig. 4.13.a, b, c, d shows the phase differences between the mutual void fractions and the Δp_{inlet}. The general trend is similar to that for a uniform heatflux, but two distinctions can be noticed:

(1) The spread of the curves is larger.
(2) The influence of subcooling is negligible.

As regards (1) during the analysis of the uniform heatflux measurements by means of the transfer function analyser it was already observed that the reproducibility of the results of the computations was better, the more unstable was the system, that means, the more the resonance frequency dominated the stochastic noise frequencies. A secondary consequence was the comparative difficulty to distinguish a clear peak in the power spectra as a function of the frequencies investigated. Both symptoms were present when analysing the sine-flux signals, thus confirming their noisy character. Referring to (2), the differences as a function of subcooling are quite gradual. This is in agreement with the constancy of the resonance frequencies, as mentioned in table 4.3.

It again confirms the relation between frequency and propagation velocity. Because of the inherent stability of the system with sine-shaped heatflux, the additional stabilising influence of increased pressure is not quite evident (Fig. 4.11.). Remarkable is the similarity of the shape of the void amplitude curves to that of the curves with subcooling, whereas one would expect a similarity to the low subcooling curves (Fig. 4.14.). Summarising, the stabilising characteristics of a sine-shaped heatflux can be concluded from:

(1) the absence of a well-definable threshold power,
(2) the signals keeping their noisy character at increased powers. There is no rapid increase of amplitude with channel power, not even near burn-out.

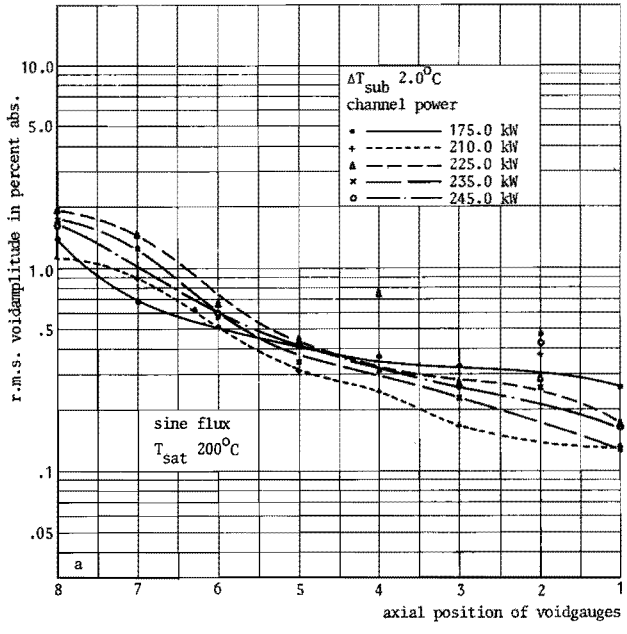
10.0
5.0
1.0
.5
.1
.05
r.m.s. voidamplitude in percent abs.
ΔT sub 2.0°C
channel power
175.0 kW
210.0 kW
225.0 kW
235.0 kW
245.0 kW
sine flux
T sat 200°C
a
8
7
6
5
4
3
2
1
axial position of voidgauges

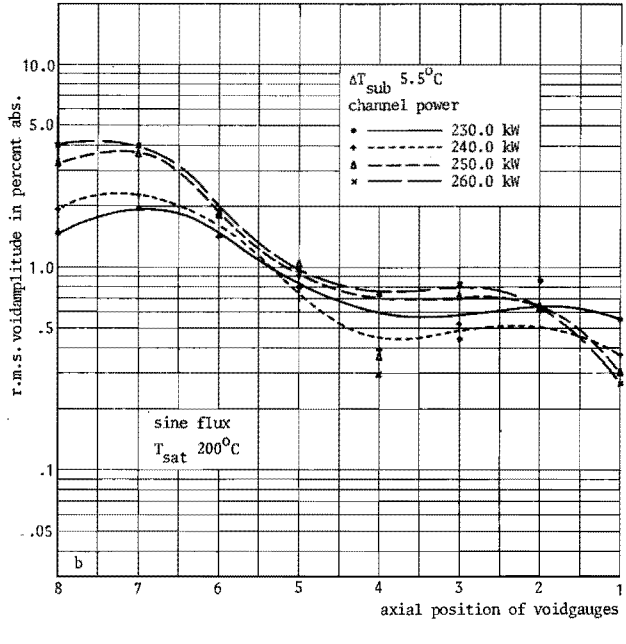
10.0
5.0
1.0
.5
.1
.05
r.m.s. voidamplitude in percent abs.
ΔT sub 5.5°C
channel power
230.0 kW
240.0 kW
250.0 kW
260.0 kW
sine flux
T sat 200°C
b
8
7
6
5
4
3
2
1
axial position of voidgauges

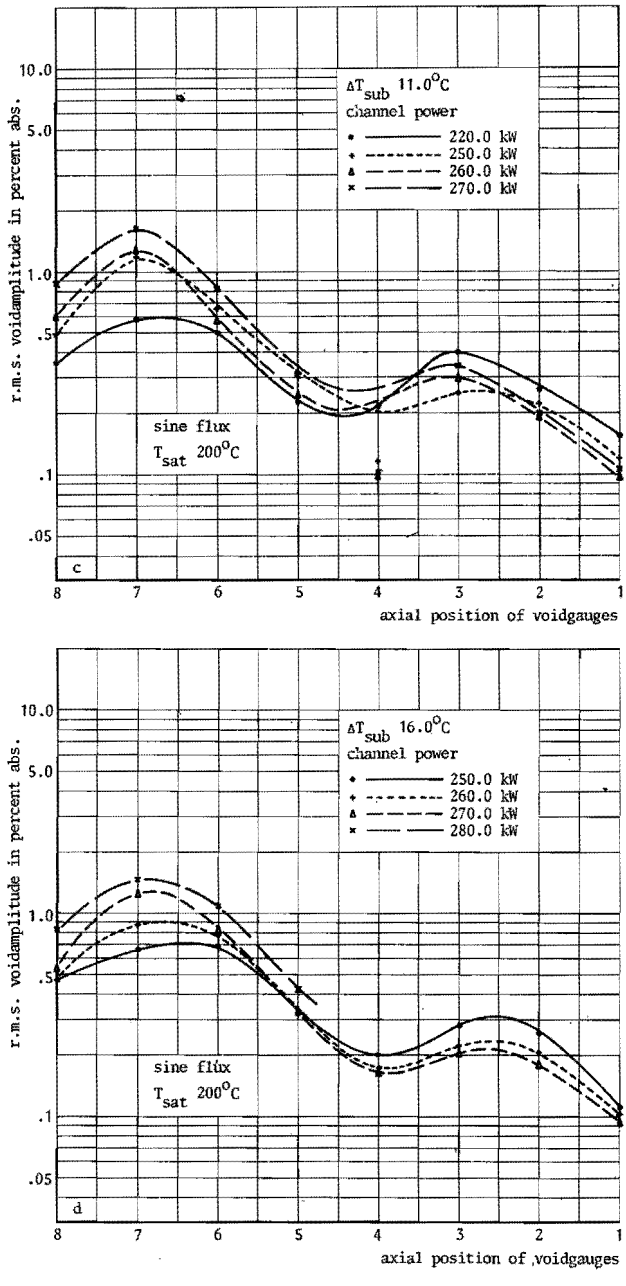

4.12.a,b,c,d. Axial distribution of void amplitudes T_{sat} 200°C, various subcoolings

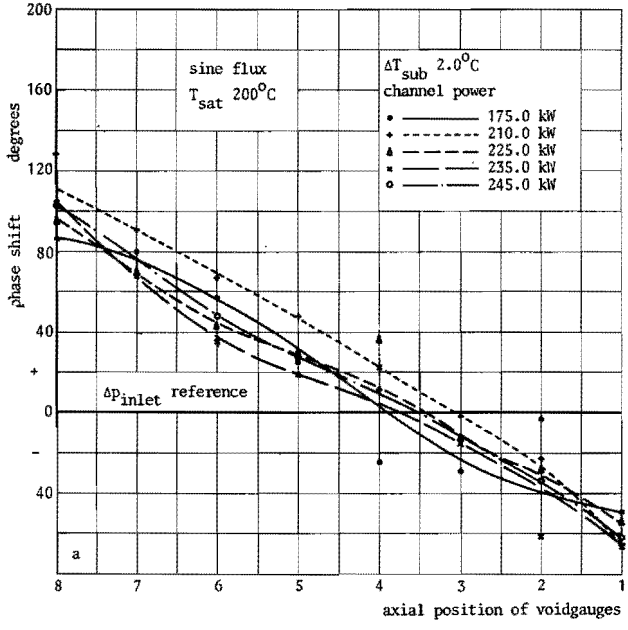
sine flux
T_{sat} 200°C
ΔT_{sub} 2.0°C
channel power
175.0 kW
210.0 kW
225.0 kW
235.0 kW
245.0 kW
Δp_{inlet} reference
phase shift
degrees
a
axial position of voidgauges

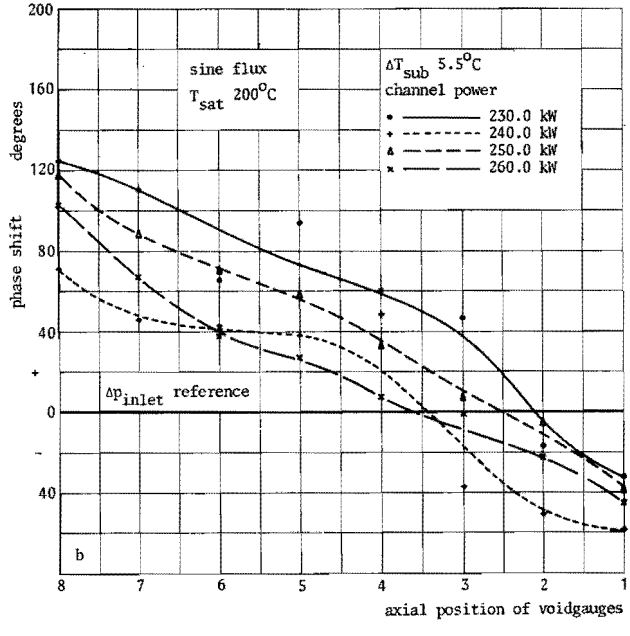
sine flux
T_{sat} 200°C
ΔT_{sub} 5.5°C
channel power
230.0 kW
240.0 kW
250.0 kW
260.0 kW
Δp_{inlet} reference
phase shift
degrees
b
axial position of voidgauges

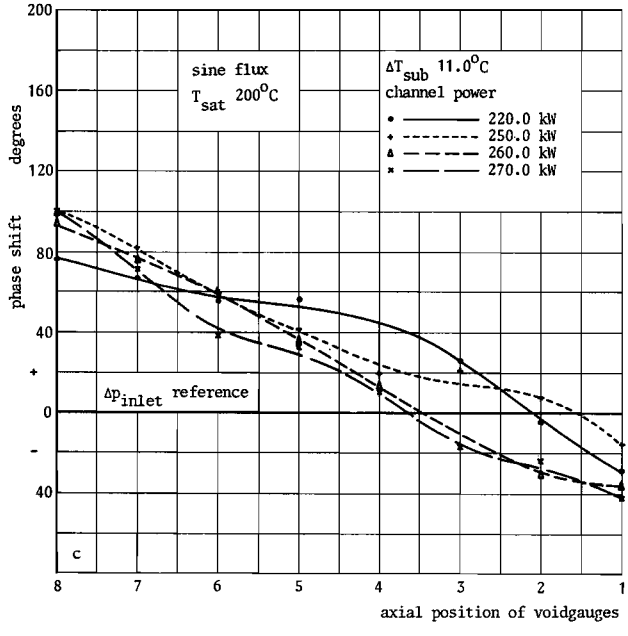

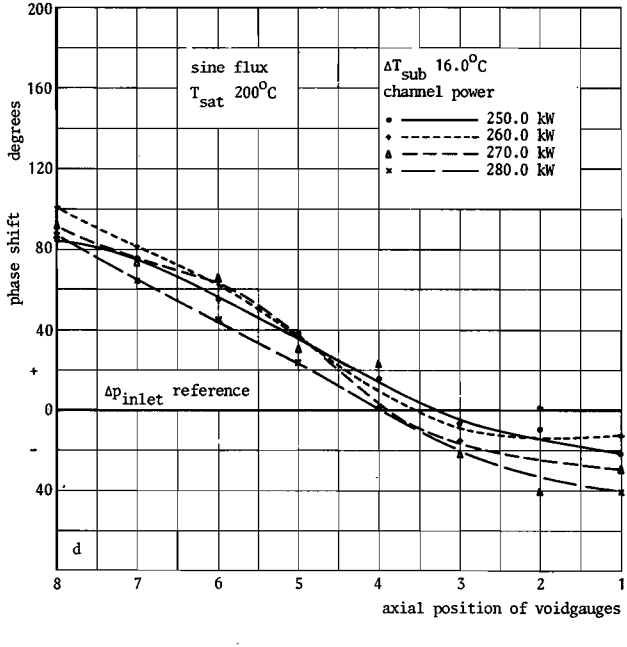

4.13. a,b,c,d. Axial phase distribution of void T_{sat} 200°C

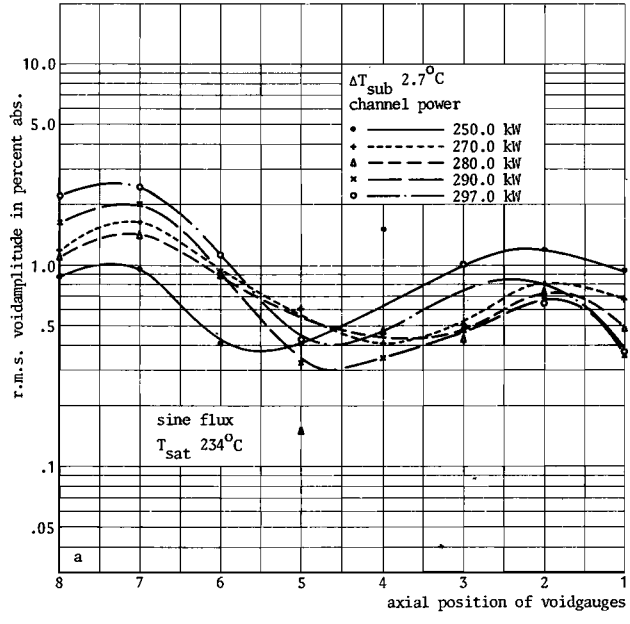

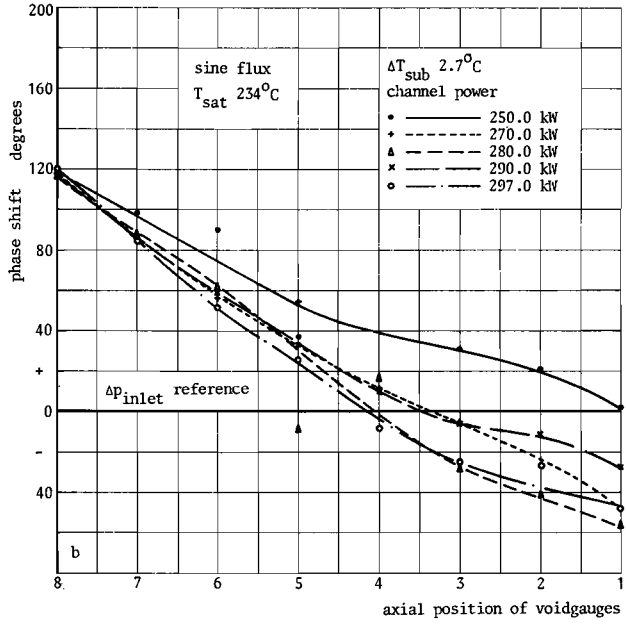

4.14. Axial distribution of void amplitudes and phase shift, T_{sat} 234°C, ΔT_{sub} 2.3°C

4.2. Transfer Function Measurements

In order to support and to supply the results as concerns the hydraulic behaviour of the boiling water system under steady state conditions a restricted number of transfer functions have been carried out. The perturbed signal was chosen to be the heating power, because it is the only external physical quantity that is independent of the other physical parameters, and because its variation with time can be programmed exactly in steady as well as non-steady conditions. Varying the heating power does not encroach upon the physical consistency of the system. Besides, it is the most convenient quantity to be perturbed.

A remark must be made with respect to the meaning of the measured power signal. The power instantaneously generated in the heating element is on the one hand transferred to the fluid and on the other hand used for increasing the temperature of the heating element. The power which easily can be measured is the instantaneous total power, but the instantaneous net power which is supplied to the fluid and which should be the correct power for correlating the transfer functions cannot be measured directly, nor can the power, dissipated in the heating element. This distinction between measured power and net power introduces immeasurable attenuation and phaseshift between them. Theoretical considerations prove that the phaseshift can be as large as 80^{o} at 1.0 Hz.

In (S 2) it has been proved that during the perturbation of the power signal the linearity of the system was maintained, provided that the amplitude was kept within certain limits and that the adjusted condition was sufficiently distant from that where spontaneous oscillations would start to occur.

P r o c e d u r e

A sinusoidally varying voltage, generated by the TFA, was connected to the transductor of the power unit, thus superimposing to the mean power a sinusoidally varying heating power with an adjustable amplitude. The variation of the power was measured by means of a Hall-generator. Contrary to the common procedure the transfer

function between the signal of the Hall generator and the different output signals was not computed on-line, but the significant signals were recorded simultaneously on the Ampex magnetic tape recorder. The motivation was that it accelerated the experimental procedure, and that, because the TFA is rather sensitive to temperature variations of the surroundings, it was preferable to carry out the analysis in an air-conditioned room remote from the loop. In addition to the signals of the Hall generator and the Δp-inlet, 4 or 8 signals were recorded, which were chosen in such a way that for reference purpose in any case the upper and lower void signals (number one and eight) formed part of them.

Although it was possible to use that part of the TFA that was suitable to analyse sinusoidal signals, the relatively poor reproducibility of the results led to the application of the unit for analysis of power spectra. The signals consequently were analysed in the same way as have been the noise signals. Unfortunately, it appeared impossible with this procedure to analyse frequencies lower than 0.2 cps.

The gain between two quantities were calculated by dividing the roots of the respective power spectra. In all figures of amplitude ratios the points have been plotted in dimensional units. The values have not been normalised by dividing them by the steady-state values of the ratio, because such a procedure veils the physical significance of the plotted quantities.

R e s u l t s

U n i f o r m h e a t f l u x

The most familiar transfer function is that between heating power and Δp-inlet, the Bode-diagram of which is given in Fig. 4.15. for the condition of 200^{o}C and a subcooling of 1.6^{o}C.
As was expected, the results concerning the amplitude ratio as well as the phaselag of Δp-inlet with respect to the power are trivial. They do not reveal new aspects. The peak in the gain is at the same frequency where the phase curve exhibits a phaselag of about 180^{o}, see (S 2). It must be emphasised that this value does not represent

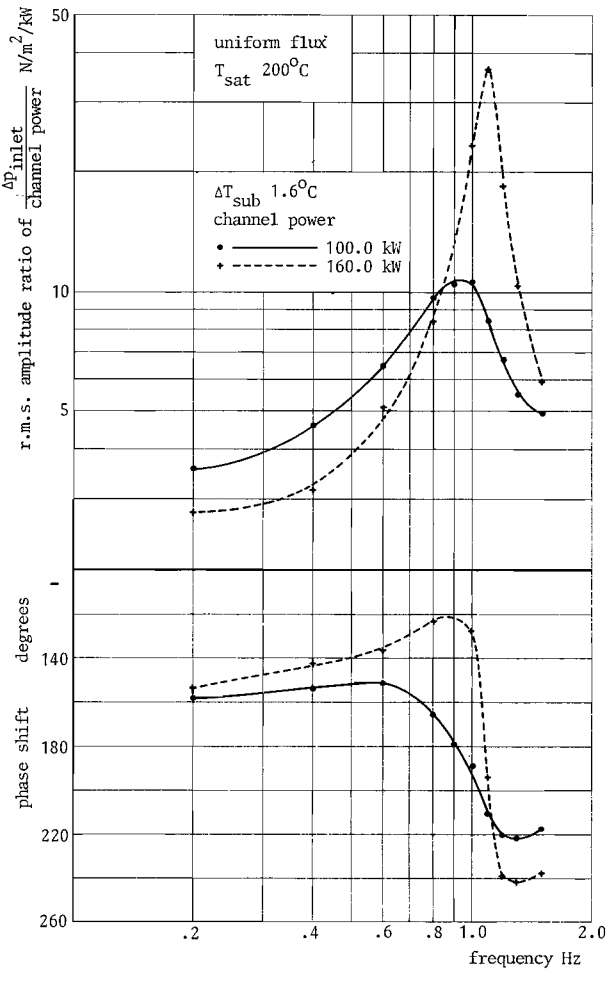

4.15. Power-to-Δp-inlet transfer function T_{sat} 200°C, ΔT_{sub} 1.6°C

the phaselag between the actually transferred power and Δp-inlet. An increase of power accentuates the curvature of the phase line and increases the gain. Similar diagrams show the relation between heating power and void fraction (Fig. 4.16.). In the vicinity of the resonance frequency the curves run parallel. The sequence of the amplitude curves corresponds in that region to the trend of the amplitude curves resulting from the noise analysis (Fig. 4.2.), i.e. the value of the void amplitude decreases when going from bottom to top. In the region of lower frequencies the sequence is somewhat irregular.

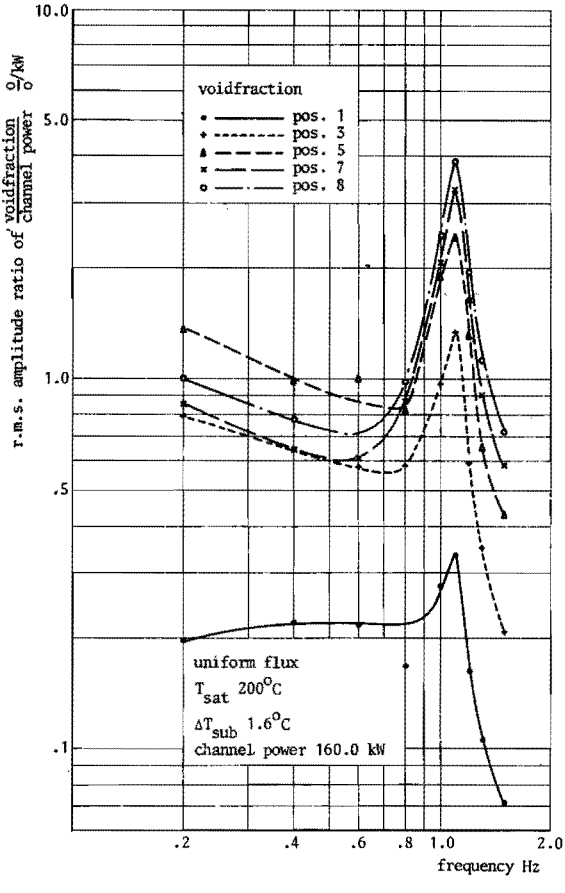

The phase differences of the void signals diverge with increasing frequencies and, for the particular condition of 200°C, 150 kW, low subcooling, and signal of void number 1, run from about 72° at 0.2 cps up to 345° at 1.5 cps. There is a rapid increase of the phaselag with respect to the power at the position of the peak in the amplitude curve, the steepness being a function of the axial void position. At low frequencies the void fraction number 8 is almost in phase with the total channel power. Concerning the phase-lead of the void fraction at position 8 with respect to the channel power at a frequency of 0.9 Hz it must be repeated that this power does not represent the net channel power. For purposes of comparison

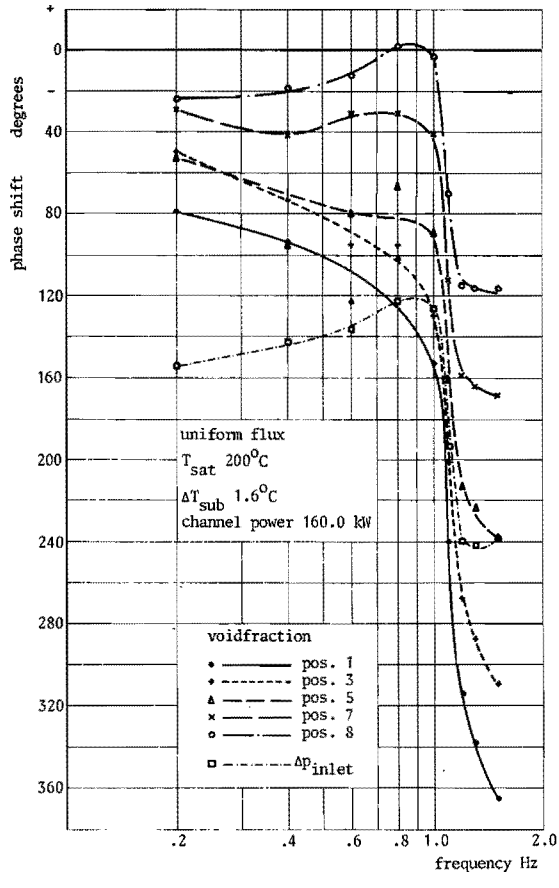

4.16. Power-to-void transfer function T_{sat} 200°C, ΔT_{sub} 1.6°C

the curve of the phaselag of the Δp-inlet signal with respect to the power has been included in the diagram.

The two sets of diagrams (4.15. and 4.16.) once being known, the relationship between heating power, void fraction and Δp-inlet is fixed. This enables the triangle to be completed by drawing the diagrams showing the mutual dependence of void fraction on Δp-inlet (Fig. 4.17.). Because the void fraction is primarily perturbed by the heating power and consequently changes the driving force of the inlet velocity, the ratio of Δp-inlet to void fraction has been plotted and not the reverse. When first attention is given to be

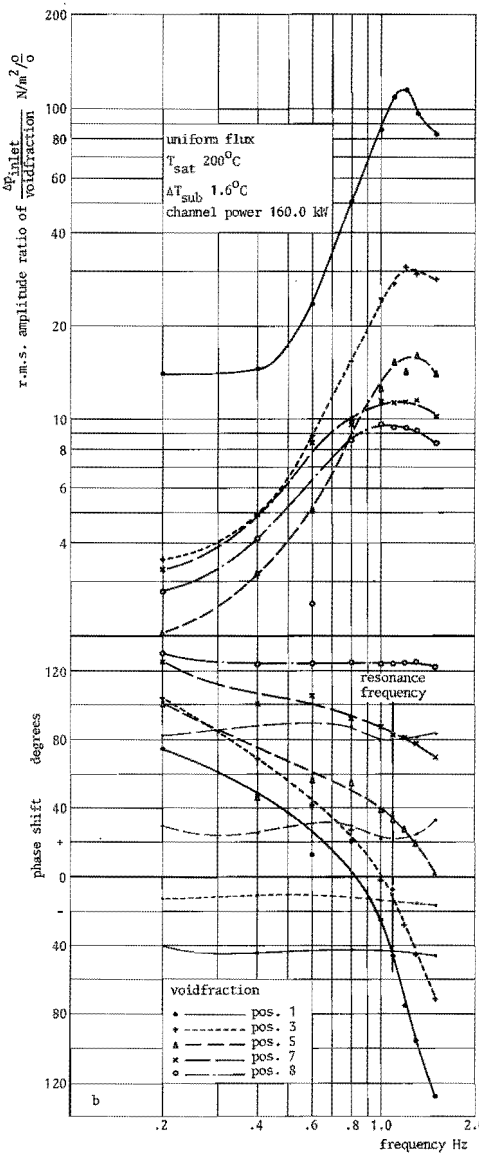

general trend of the Bode-diagram, it can be noticed that the amplitude ratio increases continuously with frequency. It means that the amplitude of Δp-inlet grows disproportionately to the void amplitudes. Reversely, this implies that a change of inlet velocity does not have an equally large effect on the void fractions.

There appears a very flat maximum in the curves. It must, however, be stressed that this occurs just beyond the resonance frequency.

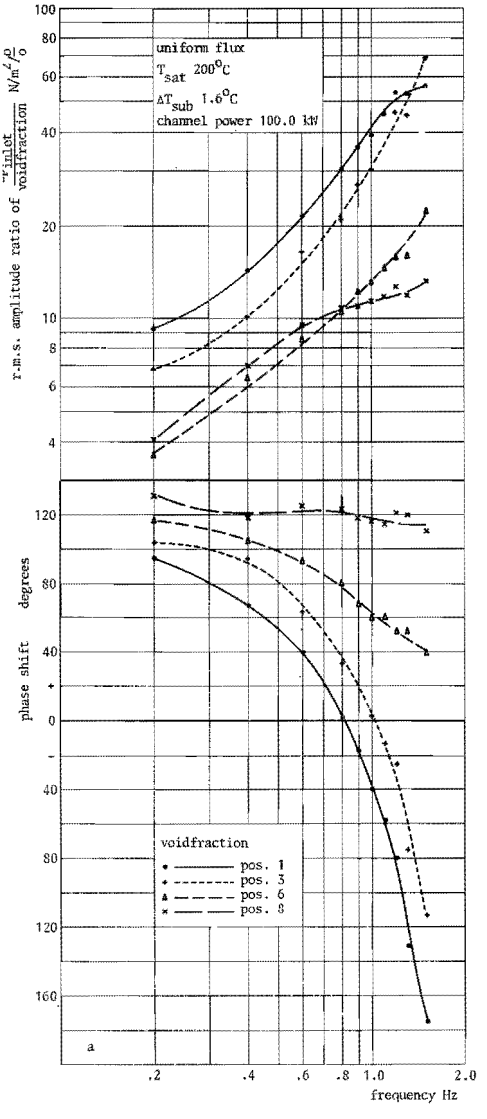

4.17. Frequency response of Δp-inlet-void T_{sat} 200°C, ΔT_{sub} 1.6°C

This is supported by the phase curves, which reveal no turning point. In this diagram 4.17. the phase angles of the void fractions have been referred to Δp-inlet. The phaselead of void number 8 with respect to Δp-inlet is practically independent of the frequency. This is quite untransparent if the void is supposed to act on the

inlet velocity, because not one particular void but the integrated void is leading. When, however, the inlet velocity is supposed to act on the void fraction via the influence on the heat transfer, then the constant phase angle is comprehensible. The dependence of the phase difference between a void (except number 8) and Δp-inlet on the frequency increases with increasing distance from the channel bottom, resulting phaselead turning to phaselag for the void fractions at higher positions and increased frequency.
It was supposed that in spite of the superimposed power perturbations, the resonance frequency of the system was still present. In order to check this, the analysis of the signals has in some

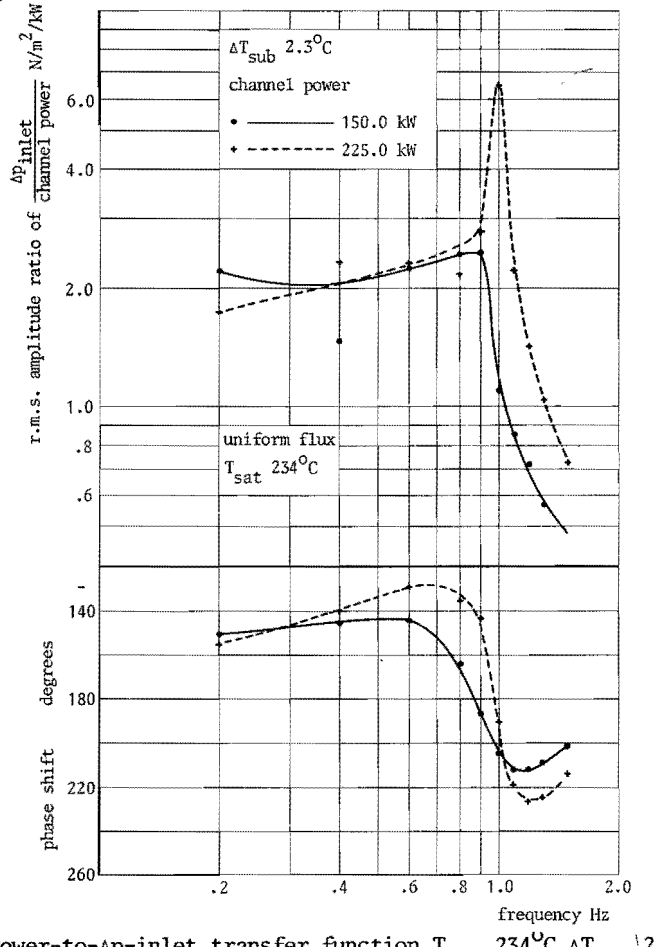

112 4.18. Power-to-Δp-inlet transfer function T_{sat} 234°C, ΔT_{sub} 2.0°C

cases also been carried out at the basic frequency. The ability of the TFA to distinguish noise superimposed on the sinusoidally varying signals, emphasises the selectivity of the device. As can be seen in Fig. 4.17. the assumption is confirmed by the results. The section across the phase curves at the resonance frequency is in perfect agreement with the results obtained from the noise analysis (Fig. 4.4.). Reminding the reader of the simple expression for the propagation velocity $v_p = \Delta z \cdot \text{frequency} \cdot 360^o/\Delta\text{-phase}$ (eq. 4.5.) and considering the phase differences in Fig. 4.17., it follows that at 0.2 Hz the propagation velocity of the excited disturbance is half that at 1.0 Hz, and that it increases proportionally

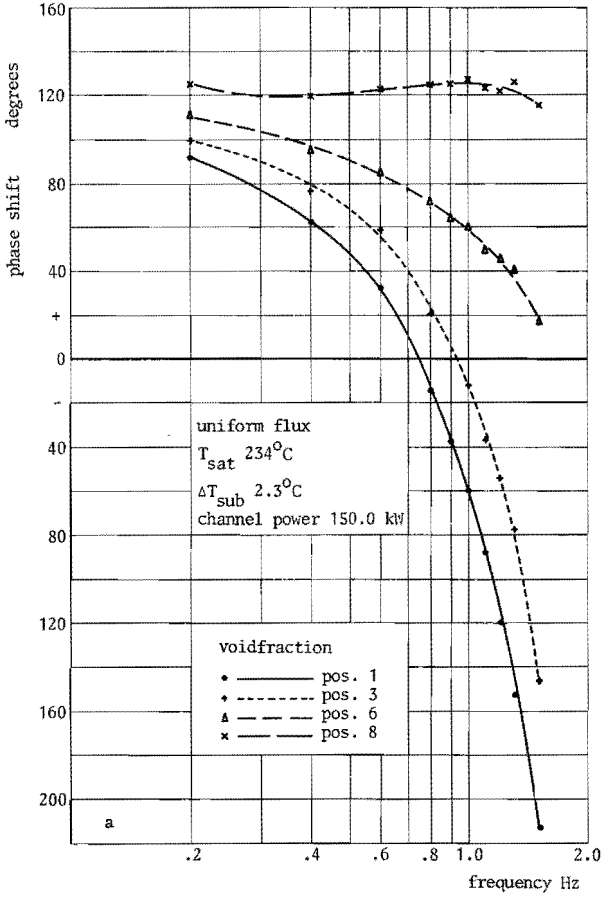

4.19a. Frequency response of Δp-inlet-void phase shift
T_{sat} 234°C, ΔT_{sub} 2°C

at higher frequencies. Therefore, there appear to exist two different propagation velocities of a void disturbance at one superimposed frequency, and both coincide at the resonance frequency. It is obvious that the diagrams prove the existence of the consistent interrelationship between void volume and inlet velocity. They form together one indissoluble physical couple. Neither of them amplifies the other, and a phaseshift of 180° between any void fraction and Δp-inlet is completely irrelevant to the origin of instabilities. Similar figures can be drawn for a higher pressure. Since curves of amplitude ratios do not show new aspects, only phase curves have been plotted (Figs 4.18. and 4.19.). There is perfect agreement with the low pressure results.

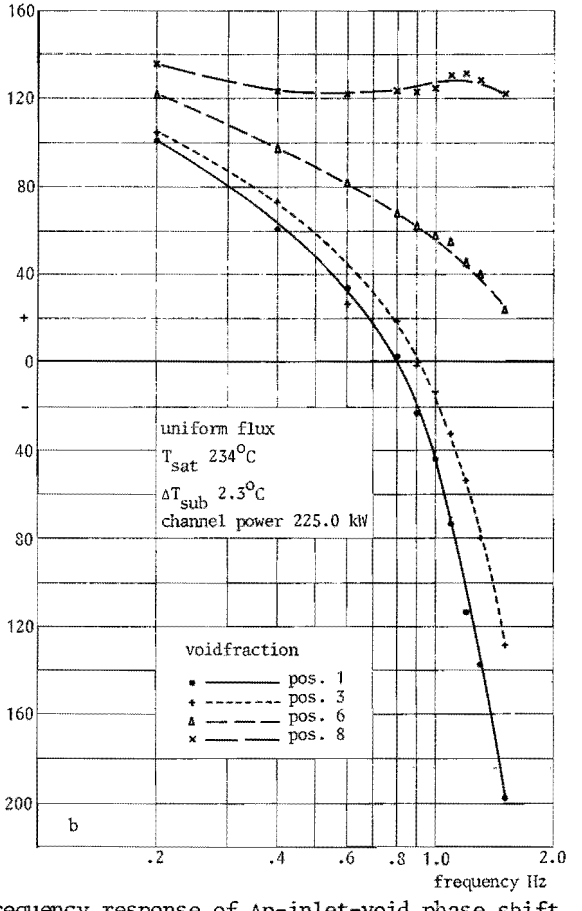

4.19b. Frequency response of Δp-inlet-void phase shift
T_{sat} 234°C, ΔT_{sub} 2°C

S i n e - s h a p e d h e a t f l u x

It is obvious that although the system under influence of the sine-shaped heatflux is much more stable than with a uniform heatflux, the presence of a resonance frequency implicates the possibility to excite the system. The Bode-diagram of power-to-Δp-inlet is given in Fig. 4.20 for two subcooling values. The oscillation power of 200 kW for the low subcooling case was 40 kW higher than the corresponding figure applied to the uniform flux. The oscillation power for the higher subcooling was 220 kW.

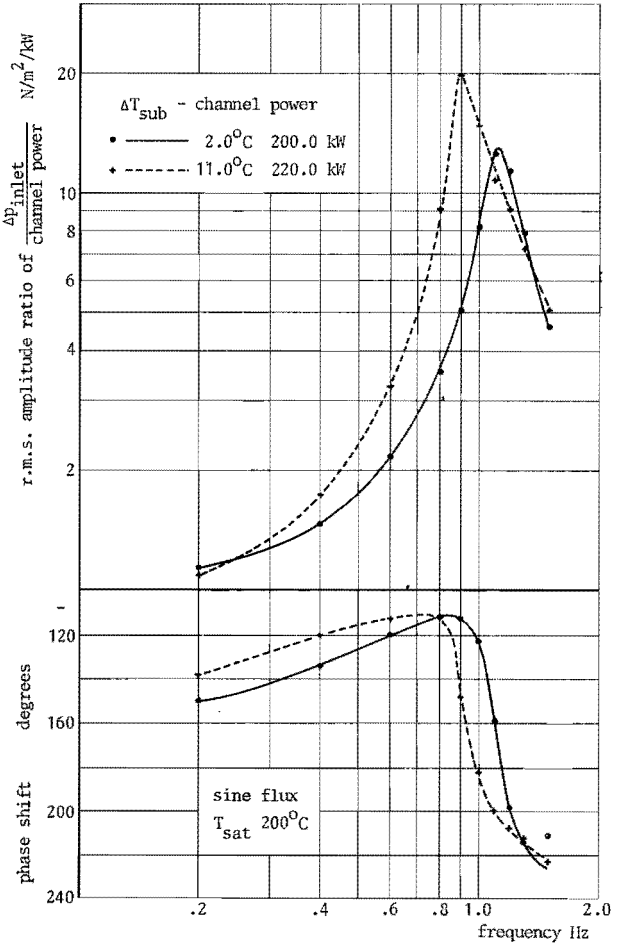

4.20. Power-to-Δp-inlet transfer function T_{sat} 200°C

In spite of this higher power in the vicinity of the resonance frequency, the phase-curve of power-to-Δp-inlet is less steep than at lowest subcooling. In both cases the phase differences at the position of the turning point are less than 180°. The curves affirm once again the greater stability of the system under a sine-shaped heatflux and emphasise that the transfer function experiments are only interesting as far as they shed light upon the stability in the presence of an external excitation force, but that they are

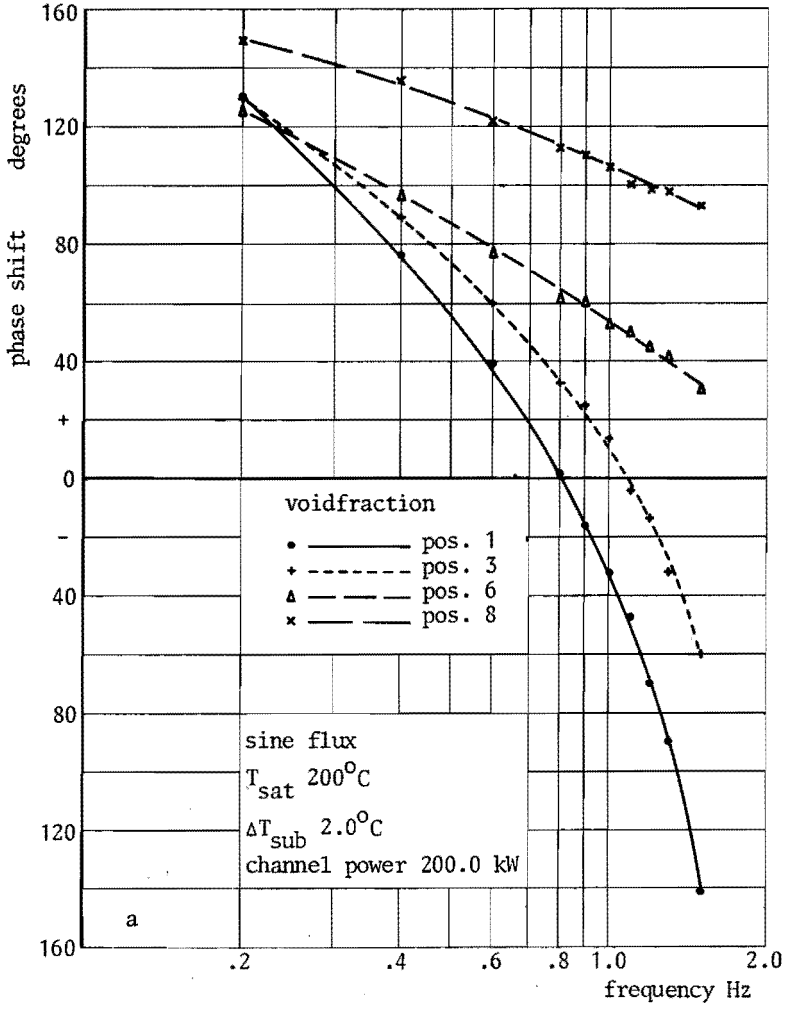

completely irrelevant with respect to the dependence of the stability on internally generated excitation forces.

The phase differences between the axially distributed void fractions and Δp-inlet are given in Fig. 4.21. The phase difference of void number 8 is less constant than at the uniform heatflux. For the rest, the curves are quite similar.

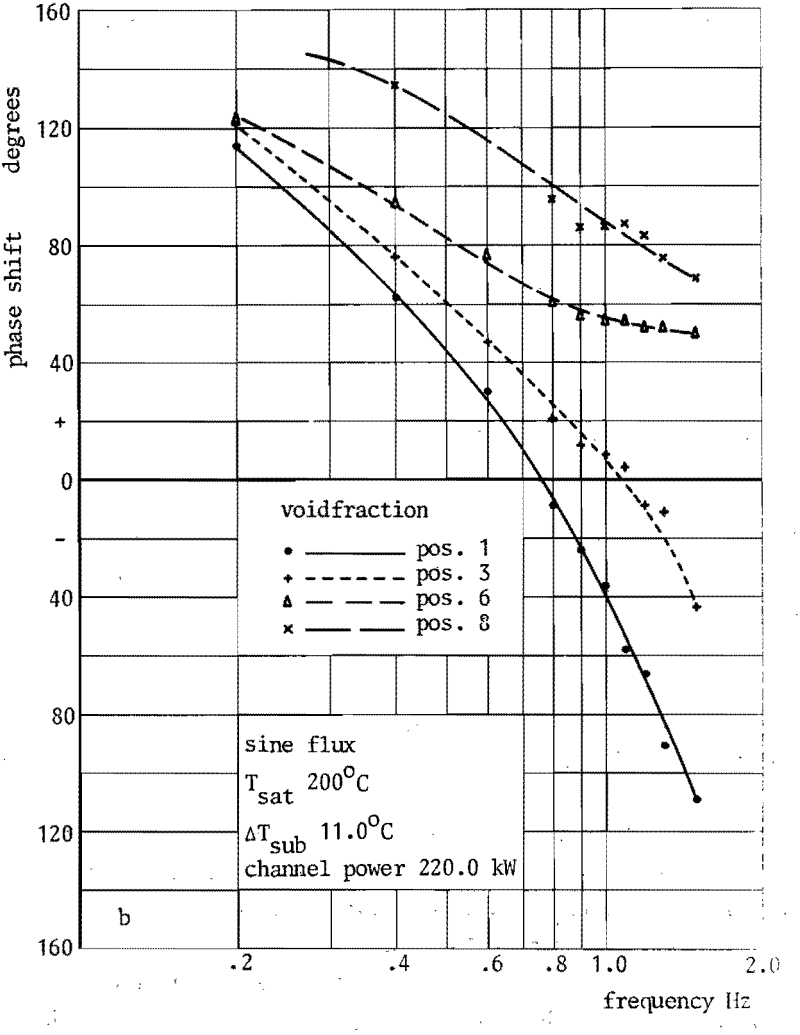

4.21. Frequency response of Δp-inlet-void phase shift T_{sat} 200°C

St. Pierre (S 1) has measured power-to-void transfer functions in a forced-circulation boiling channel at different axial positions. Owing to the absence of a resonance frequency these transfer functions are apparently different from those of the present study. Up to a frequency of 1 Hz there exists a similarity in the phase curves, but beyond this frequency, the curves of St. Pierre show notches, corresponding to nodes in the amplitude curves. The frequencies at which these notches appeared were functions of axial distance. The notch frequency was highest for those axial positions nearer the test section inlet and decreased with increasing axial distance. This notch frequency is evidently strongly dependent on the local void position. This corresponds to the image of the diagrams beyond a frequency of 1 Hz which shows a complete lack of relationship between the voids at different axial positions. Each void fraction seems to behave individually. Christensen (C 3) has derived an expression which allows the velocity of void propagation to be found from the notch frequency. The values of the propagation velocity calculated from this expression were not verified experimentally by St. Pierre. These velocities were found to be intermediate between the mixture and vapour cross-section averaged velocities.

For frequencies up to 1 Hz the axial variation in amplitude and phaselag of the transient void response was plotted, too, for two cases. In both cases the pressure was 600 psi (42.5 atm), the inlet velocity and subcooling in one case were 1.15 m/sec and 6.9°C respectively, in the other case these figures were 0.77 m/sec and 1.8°C. In both cases the void phaselag with respect to the power increased linearly with increasing axial distance. When the modulation frequency was increased, the phaselag per unit length also increased, which is consistent with a phaselag behaviour associated with transportation delay. With the lower subcooling the phase difference between the voids of upper and lower position, i.e. over a distance of 1.4 m, was 160° and with the moderate subcooling the difference was 85°, both at a perturbation frequency of 1 Hz. The flow behaviour for frequencies below 1 Hz was thus analogous to that of the present study. From the values mentioned

the void propagation velocities can be calculated as 3.1 m/sec in the lower subcooling case and 6 m/sec in the moderate subcooling case. These values are 3 to 4 times as high as the velocities calculated from the expression by Christensen. It therefore seems from the study by St. Pierre that two types of void propagation can be distinguished because the same behaviour at low frequencies demonstrates that the differences cannot be attributed exclusively to the different type of circulation.

It is interesting now to test the validity of the void propagation equation which Staub (S 3) developed. Starting from the theory of kinematic waves and accepting a number of reasonable simplifying assumptions, the ultimate solution of the void propagation equation gives the void response to both flow and power input oscillations to the fluid in a system where the power density is a function of the axial distance. The system is considered to be in thermodynamic equilibrium, i.e. the effect of subcooling is neglected.

The equation reads:

$$\frac{\partial<\alpha>}{\partial t} + C_o v_{in}(1+\varepsilon_f \sin \omega_f t) + \bar{V}_{gj} + C_o \frac{\Delta\rho}{\rho_f} \cdot \frac{q_o}{\rho_g h_{fg}} \cdot \frac{4L_b}{D} \cdot$$

$$(cz^+ + \frac{bz^{+2}}{2} + \frac{az^{+3}}{3}) \cdot (1+ \varepsilon_p \sin \omega_p t) \frac{\partial<\alpha>}{\partial z} =$$

$$\left[1- C_o \frac{\Delta\rho}{\rho_f} <\alpha>\right] \cdot \frac{q_o}{\rho_g h_{fg}} \cdot \frac{4L_b}{D} \cdot (c+bz^+-az^{+2}) \cdot (1+ \varepsilon_p \sin \omega_p t)$$

eq. 4.6.

where C_o represents the distribution parameter
$\bar{V}_{gj}$ the drift velocity of the vapour
ε_f the relative amplitude of the flow perturbation
ε_p the relative amplitude of the power perturbation
q_o the axially averaged heatflux

and the term $cz^+ + \frac{bz^{+2}}{2} - \frac{az^{+3}}{3}$ the axial shape of the heatflux.

For the meaning of the other parameters the reader is referred to the nomenclature.
In order to render the void propagation equation dimensionless, the following quantities have been defined:

length $z^+ = \frac{z}{L_b}$

time $t^+ = \frac{C_o v_{in} + \bar{V}_{gj}}{L_b} t$

vapour source term $\Gamma^+ = C_o \frac{\Delta\rho}{\rho_f} \cdot \frac{q_o}{\rho_g h_{sw}(C_o v_{in} + \bar{V}_{gj})} \cdot \frac{4L_b}{D}$

amplitude of the inlet liquid velocity $v'^+_{in} = \frac{C_o v_{in} \varepsilon_f}{C_o v_{in} + \bar{V}_{gj}}$

frequency of the power oscillations $\omega_p^+ = \frac{\omega_p L_b}{C_o v_{in} + \bar{V}_{gj}}$

frequency of the flow oscillations $\omega_f^+ = \frac{\omega_f L_b}{C_o v_{in} + \bar{V}_{gj}}$

Inserting these dimensionless parameters into eq. 4.6., the dimensionless form of the equation is obtained:

$$\frac{\partial \langle\alpha\rangle}{\partial t^+} + C_K^+ \frac{\partial \langle\alpha\rangle}{\partial z^+} = \Omega^+ \qquad \text{eq. 4.7.}$$

where C_K^+ represents the dimensionless velocity of the kinematic wave.

$$C_K^+ = 1 + v'^+_{in} \sin \omega_f^+ t^+ + \Gamma^+ (cz^+ + \frac{bz^{+2}}{2} - \frac{az^{+3}}{3}) \cdot$$

$$(1 + \varepsilon_p \sin \omega_p^+ t^+)$$

and the dimensionless reaction frequency Ω^+ is given by:

$$\Omega^+ = \left[1+C_o \frac{\Delta\rho}{\rho_f} <\alpha> \right] \frac{\rho_f}{C_o \Delta\rho} \Gamma^+ (c + bz^+ - az^{+2}) \cdot (1+ \varepsilon_p \sin \omega_p{}^+ t^+).$$

The equation 4.7. has been solved on the analogue computer for two conditions, viz. 200°C and 234°C both at 150 kW and zero subcooling.

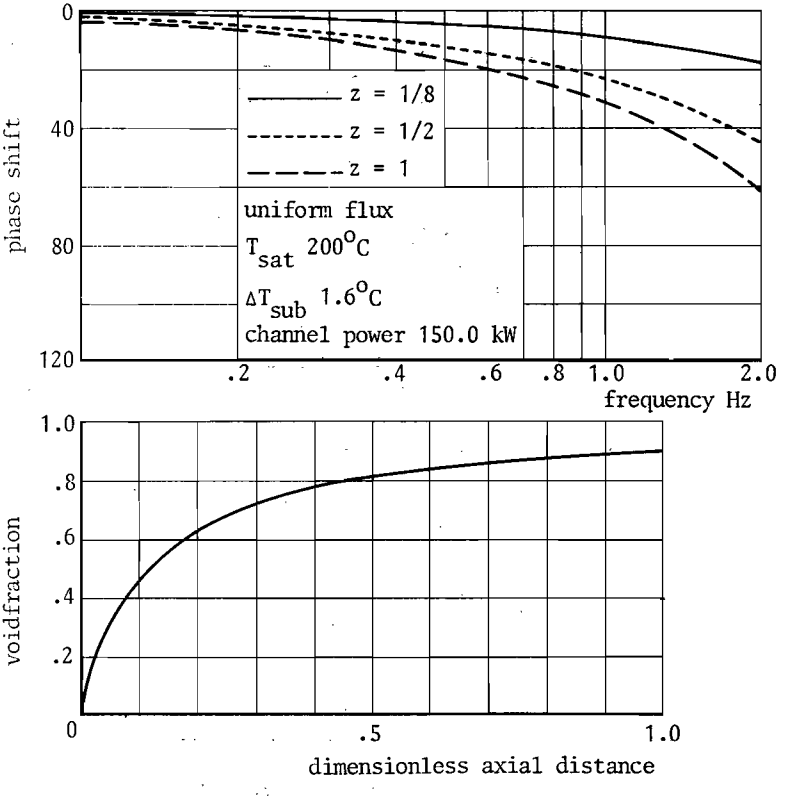

4.22. Frequency response of power-void phase shift according to Zuber (Z 1) T_{sat} 200°C

The values of the specific figures were taken to be:

200°C	234°C
C_o = 1.2	C_o = 1.2
v_{fi} = 1 m/sec	v_{fi} = 1 m/sec
$\bar{V}_{gj}$ = 0.55 m/sec	$\bar{V}_{gj}$ = 0.1697 m/sec

calculated from $\bar{V}_{gj} = 1.18 \left(\frac{\sigma . g \, \Delta\rho}{\rho_f^2}\right)^{\frac{1}{4}}$

Γ^+ = 19.8	Γ^+ = 11.12

Only the power was perturbed by setting $\varepsilon_f = 0$, and the heatflux was taken to be uniform, giving a = b = 0.

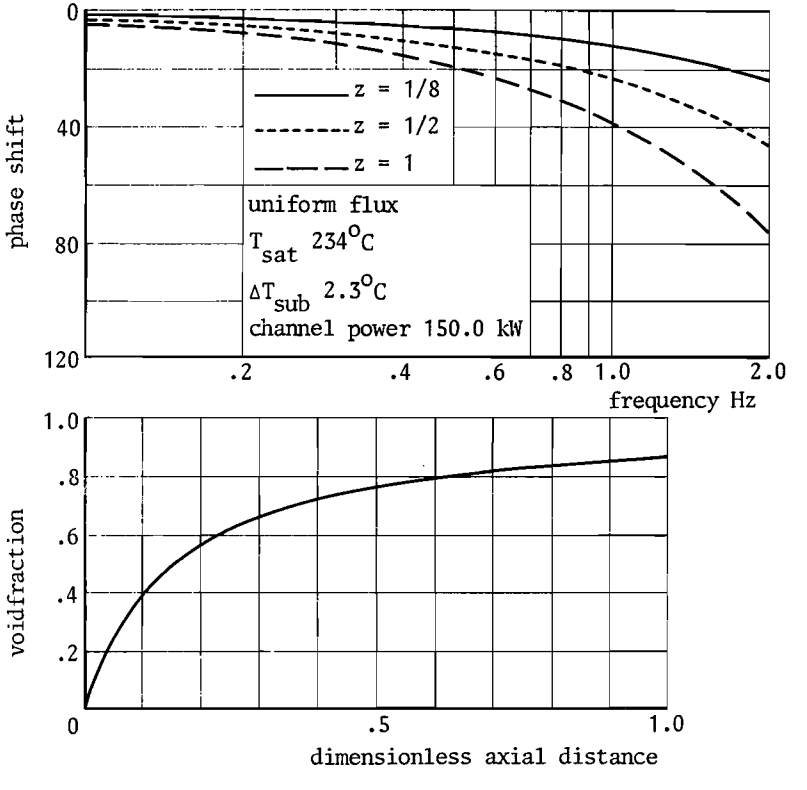

4.23. Frequency response of power-void phase shift according to Zuber (Z 1). T_{sat} 234°C

When taking $\frac{\partial<\alpha>}{\partial t^+}$ equal to zero the solution of equation 4.7. gives the stationary values of void fraction along the channel axis (Figs 4.22. and 4.23.). They are considerably higher than those measured from the experiment and also higher than one would expect on the score of a physical feeling that in connection with the high acceleration losses involved void fraction will never exceed values of 80-85%.

It must be noted that an essential lack of eq. 4.7. lies in the absence of a reasonance peak, owing to the fact that it is a differential equation of the first order. It does not describe the behaviour of a really possible system. For this reason only diagrams of the mutual phase angles of some void fractions have been given and diagrams of amplitudes have been omitted. As far as the relation to the power is concerned, the diagrams are not relevant. The values of z^+ have been chosen 1/8, $\frac{1}{2}$ and 1, assuming that they are representative of other positions. The phaseshift between the upper and lower void is 39^o at 200^oC and 34^o at 234^oC, both taken at 1.5 Hz. When extrapolating to $z^+ = 0$, the figures become 44^o and 38^o respectively. These values are substantially lower than the corresponding experimental ones. Besides, the phaseshift is not linear with z^+, especially not for the condition of 234^oC. These important deviations from the experimental results tend to the conclusion that the reliability of the void propagation equation derived by Zuber is not proportional to its complexity and intransparency and that the simple equation as inherently present in the conservation equations by far has the preference.

5. THEORETICAL STUDY

5.1. Description of the Mathematics

Introduction

Since 1960 (Q 1, F 2) many attempts have been undertaken to catch the physical behaviour of a boiling water channel in a mathematical system of differential equations, the number of which depends upon the number of physical variables one wants to take into consideration. However, in all cases the starting-point has been the formulation of the three principal laws of conservation, viz. of mass, momentum and energy, as derived for a homogeneous fluid. The necessity arose to adapt these equations so as to be able to apply them to any two-phase system, and in particular to a one-component two-phase system. A set of equations was developed that could claim a reasonable measure of probability. They have been accepted by anyone who occupies himself with the study of a boiling two-phase system. Several investigators judged it to be necessary to add some extra equations usually connected with the variation of the boiling boundary (J 2, J 5).

It is superfluous to review the models that have been developed during the last decade, because of the existence of two famous comprehensive studies, comparing a large number of mathematical models (N 2, B 4). In spite of the lapse of $2\frac{1}{2}$ years between these two studies, by which the most recent study (B 4) could contain models profiting by some more years of experience and knowledge, both studies concord in the general conclusion that the predictability of loop physics by all models is rather poor, the one being worse than another.

Contrary to other models, the HYDRO model predicts reasonably well the destabilising effect of subcooling. When applied to the Eindhoven experiments, the quantitative agreement of the computed results was, however, bad.

 The existence itself of so many models already indicates their

failure. The models can be classified in several ways, one of them being a distinction in lumped and distributed parameter models indicating the number of length increments the heated channel is divided into. The lumped parameter models having only a few increments have proved to produce the worst results. This is understandable from the fact that first the integration of the physical variables over one increment is necessarily bad, and secondly the connections of two subsequent increments introduce severe discontinuities. The division into non-linear and linearised models shows smaller differences. The general pattern of deficiency also holds with respect to the linearised model as described by Spigt (S 2). The destabilising effect of subcooling was completely absent; for certain values of subcooling it appeared to be even impossible to detect a threshold power applying the accepted criterion for it, and the frequencies did not agree, to say nothing of phase angles and other fundamental quantities. Only at zero subcooling the results were reasonably adequate. Several attempts have been undertaken to remedy these drawbacks by modifying the energy equations, paying particular attention to the region of subcooled boiling. Other correlations for slipfactor and two-phase friction were tried out, but without promising results. It therefore, was decided by the author to abandon this model.

It is the author's opinion that it is a misunderstanding to think that the rescue out of the problems related to the deficiency of theoretical models would come from models based on fundamental principles (Z 2), (W 1). It is then stated that no previous information is necessary with respect to the slip between the phases, two-phase friction, departure of nucleate boiling etcetera, because these quantities will be calculated automatically by solving the fundamental equations. Even if that is true, the solution of the equations requires foreknowledge with respect to the number of nucleation sites of a particular material, the temperature profile perpendicular to the bubble surface, the mechanisms that determine the growth of the bubbles on the heated wall and in the fluid, and the mechanisms that dominate the diffusion process of the bubbles in the liquid layer attached to the heated surface as well as in

the bulk. Whereas measurement of the familiar unknowns, owing to their character of representing average values, although difficult, is in principle possible in an existing experimental loop, it is intrinsically unfeasible with respect to fundamental data. The ability of verifying these data under practical conditions is completely lacking.The problem of the failure of theoretical models for engineering purposes still exists, with the difference that the unknown functions change from a macroscopic to a microscopic nature.

In spite of the above-mentioned bad experiences with models, and at the risk of adding a new specimen to their existing number, it was resolved to make an attempt. In any case it could be investigated to what extent one could rely upon the generally accepted set of equations. In view of the inherent disadvantages of digital computers with respect to the integration method, and on account of the requirement that the development should take only a short time and be not too costly, the choice had to fall upon the use of an analogue computer. Because of the known objections against lumped parameter models, an essential different attack was decided upon, viz. integration over length instead of over time (S 5). It is evident that this demand requires a relatively big analogue computer, equipped with about 150 amplifiers and a memory for the functions calculated in the previous time step, and unfortunately such a machine was not available in the neighbourhood of Eindhoven. But we were made aware of the existence of the Continuous System Modelling Program (CSMP) developed and owned by the IBM. This program formed the link between a digital computer, not really wanted but available, and an analogue computer, wanted but not available. It simulates all specific functions of an analogue computer in a digital way. It enables the program of the model to be written in a manner as is usual for an analogue computer, but the different blocks of the blockdiagram are simulated by digital subprograms. It is perhaps not necessary to remark that the basic functions as multiplication and adding, which take up a great deal of the capacity of an analogue computer and which constitute precisely the weak point of that type of computer from the point of view of accuracy, are realised digitally.

 The particular functions that were of fundamental importance in

order to solve the set of differential equations under consideration, were the AFGEN and the RKS procedures. The subprogram AFGEN represents a function generator, which means that giving an adequate number of coordinates causes this program to generate a suitable function through these points. The RKS subprogram is one of 7 available integration procedures. Providing the definition of the desired variable and reading its starting value is sufficient, after calling the chosen integration procedure, to put the integration proces into operation. It is this subprogram that constitutes the greatest feature of the CSMP. On account of the experience gained from a similar, but yet essentially different study (R 2), and considerations of theoretical numerical analysis, it was decided to apply the Runge-Kutta integration subprogram with variable stepsize, the size to be determined depending upon the 5th derivative of the integrated function.

Basic thoughts

It was from the beginning the intention to develop a simple, one-dimensional, more or less primitive model, without superfluous fringes in order to prevent undesired intransparency. The phenomenon of unstable behaviour was assumed to be a pure channel effect without additional influence of the external system. Therefore, the pressure difference across the channel from inlet to outlet was kept constant and the system pressure was not allowed to change with time, i.e. the effect of the condenser was omitted. Neither were the effects of heat capacity and thermal conductivity of the channel walls estimated to be essential for the occurrence of unstable behaviour of a boiling channel. The heat was assumed to be transferred instantaneously to the fluid, which suggests a heating element with an infinitely small wall-thickness. Further, in accordance with the experimental scope, it was intended to produce qualitative effects of some important independent, external parameters. The agreement of the results in absolute sense with the experimental values was assumed to be of secondary importance. Starting from good qualitative correspondence with experiments it must in principle be possible to change adequate parameters so as to fit the experimental results quite accurately. This does not mean, however, that arbitrary values

of the constants have been used. On the contrary, the values of all constants have been carefully determined from the experiment. But once having these constants fixed, they have not been changed during the computations, which might be desired in order to obtain results in better agreement with the experiment. This principle also determines the attitude with respect to the correlation functions. It is senseless to carry out an elaborate comparative study of different correlations. A generally valid correlation does not exist owing to the many imponderable parameters that differ from system to system. A rough observation of the correlation in question provides sufficient insight into the dependence of and the effect on the main variables, such as void fraction and steam quality, and the influence of these variables upon the stationary as well as the dynamic results is well known. It is unavailing to hunt for a proper correlation that fits the experimental results of its own. It is best to adopt a correlation and to adapt it rigorously to the experiment, or to develop an arbitrary function provided it fits the experimental values. It is of more importance to get correct void fractions than to use a theoretically derived correlation. The particular correlation functions which in this case have been used will be discussed separately.

Correlation for the slipfactor

In chapter 3, comprising the steady-state measurements, it was demonstrated that the correlation as proposed by Bankoff (B 2), reading $S = \frac{1-\alpha}{K-\alpha}$, is a very attractive one for two reasons. First it is based upon physical considerations, and secondly the results of the measurements when plotted in terms of void fraction and factor K give reasonable curves with a scatter only in the region of low void fractions, i.e. the region of subcooled boiling. Factor K is consequently not rather constant, as defined by Bankoff, nor a weak function of pressure as suggested by Jones (J 2), but a quadratic function of void fraction. There is an encouraging similarity between the curves belonging to different conditions of pressure and shape of heatflux. In the model factor K has been applied in the general form $K = a_1+a_2\alpha+a_3\alpha^2$, the constants a_1, a_2

and a_3 being only dependent on system pressure and flux shape. An attending feature is that the derivative of void fraction with respect to steam quality, necessary in the calculations, is a very convenient function and reads

$$\frac{\partial \alpha}{\partial x} = \frac{\rho_s}{\rho_w} \cdot \frac{\alpha^2}{x^2} \cdot \frac{1}{a_1 - a_3 \alpha^2} \quad .$$

Correlation for the two-phase friction multiplier

Despite the objections referred to in chapter 3.2. it was decided to use the two-phase friction multiplier of Martinelli-Nelson, again considering that the general form of the expression was more important than the absolute correctness of the constants. Under general form is understood the functional relationship between R and the steam quality or void fraction. The experimental results as far as they concern the two-phase friction were not sufficiently consistent to suggest another correlation, and, besides, it is a widely used correlation in theoretical models. It was, however, well kept in mind that this correlation lends itself favourably to adaptation in case the results were too divergent.

Subcooled boiling

The first investigator to tackle the problem of subcooled boiling was Bowring (B 3). He distinguished two fundamental questions, viz. Where does subcooled boiling start? and Which law governs the heat distribution between water and steam phase? He solved the first question by adopting the results of the study by Jens and Lottes (J 1). In order to answer the second question Bowring conceived a heat distribution parameter κ smaller than one, which represented the fraction of the heat supplied, used to form vapour. The remaining fraction raised the temperature of the fluid. In macroscopic sense the assumption is reasonable, but in microscopic sense it is not. For actually,studies of void generation have proved that all heat is transferred directly to the one-phase liquid layer, attached to the heated wall, and that bubbles are being generated inside this layer by transfer of heat through the liquid. In macroscopic sense, however, Bowring's postulate can be justified. The heat dis-

tribution parameter as defined by Bowring jumps from zero in the highly subcooled region to a constant value in the region of moderate subcooling and changes to one in the region of bulk boiling. This constant value κ in the region of subcooled boiling is physically very improbable and introduces serious discontinuities into a mathematical model.

Levy (L 2) has developed a conception of subcooled boiling on a theoretical basis. The point of bubble departure from the heated surface is determined from a bubble force balance and from the single phase liquid turbulent temperature distribution away from the heated wall. However, this point once determined, the physical basis is abandoned when calculation of the local vapour weight fraction in the subcooled region is concerned. Two boundary conditions are stated, namely that the derivative of steam quality with respect to the distance along the channel is zero at the point of bubble departure, and that the true local vapour weight fraction approaches the local vapour weight fraction calculated from a heat balance and thermal equilibrium at the point where the heating power integrated over the distance exceeds considerably the negative heatcontent, represented by $c.\Delta T_d$. The quantity c is the specific heat and ΔT_d the difference between the mean fluid temperature and the local saturation temperature at the point of bubble departure. Then a simple exponential relation for the true local vapour weight fraction is given which satisfies the boundary conditions. The main disadvantage of the relation is that practically the liquid temperature nowhere reaches the saturation temperature, i.e. that bulk boiling never occurs, not even at zero inlet subcooling. This is very unlikely.

In the present model the point of bubble departure was calculated by accepting the formulation by Levy. As regards the heat distribution parameter κ, neither the constant value of Bowring, nor the exponential value of Levy could convince the author of its reliability, and therefore an expression was composed which was equally arbitrary as the other two, but based upon a physical feeling. The expression reads

$\kappa = \frac{T-T_s}{T_{sat}-T_s}$, where T represents the liquid temperature,
T_{sat} the saturation temperature and
T_s the liquid temperature at the point of bubble departure.

According to this expression κ runs from zero, when $T=T_s$, to one, when $T=T_{sat}$, by a monotonic function. When testing this expression in the model it appeared that, when κ was used according to its true definition, i.e. if the fraction of heat represented by κ is used exclusively to evaporate water, then the increase of void is too large in comparison with the rise of the water temperature, resulting in a considerable steam quality at the exit of the heated channel, whereas the fluid temperature is still below the saturation temperature even at very small values of inlet subcooling. In order to remedy this effect while still maintaining the boundary values of one and zero, it was decided to raise κ to a higher power. Preliminary calculations showed that a value of 3 provided credible results. It accelerates the heating of the fluid and suppresses the generation of steam.

Set of equations

The basic equations are given in the literature (B 10)

Simplified equations

The general three-dimensional equations are commonly simplified to a one-dimensional form by accepting cross sectional averaged quantities of the physical variables. The two-phase character of the system is introduced by the definition of the void fraction.

The three simplified equations read:

conservation of mass

$$\frac{\partial}{\partial t}\{\rho_w(1-\alpha)+\rho_s\alpha\}+\frac{\partial}{\partial z}\{\rho_w v_w(1-\alpha)+\rho_s v_s\alpha\}=0$$

conservation of momentum

$$\frac{\partial}{\partial t}\{\rho_w v_w(1-\alpha)+\rho_s v_s\alpha\}+\frac{\partial}{\partial z}\{\rho_w v_w^2(1-\alpha)+\rho_s v_s^2\alpha\}=-F-\frac{\partial p}{\partial z}+$$

$$-g\{\rho_w(1-\alpha)+\rho_s\alpha\}$$

conservation of energy

$$\frac{\partial}{\partial t}\{\rho_w h_w(1-\alpha)+ \rho_s h_s \alpha\}+\frac{\partial}{\partial z}\{\rho_w h_w v_w(1-\alpha)+ \rho_s h_s v_s \alpha\} = q_m$$

When assuming the physical properties to be constant, i.e. independent of pressure and temperature, and substituting the total mass flowrate, reading

$$W = (1-\alpha)\ \rho_w v_w + \alpha\rho_s v_s$$

then the equations can be written in terms of steam quality, void fraction and mass flowrate, viz.:

conservation of mass

$$(\rho_w - \rho_s)\ \frac{\partial \alpha}{\partial t} - \frac{\partial W}{\partial z} = 0 \qquad \text{eq. 5.1.}$$

conservation of momentum

$$\frac{\partial W}{\partial t} + \frac{\partial}{\partial z}\left\{\frac{(1-x)^2}{(1-\alpha)\rho_w} + \frac{x^2}{\alpha\rho_s}\right\} W^2 = - \frac{\partial p}{\partial z} - F - \{\rho_w(1-\alpha) + \rho_s\alpha\}g \qquad \text{eq. 5.2.}$$

Owing to the assumption of a heat distribution parameter κ in the region of subcooled boiling, one is forced to split the energy equation into two parts, one for the waterphase and one for the steamphase. The splitting has been consistently realised in such a way that the two fractions of heat are exclusively used to raise the enthalpy of the waterphase and of the steamphase respectively. The split energy equation then reads:

conservation of energy of the waterphase:

$$\frac{\partial}{\partial t}\{\rho_w(1-\alpha)\left(h_w - \frac{p}{\rho_w}\right)+ \rho_s\alpha\left(h_z - \frac{p}{\rho_w}\right)\} + \frac{\partial}{\partial z}\{(1-x)h_w + xh_z\}W +$$

$$- \frac{W}{\rho_w} \cdot \frac{\partial p}{\partial z} = (1 - \kappa)q_m \qquad \text{eq. 5.3.}$$

conservation of energy of the steamphase:

$$\frac{\partial}{\partial t}\{\rho_s\alpha(h_{sw}+\frac{p}{\rho_w}-\frac{p}{\rho_s})\}+\frac{\partial}{\partial z}xWh_{sw}-\frac{xW}{\rho_s}(1-\frac{\rho_s}{\rho_w})\frac{\partial p}{\partial z}=\kappa q_m \quad \text{eq. 5.4.}$$

In view of the relative low pressures involved it was assumed valuable to take into consideration the pressure-volume terms, $\frac{p}{\rho_w}$ as well as $\frac{p}{\rho_s}$, because they make up at most 5% of the total energy.

In order to complete the 4 basic equations the following relations have been introduced:

slipfactor $S=\frac{1-\alpha}{K-\alpha}$ where $K=a_1+a_2\alpha+a_3\alpha^2$,

two-phase friction multiplier R according to Martinelli-Nelson,

heat distribution parameter $\kappa=(\frac{T-T_s}{T_{sat}-T_s})^3$.

Substitution of the slipfactor in the physical expression

$S=\frac{1-\alpha}{\alpha}\cdot\frac{x}{1-x}\cdot\frac{\rho_w}{\rho_s}$ yields:

$$\alpha=\left[1-a_2+\frac{\rho_s(1-x)}{\rho_w x}-\sqrt{\{1-a_2+\frac{\rho_s(1-x)}{\rho_w x}\}^2-4\,a_1a_3}\right]/2a_3$$

The common expression for the frictional-pressure term reads:

$$F=\frac{f_{ch}}{2\,\rho_w D}W^2R(x)$$

In the enthalpy terms the contributions of potential and kinetic energy have been neglected, resulting in:

$h_w=cT \qquad h_z=h_{w_{T=T_{sat}}}$

The saturation temperature follows from:

$$T_{sat}=p.\frac{\partial T_{sat}}{\partial p}$$

The derivatives with respect to z of the variables α and h_z have been written in the partial derivative forms

$$\frac{\partial \alpha}{\partial z} = \frac{\partial \alpha}{\partial x} \cdot \frac{\partial x}{\partial z} \qquad \frac{\partial h_z}{\partial z} = \frac{\partial h_z}{\partial p} \cdot \frac{\partial p}{\partial z}$$

The local heat input q_m is a function of z and t.
Hence, the four unknowns are W, p, x and h_w.
It must be emphasised that no extra equations have been added.
When indicating the time derivatives by t_1, t_2, t_3 and t_4 representing respectively

$$\frac{\partial \alpha}{\partial t}, \quad \frac{\partial W}{\partial t},$$

$$\frac{\partial}{\partial t}\{\rho_w(1-\alpha)(h_w - \frac{p}{\rho_w}) + \rho_s \alpha(h_z - \frac{p}{\rho_w})\} \text{ and } \frac{\partial}{\partial t}\{\rho_s \alpha(h_{sw} + \frac{p}{\rho_w} - \frac{p}{\rho_s})\},$$

and writing the equations in terms of the four variables, the equations read:

$$A_0 t_1 - \frac{\partial W}{\partial z} = 0 \qquad \text{eq. 5.5.}$$

$$t_2 + A_1 \frac{\partial W}{\partial z} + A_2 \frac{\partial x}{\partial z} + \frac{\partial p}{\partial z} + A_3 = 0 \qquad \text{eq. 5.6.}$$

$$t_3 + A_4 \frac{\partial W}{\partial z} + A_5 \frac{\partial x}{\partial z} + A_6 \frac{\partial p}{\partial z} + A_7 \frac{\partial h_w}{\partial z} = A_8 \qquad \text{eq. 5.7.}$$

$$t_4 + A_9 \frac{\partial W}{\partial z} + A_{10} \frac{\partial x}{\partial z} + A_{11} \frac{\partial p}{\partial z} = A_{12} \qquad \text{eq. 5.8.}$$

The expression for the terms A_0 up to A_{11} comprising no differential terms, have been summarised in Appendix C. Substitution of the energy equation for the steamphase in the momentum equation results in the elimination of $\frac{\partial p}{\partial z}$ in the momentum equation. The set of equations written in a changed sequence then ultimately read:

$$\frac{\partial W}{\partial z} = t_1 A_0 \qquad \text{eq. 5.9.}$$

$$(A_9-A_1A_{11})\frac{\partial W}{\partial z} + (A_{10}-A_2A_{11})\frac{\partial x}{\partial z} = A_{12}-t_4+A_{11}(t_2+A_3)$$ eq. 5.10.

$$A_1\frac{\partial W}{\partial z} + A_2\frac{\partial x}{\partial z} + \frac{\partial p}{\partial z} = -(t_2+A_3)$$ eq. 5.11.

$$A_4\frac{\partial W}{\partial z} + A_5\frac{\partial x}{\partial z} + A_6\frac{\partial p}{\partial z} + A_7\frac{\partial h_w}{\partial z} = A_8 - t_3$$ eq. 5.12.

By writing the equations in this manner it appears possible to avoid algebraic equations which would need an iterative solution or a matrix solution. Either alternative complicates the solution procedure considerably.

As mentioned earlier, the simultaneous integration in the z-direction has been carried out by means of the Runge-Kutta method with variable stepsize. Integration in the time has been executed by using the Euler approximation, thus:

$$t_1 = \frac{\alpha_i - \alpha_{i-1}}{\Delta t}$$ eq. 5.13.

$$t_2 = \frac{W_i - W_{i-1}}{\Delta t}$$ eq. 5.14.

$$t_3 = \frac{1}{\Delta t}\{\rho_w(1-\alpha_i)(h_{z_i} - \frac{p_i}{\rho_w}) + \rho_s\alpha_i(h_{w_i} - \frac{p_i}{\rho_w}) - \rho_w(1-\alpha_{i-1}).$$

$$(h_{z_{i-1}} - \frac{p_{i-1}}{\rho_w}) - \rho_s\alpha_{i-1}(h_{w_{i-1}} - \frac{p_{i-1}}{\rho_w})$$ eq. 5.15.

$$t_4 = \frac{1}{\Delta t}\rho_s\{\alpha_i(h_{sw} + \frac{p_i}{\rho_w} - \frac{p_i}{\rho_s}) - \alpha_{i-1}(h_{sw} + \frac{p_{i-1}}{\rho_w} - \frac{p_{i-1}}{\rho_s})\}$$ eq. 5.16.

The value of Δt must be a compromise between desired accuracy and minimum computing time.

Boundary conditions

The inlet conditions of the fluid for each time step were determined to be x = 0, and T equal to a prescribed value, defined by the desired subcooling.

The total pressure drop across the boiling loop was assumed to be constant in the time. Besides the pressure loss across the heated channel, this pressure drop included the pressure loss in the downcomer and across the inlet of the channel.

The iteration equation reads:

$$\Delta p = \rho_w g L - \frac{k_{in} W^2}{2\rho_w} - \frac{f_d}{2\rho_w D_d} W^2 \left(\frac{A_r}{A_d}\right)^2 \nu_d L - \frac{\partial}{\partial t}\left(\frac{A_r}{A_d} W \nu_d L\right)_{z=0}$$

eq. 5.17.

The terms of the right hand member represent consecutively the contribution of the static head, the inlet loss of the boiling channel, the friction loss in the downcomer and the acceleration loss in the downcomer . The constants f_d, D_d and A_d represent the friction factor, hydraulic diameter and cross-section of the downcomer respectively. A_r represents the cross section of the boiling channel and $\nu_d L$ the equivalent length of the downcomer taking into account the friction due to the passage through sub-cooler and belonging pipings.

For each time step this Δp was checked. When the difference between the value of Δp and zero arrived at a prescribed tolerance range the iteration stopped, else the iteration continued with an adapted value of the inlet velocity.

Order of the computation

After reading the values of the geometrical and physical constants, the following values, determined from the experiment, were fed into the machine: the factor of the inlet pressure loss k_{in}, the constants in the slip correlation a_1, a_2 and a_3, the friction factor of the downcomer f_d, and the friction factor of the channel f_{ch}. All values have been kept constant during the computations except a_1, a_2 and a_3 which have been chosen in accordance with the shape of the heatflux distribution.

The specific conditions were fixed by reading values of the inlet subcooling and the heating power. The computation was started at zero time, i.e. with all time derivatives equal to zero. The results of this run were used as starting values for the next run at time $t = \Delta t$. The computation continued by raising the time successively by Δt.

The non-linearity of the equations finds its expression in the variation of the physical quantities with time. A step input of the power, analogous to the experimental procedure, results in a sinusoidal response of the variables with a constant frequency, namely the resonance frequency of the system. The response converges or diverges with time depending on the stability of the system. This consequently determines the instability criterion. At time t=0.5 sec. the channel power was increased stepwise with 5 or 10 kW and the response of the system was computed over a period of 4.5 sec., sufficiently to establish convergency or divergency of the varying quantities. The transition from t=0 to $t = \Delta t$ caused a small disturbance. This was the motive to allow the computing process to stabilise over the period of 0.5 sec. This period, however, was too short for the system to reach the steady state condition corresponding to time t=0. The extent to which the system deviated from the steady state did not affect the stability threshold but it influenced the magnitude of amplitudes. An impression of the correctness of the amplitude values predicted by the model cannot be obtained therefore from the computations aimed at determining the stability threshold.

Transfer functions were computed by simulating the experimental procedure of sinusoidally oscillating the input power. In order to avoid the amplitudes of the various variables reaching inconveniently large values the amplitude of perturbing power was reduced for higher frequencies. In order to allow the amplitudes and phases to stabilise at a constant value after increasing stepwise the frequency the computation was continued during 5 periods for each frequency. For the purpose of limiting the computing time involved the time step was adapted to the frequency in such a way that each period contained a fixed number of 20 time steps independent of frequency.

The output of the different variables was organised in such a way that they were printed at fixed values of z, attained by interpolation between the steps as applied by the Runge-Kutta process. The variables printed are z, void fraction, water velocity, temperature, saturation temperature, slipfactor, pressure and steam quality.

5.2. Results and comparison with experiments

A limited number of characteristic conditions were selected for the computations, namely:

	T_{sat}	ΔT_{sub}
uniform heatflux	200°C	1°C
		10°C
		30°C
sine-shaped heatflux		1°C
		10°C
asymmetric axial heatflux		1°C

transfer functions - uniform heatflux, ΔT_{sub} 1°C, channel power 150 kW

The subcooling values were chosen so as to render possible the observation of the specific effects. The channel powers in each condition were chosen so as to shut in the instability threshold in case of the uniform heatflux within 5 or 10 kW.

S t e a d y - s t a t e c a l c u l a t i o n s

Because the main interest concerned the behaviour under dynamic conditions, no results are available for lower channel powers. The values of the physical quantities provided by the calculations allow, however, a sufficient comparison with the experimental results.

U n i f o r m h e a t f l u x

The inlet flow velocity (Fig. 5.1.) at moderate channel powers is quite correct, but higher powers show too great velocities, deviating up to about 10%. This is also the case for higher subcooling values. The exit void fraction (Fig. 5.2.) fits perfectly

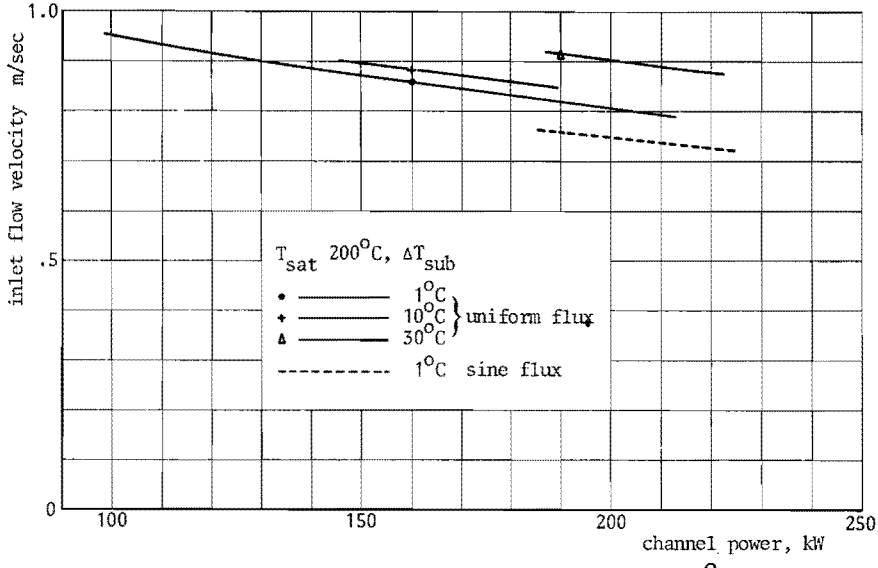

5.1. Inlet flow velocity versus channel power T_{sat} 200°C, various subcoolings

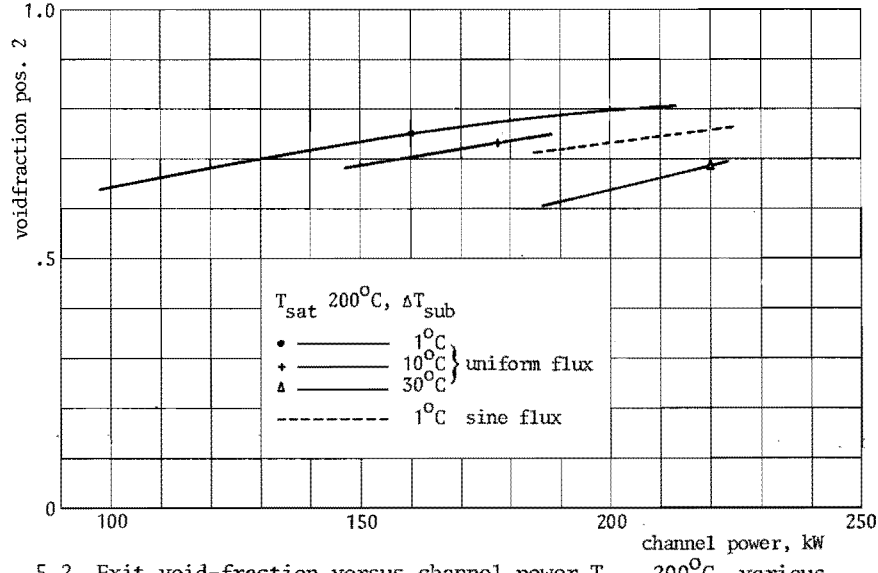

5.2. Exit void-fraction versus channel power T_{sat} 200°C, various subcoolings

cooling was 11°C. The axial void distribution (Fig. 5.3.) is almost perfect for the higher positions. At the lower positions the void fraction is too low. This trend is more pronounced at 10°C subcooling. The heat distribution parameter does not seem to be represented very adequately by the accepted function of K. The function can be improved by chosing a smaller exponent. At higher positions the void is a few per cent, too high.

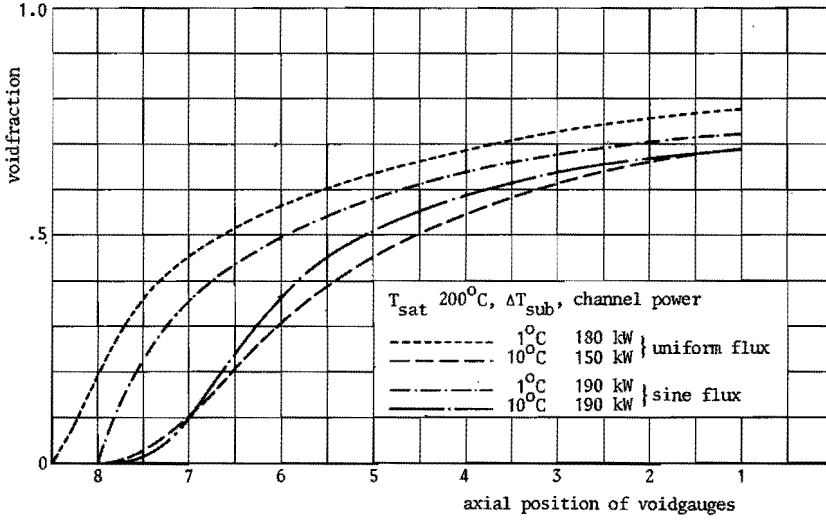

5.3. Axial void distribution T_{sat} 200°C, various subcoolings

S i n e - s h a p e d h e a t f l u x

Compared with the experimental results concerning the inlet flow velocity and the exit void fraction as well as the axial void distribution , the results obtained with the non-uniform heatflux show a similar agreement or deviation as observed from the uniform flux results. The axial void distribution at a subcooling of 10°C indicates, however, better agreement for the lower positions than for the higher.

D y n a m i c c a l c u l a t i o n s

U n i f o r m h e a t f l u x

Curves of the inlet flow velocity responding to a power perturbation

are given in Fig. 5.4. for the condition of uniform heatflux and a subcooling of $1^{o}C$. Only curves of the channel powers on both sides of the instability thresholds have been plotted. The 180 kW curve is slightly converging, the 185 and 190 kW ones are indifferent with an indication of divergency at 190 kW and the 195 kW curve is divergent. The threshold power is seen to be 190 kW. The transition from stable to unstable behaviour appears to be very smooth, with

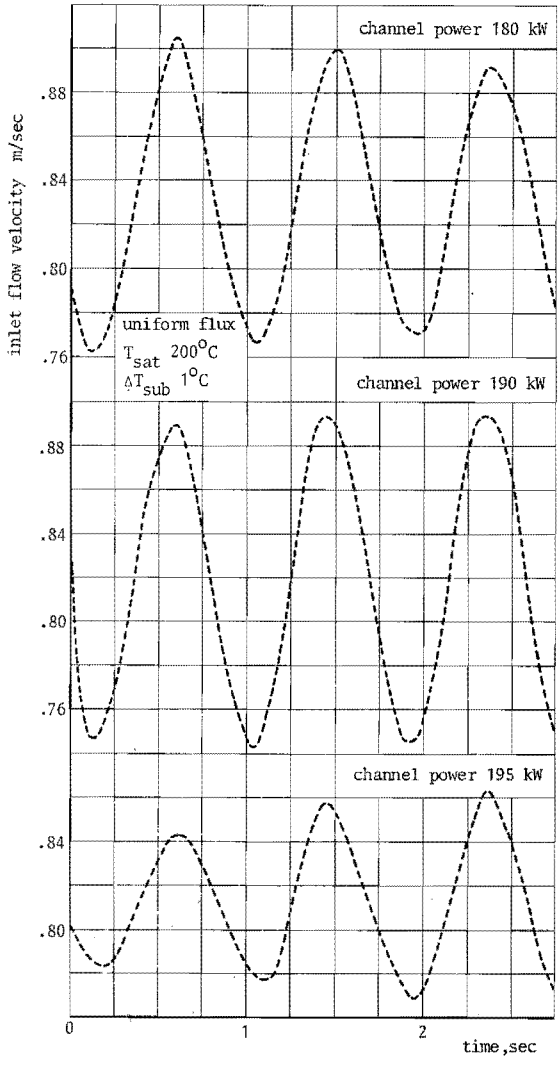

5.4. Response curves of inlet flow velocity T_{sat} 200°C, ΔT_{sub} 1°C

a transition zone of about 10 kW. This corresponds rather well with the experimental observations. Increasing the subcooling to $10^{o}C$ moves the threshold power to the considerable lower value of 155 kW and shows a quite distinct change from stable to unstable behaviour (Fig. 5.5.). The divergence at 155 kW develops very quickly

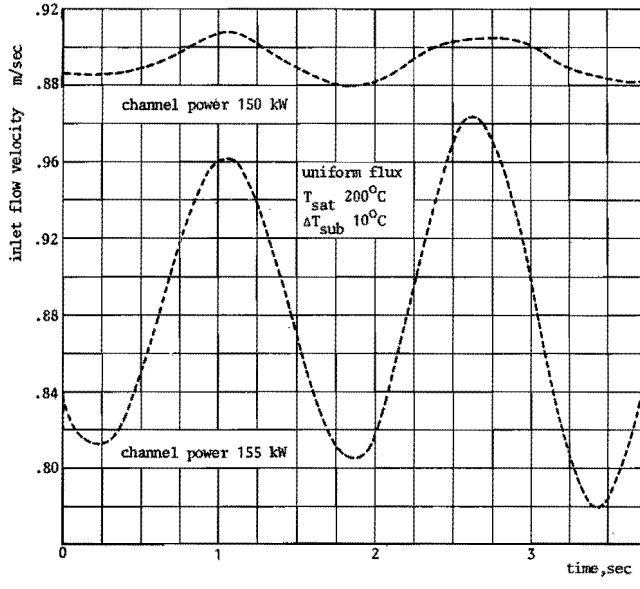

5.5. Response curves of inlet flow velocity T_{sat} $200^{o}C$, ΔT_{sub} $10^{o}C$

similarly to the experimental observations. The oscillation frequency has fallen from 1.14 cps at $1^{o}C$ subcooling to 0.63 Hz. This frequency is not affected by the change in amplitude nor by the channel power. Lower channel powers indicate that a slight power dependency of the frequency exists, viz. the frequency increases with power. A subcooling of $30^{o}C$ has a strong stabilising effect and shifts the threshold power up to 230 kW and the frequency down to 0.44 Hz (Fig. 5.6.). This stabilising influence is more pronounced than was established from the experiments. It must obviously be imputed to the effect of subcooled boiling. The steady-state results showed the void fraction at lower positions to be less than the measured values and it is clear that this is very important, in

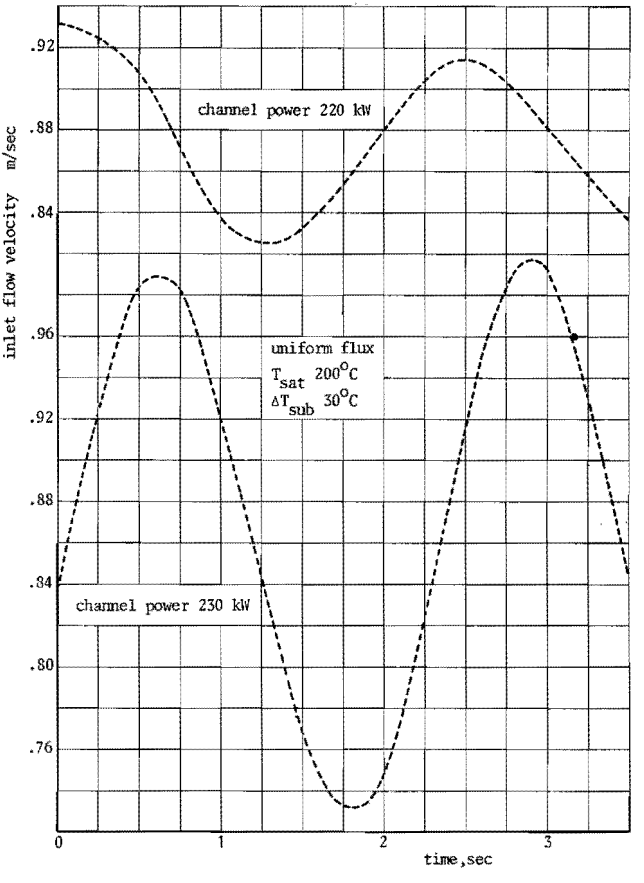

5.6. Response curves of inlet flow velocity T_{sat} 200°C, ΔT_{sub} 30°C

particular to high subcooling values. The computations showed that even at the exit the saturation temperature had not been reached. This means that all over the channel length only subcooled boiling was present at 30°C subcooling. The results mentioned have been summarised in table 5.1.

Comparison with table 4.1. indicates a promising correspondence with the experimental results. Although the absolute figures do not fit completely, the trend of the subcooling effect is obvious.

Table 5.1. Threshold powers and related frequencies obtained from the non-linear model

Uniform heatflux T_{sat} 200°C

ΔT_{sub}	threshold power in kW	frequency in Hz
1°C	190	1.14
10°C	155	0.63
30°C	230	0.44

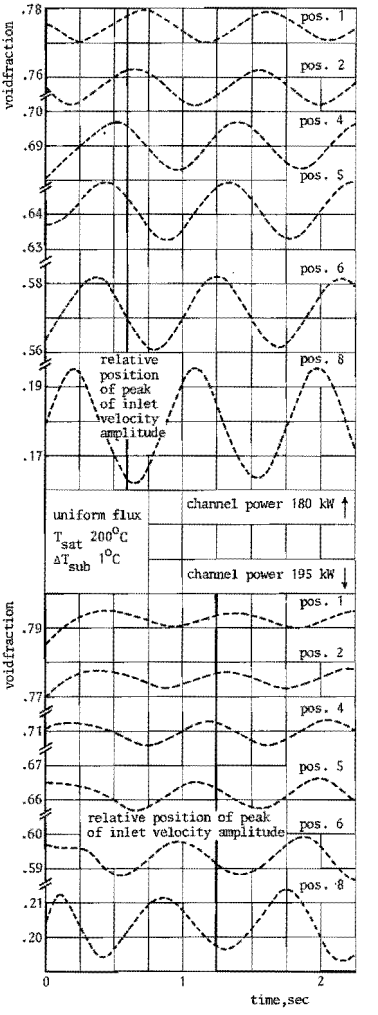

144 5.7. Response curves of axial void distributions T_{sat} 200°C, ΔT_{sub} 1°C

The curves of the void fraction at different axial positions have been given in Figs 5.7. up to 5.9. for different subcoolings. At a subcooling of $1^{o}C$ the void amplitudes are not comparable owing to the dependence of the amplitudes on the magnitude of the disturbance. The upper voids show a short running time before the correct phase and amplitude are established. In the diagrams the position of a maximum has been indicated in the curve of the inlet flow velocity, which enables the phase shifts between voids and flowrate to be determined. For the case of $10^{o}C$ subcooling (Fig. 5.8.), the maximum void amplitude lies at a position intermediate between positions 6 and 7. Position 8 is lacking owing to the absence of void there. The

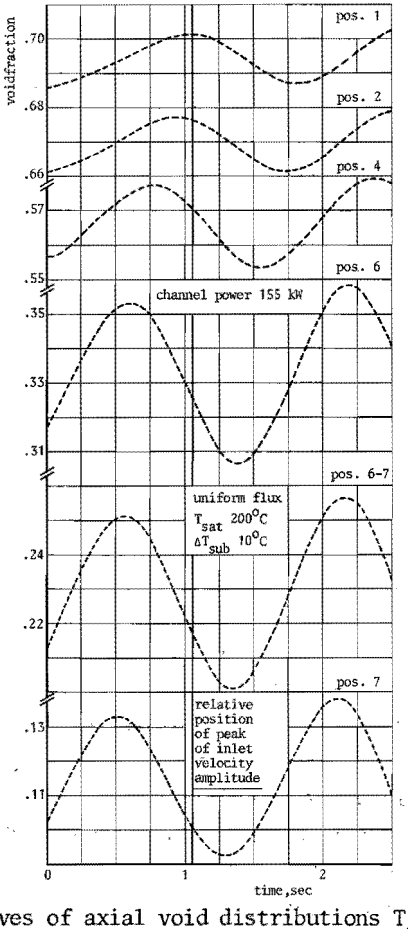

5.8. Response curves of axial void distributions T_{sat} 200°C, ΔT_{sub} 10°C

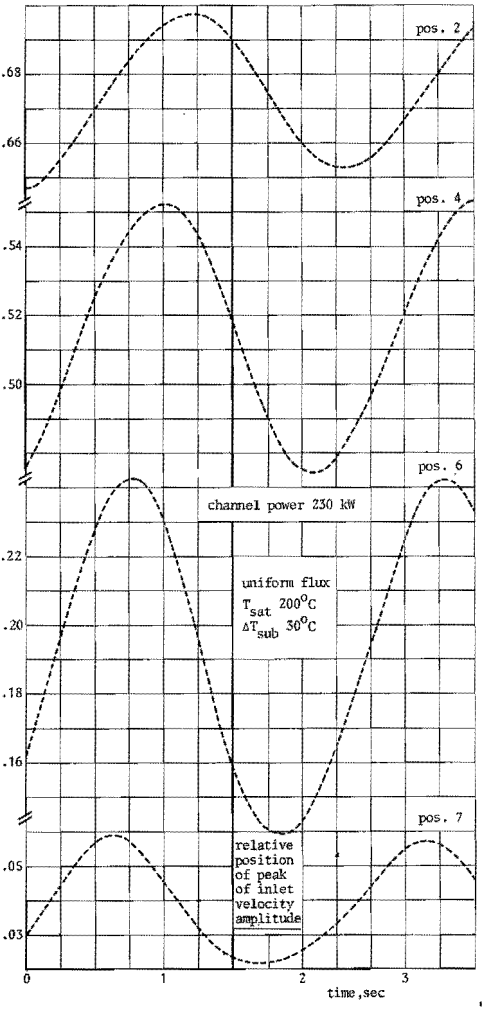

5.9. Response curves of axial void distributions T_{sat} 200°C, ΔT_{sub} 30°C

boiling boundary was calculated to be at position 4 (see Fig. 5.11. It implies that the model, too, does not predict a relationship between maximum void amplitude and boiling boundary, i.e. that the boiling boundary is not a significant quantity for the hydrodynamic behaviour of the system. During the experiments the maximum amplitude was at position 7 (Fig. 4.7.). The irrelevance of the boiling boundary is emphasised by Fig. 5.9. for 30°C subcooling, where a

position intermediate between positions 5 and 6 indicates the maximum void amplitude whereas all along the channel no bulk boiling occurs and consequently no boiling boundary exists. The experiments showed the maximum amplitude at position 6 (Fig. 4.7.).

The axial phase distribution of voids with respect to the inlet flow velocity (Fig. 5.10.) shows perfect agreement with the experimental curves (Fig. 4.4. and 4.8.). The differences are only a few degrees. The influence of subcooling is similar to that observed from the experiments. The common conservation equations are thus found to be fully suitable to predict phase relationships between different physical variables.

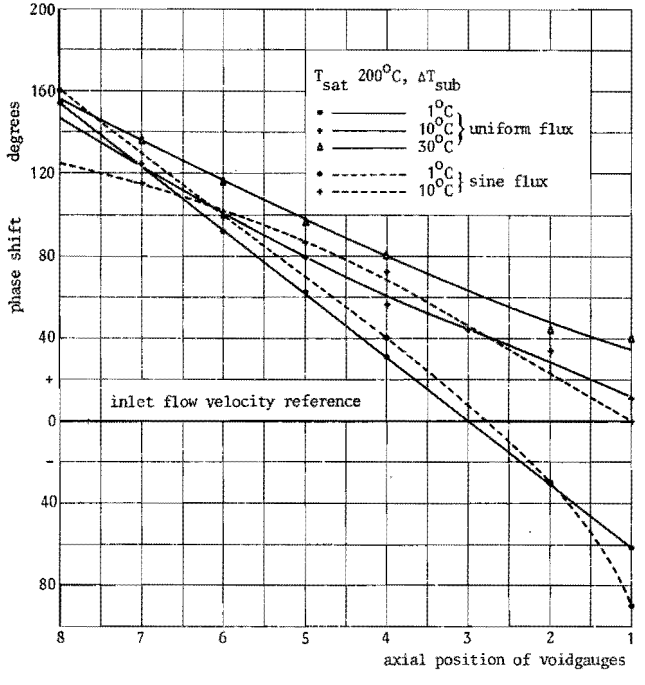

5.10. Axial phase distribution of void T_{sat} 200°C, various subcoolings

For the case of 10°C subcooling the response of the temperature of the liquid at various axial positions has been plotted in Fig. 5.11. In order to avoid overcrowding the diagram, the variations at lower

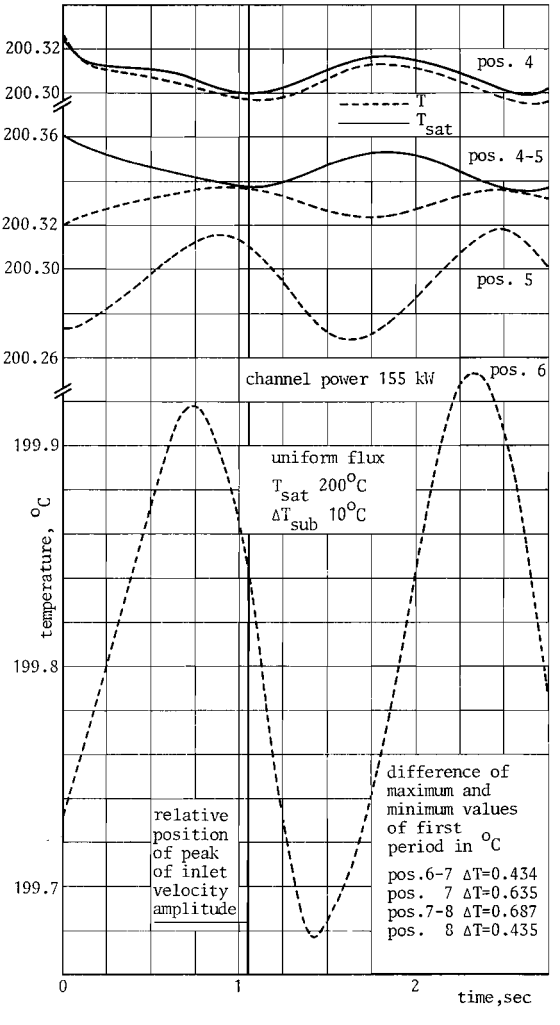

5.11. Response curves of axial temperature distributions T_{sat} 200°C, ΔT_{sub} 10°C

positions have been omitted but the values have been mentioned which indicate the maximum and minimum of the first period of the liquid temperature in question. The largest amplitude appeared between positions 7 and 8. It is supposed that this corresponds to the position of the steepest slope of the axial steady-state liquid

 temperature distribution. Actually the slope is largest immediate-

ly at the beginning of the heating element; however, that boundary condition which dictates the inlet temperature to be constant impedes the maximum amplitude to occur at the entrance. The amplitude decreases when reaching position 4 where the liquid temperature equals the saturation temperature. For position 4 and 4½ (between positions 4 and 5) the variation of the saturation temperature has been plotted, too. The liquid temperature approaches smoothly the saturation temperature without overshoot. This is, of course, caused by the formulation of the heat distribution parameter. There appears to exist a steadily changing phase difference between the liquid temperatures but that between the saturation temperatures does not change at all. The phase shifts have been plotted for only two positions. The phase of the liquid temperature at position 4½ can be thought to be extrapolated from the lower positions and is 180° with respect to the saturation temperature. This is quite remarkable because the liquid temperature has to equal in magnitude as well as in phase the saturation temperature at position 4. This is, indeed, the case and it causes a turn of the phase from 180° to 0° over a distance of 16.7 cm.

Sine-shaped heatflux

The response of the inlet flow velocity to a power disturbance is given in Fig. 5.12. for the condition of T_{sat} 200°C and ΔT_{sub} 1°C. The computations have been performed up to 230 kW. At this power the convergence appeared still to be so rapid that it was judged unfruitful to continue the calculations because the threshold power, if any, would 250 kW exceed, and beyond this power the threshold of oscillations is of no further interest, since burn-out would have occurred at this figure. The same procedure was followed for the condition of 10°C subcooling. The variables showed stable situation at 200 kW and unstable at 230 kW. The threshold was not shut in more accurately. It is expected that the threshold will lie between 210 and 230 kW. The destabilising effect was obviously also present under an axial heatflux distribution,contrary to the experi-

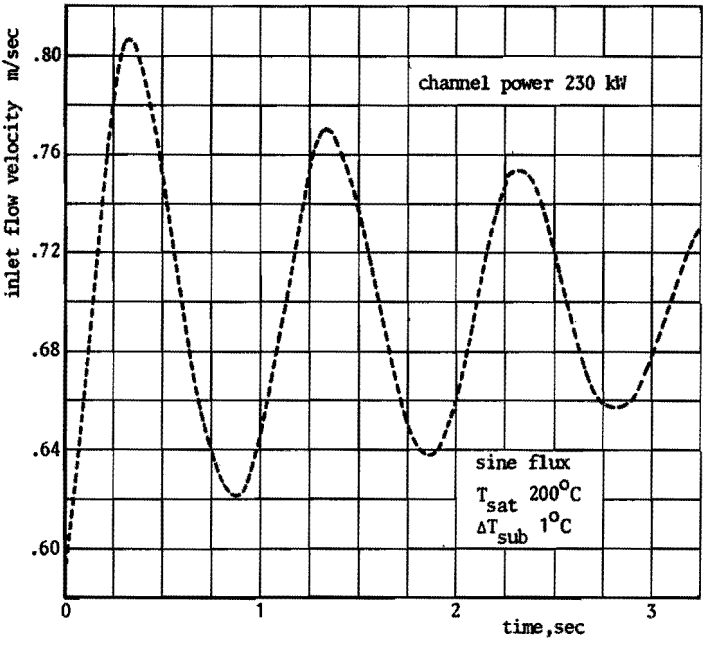

5.12. Response curves of inlet flow velocity T_{sat} 200°C, ΔT_{sub} 1°C

mental observations. The stability level, however, was really shifted towards considerably higher channel powers compared with the uniform heatflux, but not to the extent as indicated by the experiments. The frequencies for 1°C and 10°C subcooling were 1.11 and 0.84 Hz respectively. The frequency is less sensitive to subcooling than it was for the uniform heatflux, in correspondence with the experiments.

The void variations at various axial positions do not really differ from the results of the uniform flux (Fig. 5.13.). The amplitudes of position 4 and higher differ only slightly mutually. At 10°C subcooling (Fig. 5.14.) the amplitude is maximum at position 7, whereas the maximum for the uniform heatflux occurred at a slightly higher position. The phase differences between void and inlet flow velocity (Fig. 5.10.) differ somewhat from the experimental values, particularly visible in the lower positioned voids. The deviations

may probably be attributed to a less correct slip correlation and on the other hand to the less adequate exponent of the heat distribution parameter.

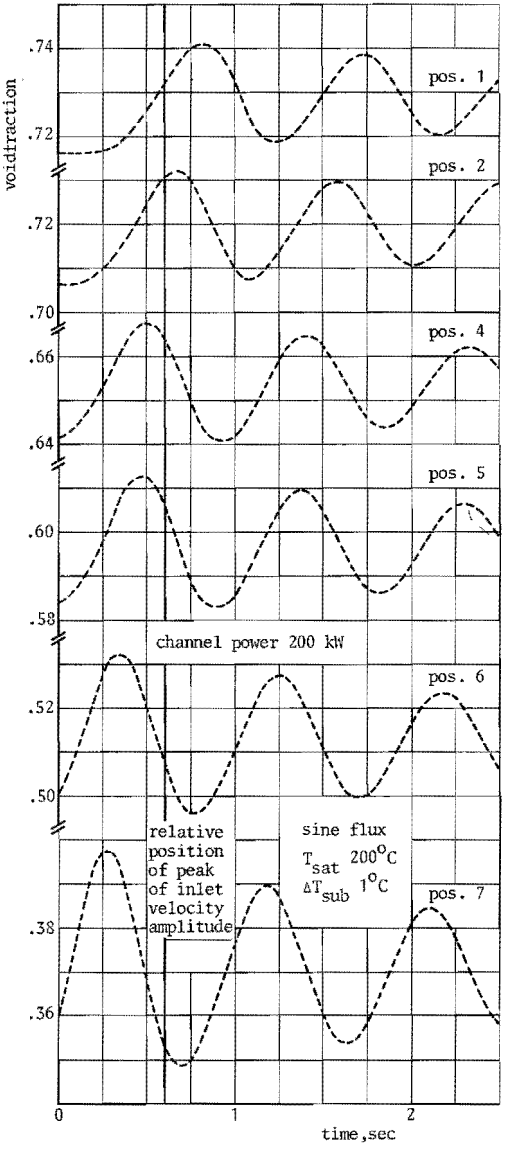

5.13. Response curves of axial void distributions T_{sat} 200°C, ΔT_{sub} 1°C

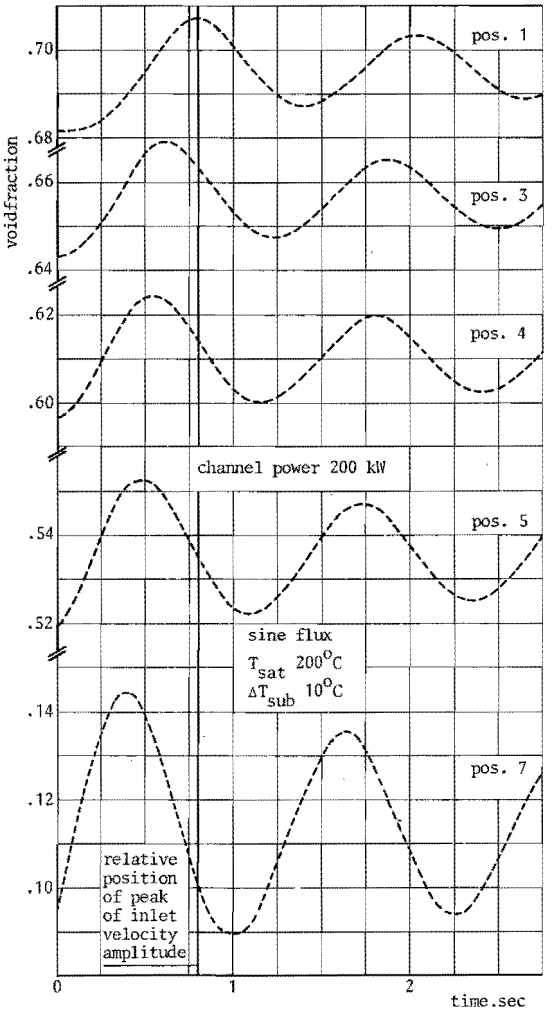

5.14. Response curves of axial void distributions T_{sat} 200°C, ΔT_{sub} 10°C

A s y m m e t r i c , a x i a l h e a t f l u x

It was thought valuable to perform some calculations with an asymmetric axial heatflux distribution in view of the reactor flux distribution being of an asymmetric shape. The shape was approximated by a 5th order expression, which is a function of axial distance, and is represented in Fig. 5.15. The results are quite identical to those of the sine-shaped heatflux (Fig.5.16). At 230 kW the system was still stable.

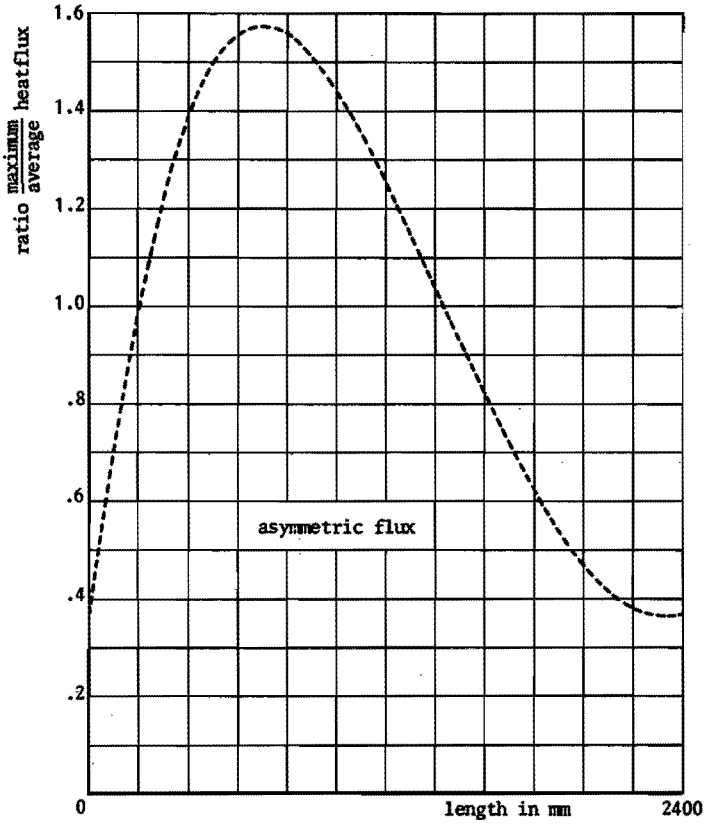

5.15. Axial distribution of asymmetric heatflux

Transfer functions

For the condition of uniform heatflux, T_{sat} 200°C, ΔT_{sub} 1°C and channel power 150 kW transfer functions were computed between the disturbing channel power and the dependent physical variables. The Bode-diagram of inlet flow velocity versus channel power is given in Fig. 5.17. The illustration represents the trivial characteristics of an amplitude peak and a sharp turn of phase shift at the resonance frequency.

The phase shift between inlet flow velocity and local voids is given in Fig. 5.18. There exists a good agreement with the corresponding experimental illustration (Fig. 4.16.).

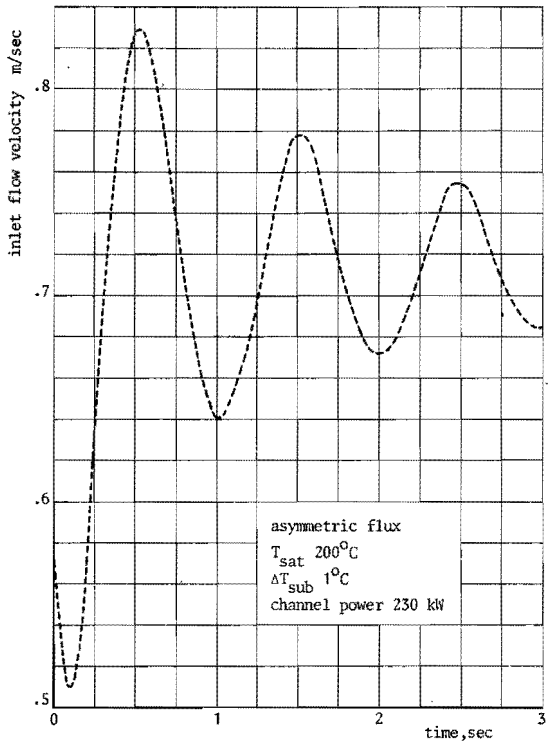

5.16. Response curves of inlet flow velocity T_{sat} 200°C, ΔT_{sub} 1°C

Conclusive remarks

The results of the computations answered perfectly the intention to develop a simple model that qualitatively should predict correctly the influence of subcooling and axial heatflux distribution. Although, or perhaps because+, the steady-state results did not fit exactly the experimental results, yet in quantitative respect, too, the results were quite promising. The axial phase distributions for the uniform heatflux corresponded perfectly with the experimental values. The

+ In (B 4) it is stated that modifying a model to better predict steady-state results often has a reverse effect on the dynamic results.

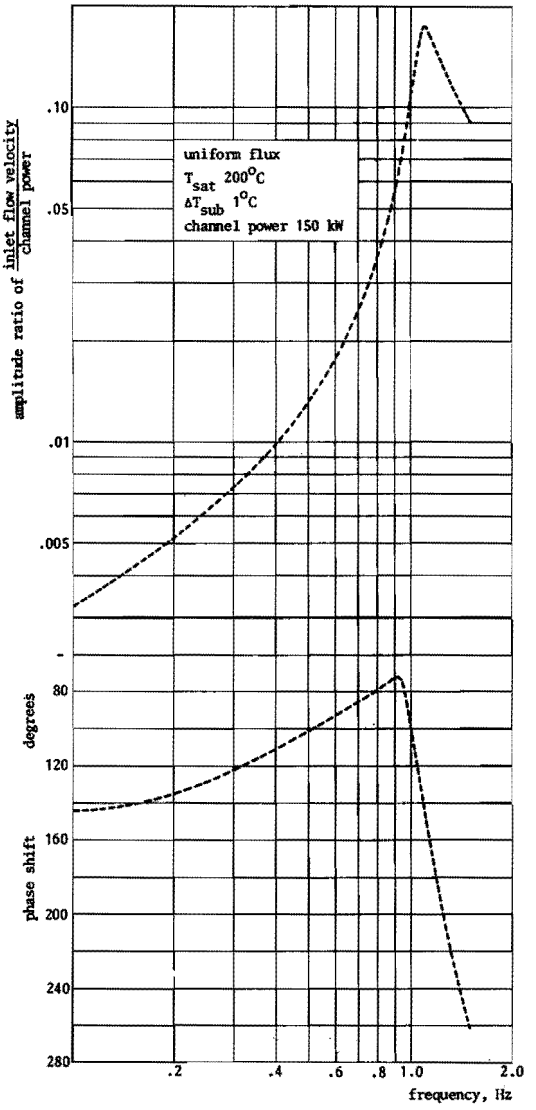

5.17. Transfer function between inlet flow velocity and channel power T_{sat} 200°C, ΔT_{sub} 1°C

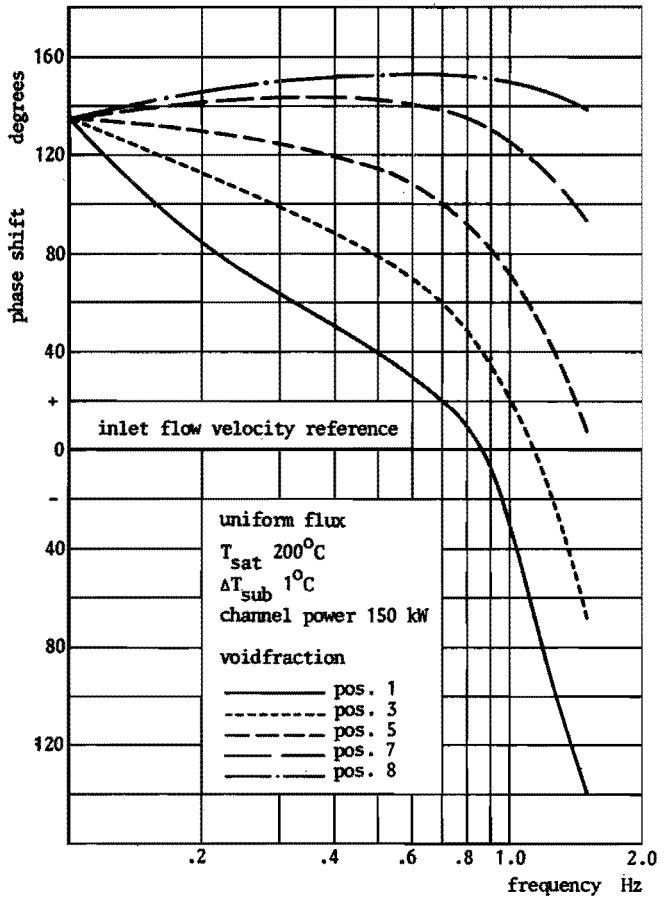

5.18. Axial phase distribution of void as a function of frequency T_{sat} 200°C, ΔT_{sub} 1°C, 150 kW

destabilising effect of subcooling was a little more pronounced when comparing the threshold powers, but there was little or no difference when comparing the powers in unstable condition.
The sine-shaped heatflux did not show instabilities at lowest subcooling and 230 kW nor did the asymmetric heatflux. Moderate subcooling caused instabilities to occur between 210 and 230 kW which is at least 55 kW higher than the corresponding threshold under the uniform heatflux.

6. CONCLUSIONS

Instabilities in boiling water reactors are very significant to the reactor industry because the safe operating power of a boiling water reactor can be determined by the threshold of instability. It must be emphasised that the subject of interest is boiling water. This is important because in many experiments the fluid properties are simulated by air-water mixtures. One has to be very cautious when transfer results and observations obtained from an air-water rig to a boiling water system. Instabilities of the type as are encountered in a boiling water channel are essentially impossible in an air-water mixture (J 4). For instance, the oscillations in the latter type of fluid can be of the slug type (A 1). Thus, the analogy between single-component and two-component two-phase systems, so often employed, could lead to erroneous conclusions (J 4, F 1). This is supported by the experience with the calibration of the present void gauges. The results obtained from air-water tests deviated substantially from the loop results. This is not really surprising because of the lack of physical interrelationship between air and water.

The experiments revealed that the oscillations can to a great extent be reduced to steady-state conditions. The phase differences between axially distributed voids and Δp-inlet were very constant and did not change when entering the unstable region. A change in the phase-lag between any void and the flowrate to 180° could not be detected from the experiments. Consequently, the void-propagation velocities are constant. An analytical expression as derived by Neal (N 3) from the laws of conservation succeeds very well in predicting the propagation velocity, whereas the kinematic wave theory, as applied by Staub (S 3), is not very successful. The rate of increase of the amplitudes of the different physical variables as a function of power is at the lowest subcooling smoother than at higher subcoolings, where the transition from stable to unstable is very abrupt. During unstable behaviour the twin-type relation between void and inlet

flow velocity is maintained, which is supported by an observation of the relationship between the amplitudes of the signals.

The effect of two important operating parameters, acting on loop stability either separately or in combination is unexpectedly large. The destabilising effect of moderate values of subcooling has been reported by several authors (J 3, B 5, B 6, S 2, Å 2), but in combination with a sine-shaped heatflux the effect is reversed. The stabilising influence of an axial flux distribution appeared to be so great that no oscillations at all could be observed up to burn-out point. Increased subcooling does not promote instabilities but moves the burn-out power up to higher values.

The phase differences between void and flow velocity, the threshold powers of instabilities, the oscillation frequencies, the axial position of the amplitude maxima of void, the destabilising effect of subcooling and the strong stabilising effect of a sine-shaped heatflux were correctly predicted by a simple non-linear model. The success of the model implied a justification of the basic assumptions and of the neglect of estimated second order effects. It affirmed the validity of steady-state physical correlations for dynamic computations and the correctness of the basic conservation equations. According to Neal (N 5), in case of saturated boiling flow it is not necessary to apply separate momentum equations for the two phases. This is supported by the model. The promising results of the model are a stimulus to proceed with non-linear programming as a beginning of optimalisation (B 7). The successful application of the CSMP-program evidently suggests the suitability of hybrid-computers in order to increase accuracy and to diminish the computing time considerably.

From the measurements it is obvious that one must seriously query the results of experiments with a uniform flux in view of the enormous influence of axial power distribution. It is, however, this shape that is being generated in a nuclear reactor. It means that it is questionable whether any instabilities of the type as described in this report can occur in a boiling water reactor. This can be related also to steamboilers with asymmetric heating.

 Therefore, the experiments reported here seem to prove their own superfluity

ACKNOWLEDGEMENTS

I gratefully record my indebtedness to Professor Dr. M.Bogaardt for affording me the opportunity to carry out this research. Further I would express my obligation to the members of the Laboratory of Heat Transfer and Reactor Engineering for their technical assistance and moral support; to Mr. J.M.H.Verspagen, who was responsible for the rig and its operation and who was indispensable for providing the experimental data; to Mr. M.L.C.Sluiter, whose exertion and ideas have contributed to the success of the non-linear model; to Mr. J.F.Tummers, whose imperturbable assistance and punctuality overcame a period of set-back; and to Miss A.M.E.T.Hammes for her conscientious typing of the manuscript, and in particular for her cordiality which has been an imponderable support for me.
Besides I thank the members of the mathematical department of the Catholic University of Nijmegen for their exceptional service which has contributed considerably to the development of the model in such a short time.

Appendix A. Rough data computed by the Transfer Function Analyser.

Condition of uniform heatflux, T_{sat} 200°C, ΔT_{sub} 16°C and 150 kW

signals x	signals y	power spectra Φ_{xx}	power spectra Φ_{yy}	cross-spectrum Φ_{xy}	phase angle in degrees
Δp_{inlet}	void pos.	45.4	34.8	31.0	173.7
	1	44.7	32.6	26.4	172.9
		45.5	30.2	26.4	174.4
	2	45.2	24.8	26.5	172.8
		44.8	24.9	28.0	172.5
		44.0	26.4	28.6	172.8
	3	44.4	18.8	17.9	154.9
		43.9	19.7	22.1	155.1
		44.0	18.5	19.7	155.5
	4	44.6	7.7	15.0	138.2
		45.2	7.1	15.4	139.4
		44.6	8.0	15.4	137.8
	5	44.8	5.5	13.8	103.7
		43.0	6.3	13.9	105.1
		43.7	6.4	14.4	103.8
	6	44.7	6.0	15.1	78.3
		44.7	5.7	14.6	78.3
		43.2	5.0	13.3	79.1
	7	44.1	10.2	13.0	54.2
		43.0	9.7	13.0	55.3
		44.2	11.2	13.1	54.5
	8	43.4	2.1	9.0	31.2
		43.4	2.4	9.0	29.9
		43.4	2.3	9.4	31.2

Appendix B. Review of experimental conditions.

	steady state ΔT_{sub} in ^{o}C	noise analysis ΔT_{sub} in ^{o}C	transfer functions ΔT_{sub} in ^{o}C	channel power
uniform heatflux T_{sat} 200^{o}C	1.6	1.6	1.6	100 kW
	5.6	11.0		160 kW
	8.6	16.0		
	11.0	30.0		
	16.0			
	21.0			
	30.0			
T_{sat} 234^{o}C	2.3	2.3	2.3	150 kW
	7.0	7.0		225 kW
	13.0	13.0		
	30.0	30.0		
sine-shaped heatflux T_{sat} 200^{o}C	2.0	2.0	2.0	200 kW
	5.5	5.5		
	11.0	11.0	11.0	220 kW
	16.0	16.0		
	21.0			
T_{sat} 234^{o}C	2.7	2.7		
	11.0			
	21.0			
	30.0			

Appendix C. Terms incorporated in the model equations.

$$A_1 = 2W\left\{\frac{(1-x)^2}{\rho_w(1-\alpha)} + \frac{x^2}{\rho_s\alpha}\right\}$$

$$A_2 = W^2\left[\frac{\rho_s}{\rho_w}\cdot\frac{\alpha^2}{x^2}\cdot\frac{1}{a_1-a_3\alpha^2}\left\{\frac{(1-x)^2}{\rho_w(1-\alpha)^2} - \frac{x^2}{\rho_s\alpha^2}\right\} - \frac{2(1-x)}{\rho_w(1-\alpha)} + \frac{2x}{\rho_s\alpha}\right]$$

$$A_3 = \{\rho_w(1-\alpha) + \rho_s\alpha\}g + \frac{f_{ch}}{2\rho_w D} R W^2$$

$$A_4 = cT(1-x) + cT_{sat}\, x$$

$$A_5 = c(T_{sat}-T)\, W$$

$$A_6 = W\left(xc\,\frac{\partial T_{sat}}{\partial p} - \frac{1}{\rho_w}\right)$$

$$A_7 = W(1-x)$$

$$A_8 = (1-\kappa)q_m$$

$$A_9 = h_{sw}x$$

$$A_{10} = h_{sw}\dot{W}$$

$$A_{11} = \frac{-xW}{\rho_s}\left(1 - \frac{\rho_s}{\rho_w}\right)$$

$$A_{12} = \kappa q_m$$

LIST OF REFERENCES

A 1 K. Akagawa.
Fluctuation of void ratio in two-phase flow. Bulletin of JSME, vol. 7, no. 25, 1964.

A 2 C. Arneodo, G. Gaudiosi, A. Merelli, C. Merlini, B. Migliorati.
Thermal Hydraulic Instability Tests at 60 kg/cm^2 performed on the Natural Circulation, Pressurised Water Loop of the Polytechnic School of Turin in 1962. FIAT-GN 42.

A 3 N. Adorni, P. Alia, L. Cravarolo, A. Hassid, E. Pedrocchi.
An isokinetic sampling probe for phase and velocity distribution measurements in two-phase flow near the wall of the conduit. CISE-Report R89, 1963.

A 4 R.P. Anderson.
The calculation of steady-state hydraulics and stability studies at ANL of natural circulation boiling water reactors.
Section IX, Advanced Course, Kjeller, Norway, 1962.

A 5 Anonymous.
Studies on the steady-state and dynamic behaviour of boiling water reactors. Final Report, Technological University of Eindhoven, EUR-3789, 1968.

B 1 O. Baker.
Simultaneous flow of oil and gas.
Oil and Gas Journal, vol. 33, July 1954.

B 2 S.G. Bankoff.
A variable density single-fluid model for two-phase flow with particular reference to steam-water flow. Journal of Heat Transfer, Trans. ASME, Series C, vol. 82, 1960.

B 3 R.W. Bowring.
Physical model, based on bubble detachment, and calculation of steam-voidage in the subcooled region of a heated channel. OECD Halden Reactor Project. HPR 10, 1962.

B 4 T.J. Bjørlo, T. Eurola, R. Grumbach, P. Hansson, A. Olsen, J. Rasmussen, K. Romslo.
Comparative studies of mathematical hydrodynamic models applied to selected boiling channel experiments. Institutt for Atomenergi, Halden, HPR 97, 1967.

B 5 T.J. Bjørlo, T. Eurola, R. Grumbach, J.E. Lunde, J.H. Post, K. Romslo, V. Tosi, H.G. Walger.
In-pile and out-of-pile hydrodynamic studies on natural circulation boiling water channels. Institutt for Atomenergi, Halden HPR 82, 1967.

B 6 K. Becker, R. Mathisen, O. Eklind, B. Norman.
Measurements of hydrodynamic instabilities, flow oscillations and burn-out in a natural circulation loop. EAES Symp. on Two-Phase Flow, Studsvik, Sweden, October 1963, S. 316.

B 7 S.G. Bankoff.
Chairman's remark. Symp. on Two-Phase Flow Dynamics, Eindhoven, 1967.

B 8 Babcock & Wilcox.
Non-uniform heat generation - Experimental program. Final Report 1967.

B 9 C.J. Baroczy.
A systematic correlation for two-phase pressure drop. Atomics International, NAA-SR-MEMO-11858, 1966.

B 10 R. Bird, W. Stewart, E. Lightfoot.
Transport phenomena, Wiley, New York, 1965.

C 1 L. Cimorelli, R. Evangelisti.
The application of the capacitance method for void-fraction measurements in bulk boiling conditions. Int. J. Heat Mass Transfer, vol. 10.

C 2 H. Christensen.
Chairman's remark, Symp. on Two-Phase Flow Dynamics, Eindhoven, 1967.

C 3 H. Christensen.
Power-to-void transfer functions, ANL-6385, 1961.

D 1 F.J.M. Dijkman, J.F. Tummers, M. Bogaardt.
Influence of the stability criterion on the threshold power of boiling water systems. Technological University of Eindhoven, R-134, 1968.

D 2 A.L. Davies, R. Potter.
Hydraulic Stability. An analysis of the causes of unstable flow in parallel channels. Paper 9.3. Symp. on Two-Phase Flow Dynamics, Eindhoven, 1967.

F 1 H.K. Fauske.
Chairman's remark. Symp. on Two-Phase Flow Dynamics, Eindhoven, 1967.

F 2 J.A. Fleck.
The dynamic behaviour of boiling water reactors. Journal of Nuclear Energy, 11, A, 114, 1960.

E 1 R. Evangelisti.
Personal communication concerning the application of the impedance method.

H 1 G.F. Hewitt, D.C. Leslie.
Two-phase flow and heat transfer. The Engineer, 1967.

H 2 P.T. Hansson, R.P. Mathisen, O. Eklind.
A study of loop stability dependence on axial heatflux distribution in round duct test sections. A.B. Atomenergi, Studsvik, RTL-759.

J 1 W.H. Jens, P.A. Lottes.
Analysis of heat transfer, burn-out, pressure drop and density data for high pressure water, ANL-4627, 1951.

J 2 A.B. Jones, Hydrodynamic stability of a boiling channel. KAPL-2170, 1961.
A.B. Jones, A.G. Dight. Hydrodynamic stability of a boiling channel, part II, KAPL-2208, 1962.

J 3 K.C. Jain.
Self-sustained hydrodynamic oscillations in a natural circulation two-phase flow boiling loop. ANL-7073, 1965.

J 4 F.A. Jeglic, T.M. Grace.
Onset of flow oscillations in forced-flow subcooled boiling. NASA-TN D-2821, 1965.

J 5 S. Jahnberg.
A one-dimensional model for calculation of non-steady two-phase flow. EAES Symposium on Two-Phase Flow, Studsvik, 1963.

K 1 G. Kjaerheim, E. Rolstad.
In-pile hydraulic instability experiments with a 7-rod natural circulation channel. Paper 1.7. Symp. on Two-Phase Flow Dynamics, Eindhoven, 1967.

K 2 A. Kirchenmayer, H.E. Scholz.
Stability problems of boiling water reactors. Paper 8.3. Symp. on Two-Phase Flow Dynamics, Eindhoven, 1967.

L 1 P.A. Lottes, W.H. Cook, K.F. Neusen, R.W. Wright, S.M. Zivi, N. Zuber.
Fluid dynamics, stability and vapour-liquid slip in boiling reactor systems. Paper 230, Geneva Conference, 1964.

L 2 S. Levy.
Forced convection subcooled boiling-prediction of vapour volumetric fraction. Int.J.Heat Mass Transfer. vol. 10, 1967.

L 3 C. Lackmé.
Structure et cinematique des écoulements diphasiques à bulles. CEA. Grenoble TT-71, 1966.

M 1 R.C. Martinelli, D.B. Nelson.
Prediction of pressure drop during forced-circulation boiling of water. Trans. ASME, vol. 70, 1948.

M 2 J.C. Maxwell.
A treatise on electricity and magnetism. Clarendon Press, Oxford, 1881.

M 3 R.P. Mathisen.
Natural circulation with boiling. Nukleonik 11 Bd, Heft 1, 1968.

N 1 G.P. Nassos.
Propagation of density disturbances in air-water flow. ANL-7053, 1965.

N 2 L.G. Neal, S.M. Zivi.
Hydrodynamic stability of natural circulation boiling systems. A comparative study of analytical models and experimental data. TRW-Systems, STL 372-14 (1), 1965.

N 3 L.G. Neal, S.M. Zivi, R.W. Wright.
The mechanisms of hydrodynamic instabilities in boiling systems. Paper 8.1. Symp. on Two-Phase Flow Dynamics, Eindhoven, 1967.

N 4 L.G. Neal, S.M. Zivi.
The stability of boiling water reactors and loops. Nucl.Sci. Eng., vol. 30, 1967.

N 5 L.G. Neal.
Chairman's remark. Symp. on Two-Phase Flow Dynamics, Eindhoven, 1967.

O 1 H.O. Olsen.
Theoretical and experimental investigation of impedance void-meters. Institutt for Atomenergi, Kjeller, KR-118.

P 1 M. Petrick, A.A. Kudirka.
On the relationship between the phase distribution and relative velocities in two-phase flow. Vol. IV Proceedings Chicago Conference, 1966.

P 2 G. Possa, G. Valli, J.B. van Erp.
Measurement of total steam volume in a heated channel at 70 kg/cm^2, paper E 4, Symp. on Two-Phase Flow, Exeter, 1965.

Q 1 E. Quandt.
Analysis and measurement of flow oscillations.
WAPD-T-1134, 1960.

R 1 Z. Rouhani.
Calculation of steam volume fraction in subcooled boiling.
Trans. ASME, febr. 1968.

R 2 F. Reisch, G. Vayssier.
A non-linear digital computer model requiring short computation time for studies concerning the hydrodynamics of boiling water reactors., Nucl.Eng.Design 9, no. 2, 1969.

S 1 C.C. St. Pierre.
Frequency-response analysis of steam voids to sinusoidal power modulation in a thin-walled boiling water coolant-channel.
ANL-7041.

S 2 C.L. Spigt.
On the hydraulic characteristics of a boiling water channel with natural circulation. Technological University of Eindhoven 1966.

S 3 F.W. Staub, N. Zuber.
Void response to flow and power oscillations in a forced-convection boiling system with axially non-uniform power input.
Nucl.Sci.Eng. 30, 1967.

S 4 G.F. Stevens, R.W. Wood, J. Pryzbylski.
An investigation into the effects of a cosine axial heatflux distribution on burn-out in a 12 ft long annulus using Freon-12, UKAEA, AEEW - R 609.

S 5 M.L. Sluiter, Personal communication concerning the solution procedure of the set of non-linear equations.

T 1 A. Thie.
Reactor noise, Rowman and Littlefield, Inc., New York.

T 2 R. S. Thom.
Prediction of pressure drop during forced circulation boiling of water. Int.J.Heat Mass Transfer vol. 7.

T 3 N.V. Tarasova, A.I. Leontiev, V.I. Hlopushin, V.M. Orlov.
Pressure drop of boiling subcooled water and steam-water mixture flowing in heated channels. Vol. IV Proceedings Int. Heat Transfer Conference, Chicago, 1966.

T 4 G. del Tin, C. Merlini.
Instabilité débit dans une boucle à circulation naturelle. Revue générale de Thermique No. 88, 1969.

T 5 N.E. Todreas, W.M. Rohsenow.
The effect of axial heatflux distribution on critical heatflux in annular two-phase flow.

W 1 F. van der Walle, H.J. Lamein.
On the hydrodynamic aspects of two-phase flow in vertical boilers. Part I: Theory. Technological University of Eindhoven, 1963.

Z 1 N. Zuber, J.A. Findlay.
The effects of non-uniform flow and concentration distributions and the effect of the local relative velocity on the average volumetric concentration in two-phase flow. GEAP-4592, 1964.

Z 2 N. Zuber, F.W. Staub.
An analytical investigation of the transient response of the volumetric concentration in a boiling forced-flow system. Nucl.Sc.Eng. 30, 1967.

Å 1 H. Åkesson.
Local void measurements in oscillation two-phase flows. Aktiebolaget Atomenergi, Studsvik. AE-RTL-1010.

Å 2 F. Åkerhielm, P.T. Hansson, O. Nylund.
Experimental and theoretical determination of dynamic characteristics and stability limits in natural circulation boiling channels with rod clusters. Paper 1.2. Symp. on Two-Phase Flow Dynamics, Eindhoven, 1967.

LIST OF ILLUSTRATIONS

Chapter 2

Chapter 3

3.16†.	Inlet flow velocity versus channel power	T_{sat} 234°C
3.17.	Inlet flow velocity versus channel power	T_{sat} 234°C, ΔT_{sub} 2.7-2.3°C and 30°C
3.18†.	Exit void fraction versus channel power	T_{sat} 234°C
3.19.	Exit void fraction versus channel power	T_{sat} 234°C, ΔT_{sub} 2.7-2.3°C and 30°C
3.20†.	Axial void distributions	T_{sat} 234°C, ΔT_{sub} 2.7°C
3.21.	Void parameters defined by Zuber (Z 1)	T_{sat} 200°C and 234°C
3.22†.	Void parameters defined by Zuber (Z 1)	T_{sat} 200°C and 234°C
3.23.	Void parameters based on study by Bankoff (B 2)	T_{sat} 200°C and 234°C
3.24†.	Void parameters based on study by Bankoff (B 2)	T_{sat} 200°C and 234°C
3.25.	Two-phase friction parameters defined by Martinelli-Nelson (M 1)	T_{sat} 200°C

Chapter 4

4.1.	Stability curves defined by Δp-inlet	T_{sat} 200°C and 234°C
4.2.	Axial distribution of void amplitudes	T_{sat} 200°C, ΔT_{sub} 1.6°C
4.3.	Axial distribution of amplitude ratio Δp-inlet - void	T_{sat} 200°C
4.4.	Axial phase distribution of void	T_{sat} 200°C, ΔT_{sub} 1.6°C
4.5.	Axial phase distribution of void compared to Neal's expression	T_{sat} 200°C
4.6.	Residence times of water and steam	T_{sat} 200°C
4.7.	a,b,c. Axial distribution of void amplitudes	T_{sat} 200°C, various subcoolings
4.8.	a,b,c,d. Axial phase distribution of void	T_{sat} 200°C, various subcoolings
4.9.	a,c,b,d. Axial distribution of void amplitudes	T_{sat} 234°C, various subcoolings
4.10.	a,b,c,d. Axial phase distribution of void	T_{sat} 234°C

4.11. Stability curves defined by Δp-inlet — T_{sat} 200°C and 234°C

4.12†. a,b,c,d.
Axial distribution of void amplitudes — T_{sat} 200°C, various subcoolings

4.13†. a,b,c,d.
Axial phase distribution of void — T_{sat} 200°C

4.14†. Axial distribution of void amplitudes and phase shift — T_{sat} 234°C, ΔT_{sub} 2.3°C

4.15. Power-to-Δp-inlet transfer function — T_{sat} 200°C, ΔT_{sub} 1.6°C

4.16. Power-to-void transfer function — T_{sat} 200°C, ΔT_{sub} 1.6°C

4.17. Frequency response of Δp-inlet-void — T_{sat} 200°C, ΔT_{sub} 1.6°C

4.18. Power-to-Δp-inlet transfer function — T_{sat} 234°C, ΔT_{sub} 2.0°C

4.19. Frequency response of Δp-inlet-void phase shift — T_{sat} 234°C, ΔT_{sub} 2°C

4.20†. Power-to-Δp-inlet transfer function — T_{sat} 200°C

4.21†. Frequency response of Δp-inlet-void phase shift — T_{sat} 200°C

4.22. Frequency response of power-void phase shift according to Zuber (Z 1) — T_{sat} 200°C

4.23. Frequency response of power-void phase shift according to Zuber (Z 1) T_{sat} 234°C.

Chapter 5

5.1. Inlet flow velocity versus channel power — T_{sat} 200°C, various subcoolings

5.2. Exit void-fraction versus channel power — T_{sat} 200°C, various subcoolings

5.3. Axial void distribution — T_{sat} 200°C, various subcoolings

5.4. Response curves of inlet flow velocity — T_{sat} 200°C, ΔT_{sub} 1°C

5.5. Response curves of inlet flow velocity — T_{sat} 200°C, ΔT_{sub} 10°C

5.6. Response curves of inlet flow velocity — T_{sat} 200°C, ΔT_{sub} 30°C

5.7. Response curves of axial void distributions — T_{sat} 200°C, ΔT_{sub} 1°C

5.8. Response curves of axial void distributions — T_{sat} 200°C, ΔT_{sub} 10°C

5.9. Response curves of axial void distributions — T_{sat} 200°C, ΔT_{sub} 30°C

† indicates experiments and computations with sine-shaped heatflux

LIST OF TABLES

LIST OF APPENDICES

SAMENVATTING

In deze studie wordt verslag gedaan van een experimenteel en theoretisch onderzoek naar het hydraulisch gedrag van een kokend water kanaal, waarin het stoom-water mengsel circuleert onder invloed van natuurlijke convectie, onder invloed van een hoge warmtebelasting. Uitgaande van een stationaire toestand, die gekenmerkt wordt door een grote mate van stabiliteit van de gemeten fysische grootheden: inlaatsnelheid en lokale dampfracties, temperaturen en drukken, ontstaan bij voldoend hoog vermogen heftige oscillaties in het systeem. Deze instabiliteiten zijn zichtbaar aan alle gemeten parameters en hebben een zeer regelmatig karakter. Alle meetsignalen vertonen een constante amplitude en een constante frequentie. De amplitude is een functie van het ingestelde vermogen, de frequentie niet of nauwelijks. Deze frequentie of resonantie-frequentie is wel afhankelijk van andere systeemgrootheden. Het type instabiliteiten wordt algemeen toegeschreven aan een wederkerige terugkoppeling tussen inlaatsnelheid en dampfractie.

In hoofdstuk 1 wordt een visie gegeven op de problematiek van de dynamica van een kokend-water systeem en wordt de achtergrondgedachte uiteengezet van waaruit de experimenten werden opgezet.

Hoofdstuk 2 geeft een beschrijving van de meetopstelling en de instrumentatie. Extra aandacht is besteed aan de techniek van het meten van dampfractie, die door de aard van het meetobject de grootste moeilijkheden oplevert.

De stationaire metingen worden vermeld in hoofdstuk 3. De invloed op de eigenschappen van het systeem is nagegaan voor de volgende onafhankelijk instelbare grootheden: kanaalvermogen, systeemdruk, onderkoeling aan de inlaat, de vorm in axiale richting van de verdeling van de warmtestroomdichtheid en een combinatie van deze

parameters. De invloed van de drie eerstgenoemde grootheden is triviaal en ook die van de vierde vertoont weinig aspecten die niet van te voren te voorzien waren.

Terwijl het stationaire gedrag zich heel goed laat verklaren uit een fysische beschouwing, blijkt dit voor het dynamische gedrag, als uiteengezet in hoofdstuk 4, niet mogelijk. Dit is niet verwonderlijk als men bedenkt dat de fundamentele kennis van de dynamica van een kokend water systeem tijdens 10 jaar ingespannen speurwerk slechts betrekkelijk weinig is gegroeid. De meest intrigerende parameter voor de onderzoeker is (was) de onderkoeling van het water aan de ingang van het kanaal. Bij betrekkelijk lage waarden blijkt onderkoeling een sterk instabiliserend effect te vertonen, dat bij hogere waarden weer afneemt. Dit is door verschillende onderzoekers bevestigd. Wat men echter in de literatuur tevergeefs zoekt is een publicatie over de invloed van een ongelijkmatig verdeelde warmtebelasting d.w.z. een die aan de uiteinden van het kanaal lager en in het midden hoger is dan gemiddeld over de lengte van het kanaal. Dat hiervan geen metingen bekend zijn is des te verwonderlijker, omdat het effect buitengewoon groot is. De stabiliteit van het systeem bleek aanzienlijk beter te zijn dan voor een gelijkmatige warmtebelasting en dit vooral wanneer het water aan de inlaat onderkoeld was, omdat het effect in plaats van instabiliserend nu juist stabiliserend was geworden. Van oscillaties was zelfs geen sprake meer en doorbranden van de staaf trad op voordat instabiliteiten konden optreden.

In een poging om dieper in te gaan op het fenomeen van instabiliteiten werden uit de meetsignalen, verkregen tijdens stationaire zowel als instationaire toestanden, amplitudes en faseverschillen berekend van lokale dampfracties en de inlaatsnelheid. Opvallend was dat de onderlinge fasverschillen nauwelijks een functie waren van de mate van stabiliteit d.w.z. er viel geen omslag te bespeuren bij de overgang van stationair naar instationair gedrag. Wel veranderde uiteraard de amplitude van de meetgrootheden.

De metingen werden aangevuld met een aantal overdrachtsfunctiemetingen, waarbij het vermogen werd geslingerd. De eerder gevonden
 resultaten werden volledig bevestigd. Als de slingerfrequentie

samenviel met de resonantiefrequentie werd wel een fase omslag geconstateerd tussen het vermogen en de interne responsie signalen, maar niet tussen deze signalen onderling. Zoals te verwachten was bleek ook bij de lage frequenties de resonantiefrequentie aanwezig te zijn.

Ondanks het geringe succes van bestaande mathematische beschrijvingen van het fysische gedrag van een twee-fase systeem werd een nieuw model ontwikkeld, beschreven in hoofdstuk 5, dat zich op twee punten van andere modellen onderscheidt:

1) het is uitsluitend gebaseerd op de behoudswetten, welke zijn geformuleerd op een wijze die algemeen aanvaard is voor een twee-fase systeem. Wel zijn de vergelijkingen aangevuld met correlaties voor slipfactor, twee-fase weerstand en onderkoeld koken, maar geen aandacht werd besteed aan kookgrensvariaties, warmteoverdracht aan de wand van het verhittingselement en dergelijke.
2) de niet-lineaire vergelijkingen werden opgelost met behulp van het CSMP-programma van de IBM. Dit bevat een aantal integratiesubroutines, die het programmeren van de oplossingsprocedure voor een stelsel differentiaalvergelijkingen zeer sterk vereenvoudigen.

De resultaten waren opvallend goed. In kwalitatief opzicht werd het gedrag van het systeem als functie van onderkoeling en ongelijkmatige warmtebelasting, volkomen correct voorspeld. Ook kwantitatief weken de resultaten slechts weinig af van de experimentele. Zo werden niet alleen de drempel-vermogens, waarbij instabiliteiten gaan optreden, maar ook faseverschillen en frequenties heel behoorlijk berekend. Het is verheugend dat een dergelijk simpel model zulke uitstekende resultaten produceert. Een nadeel van het model is de grootte van de benodigde rekentijd. Deze kan echter aanzienlijk worden teruggebracht door toepassing van een hybridecomputer.

In hoofdstuk 6 wordt de betekenis uiteengezet die de resultaten van het onderzoek en van de theoretische studie hebben voor het ontwerp van kernreactoren en conventionele stoominstallaties. In

de praktijk is een gelijkmatige warmtestroomdichtheid onbestaanbaar. Zowel in een reactorkern als in een vuurhaard bestaat een asymmetrisch profiel van de warmtebelasting. Het is daarom zeer twijfelachtig of resultaten van experimenten uitgevoerd met een gelijkmatige warmtebelasting vertaald kunnen worden naar condities zoals deze in de praktijk aanwezig zijn. Het is zelfs de vraag of onder praktische omstandigheden wel instabiliteiten kunnen optreden. Dit houdt in dat het twee-fase onderzoek nog sterker dan tot nu toe geconcentreerd moet worden op het optreden van doorbranden van splijtstofstaven en stoompijpen tijdens stationaire toestanden.

S T E L L I N G E N

1. Het vertalen van resultaten, verkregen uit experimenten met een twee-fase, twee-componenten systeem, naar toepassing in een twee-fase, een-component systeem is slechts in kwalitatieve zin mogelijk.

2. Onderzoek naar instabiliteiten, optredend onder invloed van een uniforme warmtestroomdichtheid, moet, gezien de grote invloed van een niet-uniforme warmtestroomdichtheid, welke laatste in praktische installaties altijd aanwezig is, met grote reserve beschouwd worden.

3. De hypothese, dat de oorzaak van instabiliteiten, van de soort als beschreven in deze studie, gezocht moet worden in een faseverschil van 180^{o} tussen inlaatsnelheid en dampvolume wordt noch door het experiment noch door de theorie bevestigd.

4. Aangezien de organisatie van ziekenhuizen meer gericht is op behandeling van de ziekte dan van de zieke, zijn weerstanden tegen technisch-medische integratie op grond van humanitaire overwegingen van hypocriet karakter.

5. Invoering van dienstplicht voor meisjes is geen adequaat middel voor het opheffen van het tekort aan verpleegsters, omdat het zal leiden tot een verdere dehumanisering van de verpleging.

6. Begeleiding van onderwijs - en onderzoekgroepen door sociologen zou de persoonlijke voldoening in en het rendement van het werk binnen deze groepen ten goede komen.

7. Met het oog op een betere communicatie tussen beoefenaren van de medische en technische wetenschap is het gewenst dat bij het medische onderwijs een aantal exacte vakken wordt gedoceerd.

8. Voor een optimaal bestuur is het gewenst dat gestreefd wordt naar een ontkoppeling van vakspecialistische deskundigheid en bestuurlijke functies.

9. Voor een betere waardering van individuele medewerkers is het wenselijk dat het salarisbeleid aan de THE gedecentraliseerd wordt.

10. Het stromingskarakter van het verkeer wordt bevestigd door de analogie tussen de instabiliteit van verkeersstromen en die, welke beschreven is in deze studie.

11. Dampfractiemetingen van anderen zijn altijd onbetrouwbaar.

Eindhoven, 30 december 1969 F. J. M. Dijkman